THE UNIVERSITY OF OKLAHOMA

GRADUATE COLLEGE

INVESTIGATION OF EFFECTS OF SURFACE ROUGHNESS

UPON REFLECTANCE

A DISSERTATION

SUBMITTED TO THE GRADUATE FACULTY

in partial fulfillment of the requirements for the

degree of

DOCTOR OF PHILOSOPHY

BY

DWIGHT C. LOOK, JR.

Norman, Oklahoma

1969

INVESTIGATION OF EFFECTS OF SURFACE ROUGHNESS

UPON REFLECTANCE

APPROVED BY
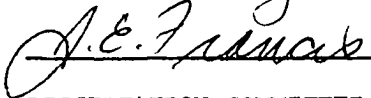
DISSERTATION COMMITTEE

ACKNOWLEDGMENTS

ABSTRACT

The directional reflectance in the plane of incidence, from a statistically constructed rough surface, is investigated. The V-groove character of the surface geometry is assumed describable by the RMS peak to valley and RMS peak to peak dimensions, $\bar{\sigma}$ and $\bar{a}$, respectively. The peaks of these surfaces are assumed to be rounded, dependent on a parameter P.

The analytical approach of this investigation involves a Monte Carlo technique of following an energy bundle as it is reflected about the rounded V-groove, obeying the rules of geometrical optics and thus includes multiple reflections. The peak to valley and peak to peak dimensions are assumed to be Rayleigh distributed random numbers, thus each energy bundle encounters essentially a different surface. The concept of a localization circle, whose radius is the wavelength of the incident radiation in the plane of incidence, is used in an attempt to restrict regions of the rounded V-groove from first incidence. Upon escape of the energy bundle from the rounded V-groove, its angle of escape is categorized into angular regions.

The results of this analysis are graphically compared to published experimental data of other investigators. It is evident from these comparisons that this approach yields a close approximation to experimental data under variations of the angle of incidence and the

wavelength of the incident radiation.

TABLE OF CONTENTS

APPENDICES

LIST OF TABLES

LIST OF FIGURES

LIST OF SYMBOLS

a	= Peak to peak dimension
$\bar{a}$	= RMS peak to peak dimension
a'	= autocovariance length
A	= macroscopic surface area
A'	= projected macroscopic surface area
$\bar{A}$	= arbitrary coefficient in smoothness function F
b_i	= radius of curvature of rounded portion
c	= length of slanted side of V-groove
(c,b)	= horizontal and vertical coordinates of center of curvature of localization circle
E	= radiant energy (watts)
F	= radiant flux (watts/cm^2)
$\bar{F}$	= smoothness function
F_N	= normalized detecting area
h	= penetration depth
H_i	= center of curvature for ith side rounded portion of V-groove
H'	= irradiance (watts/cm^2)
I	= intensity (watts/sr cm^2)
J	= radiant intensity (watts/sr)
$N(\psi;\ \theta,\varphi)$	= number of energy bundles received about the direction (θ,φ) when ψ is the angle of incidence

(n_x, n_y)	= horizontal and vertical components of normal to left side of V-groove
(N_x, N_y)	= horizontal and vertical components of normal to right side of V-groove
p	= probability of success in Bernouilli trial
P	= roundedness parameter
$P(LIM)$	= limiting value of P for basic surface configuration
$P(left)$	= probability that first incidence is on left side of rounded V-groove
Q	= radiance (watts/sr cm^2)
Ra	= random number
$\bar{R}$	= random number that will make $y_2(\bar{x}, \bar{y}) = y_Q(\bar{x}, \bar{y})$
X_o	= V-groove vertex position
x^*_i	= horizontal coordinate of the intersection of the penetration depth and i-th side of rounded V-groove
$(\bar{x}_i, \bar{y}_i)$	= transition point from rounded to straight portion of the i-th side of rounded V-groove
(x'_o, y_o)	= shadow boundary on right side of V-groove
(x', y')	= shadow boundary on left side of V-groove
(x, y)	= point of interaction of energy bundle and rounded V-groove
$y_1(x)$	= equation of left side of V-groove
$y_2(x)$	= equation of right side of V-groove
$y_3(x)$	= equation of rounded portion on left side
$y_4(x)$	= equation of rounded portion on right side
$\widehat{y_1}(x)$	= equation of the line of incidence that will intersect the rounded V-groove at the left extreme, on side of V-groove
$\widehat{y_2}(x)$	= equation of the line of incidence that will intersect the rounded V-groove on the right extreme, on either side of the V-groove

$y_Q(x)$ = equation of the line of incidence that will inter-sect the rounded V-groove on either side of the V-groove at $(\bar{x}, \bar{y})$

$y_?(x)$ = equation of the line of incidence that is randomly selected to be between $\widehat{y_1}(x)$ and $\widehat{y_2}(x)$

β = angle measured from nadir of center point of localization circle to (x_o', y_o)

θ = angle of relection (in degrees)

θ_i = $\tan^{-1}$ (slope of i-th side of V-groove)

λ = wavelength of incident energy bundle

λ_{max} = maximum wavelength of localization circle for the the radius of the circle to be perpendicular to the side of the V-groove

μ = micron $(10^{-6}\,m)$

π = 3.14159

ρ = reflectance

σ = peak to valley dimension

$\bar{\sigma}$ = RMS peak to valley dimension (roughness)

σ_o = RMS optical roughness

φ = azimuthal angle of reflected energy measured from the plane of incidence

ψ = angle of incidence (in degrees)

ψ_c = angle of tangential incidence at the point (x^*, h)

$d\omega_i$ = incremental solid angle

subscripts

ba = biangular

d = diffuse

s = specular

1 = left side

2 = right side

INVESTIGATION OF EFFECTS OF SURFACE ROUGHNESS

UPON REFLECTANCE

CHAPTER I

INTRODUCTION

This research is directed toward the question of why surfaces
reflect as they do. It is assumed once this is understood, accurate
theories may be developed to describe the reflectance (thus emittance
properties (1)) of surfaces as functions of surface geometry, both large
and small scale, and electrical properties as well as the angles of
irradiation and observation. The question of how these characteristics
should be defined is directly linked to what characteristics can be
measured with confidence. Thus the decision must be made as to what to
measure and how to measure it. The work reported herein is an attempt
to determine the effects of surface characteristics upon reflected energy
distributions, thereby indicating what surface properties should be
measured.

Classically there are two extremes for classification of re-
flected energy: the so-called "specular" and the "diffuse". The
specular (hereafter referred to as "regular") results when radiant
energy strikes a smooth surface. Academically, "smooth" implies the
surface is exactly flat with no small scale variations. The Fresnel
laws of reflection and refraction discussed in all standard optics

1

textbooks (2) appear to adequately describe the fractions of the incident radiation that are reflected and refracted. That is, in the plane of incidence the angle of incidence equals the angle of reflection and the refracted angle is related to the incident angle by Snell's law. It is interesting to note that the regular reflection rule was stated more than 650 years ago (3). Thus if it were possible to have a "smooth" surface, the surface would appear dark, except when viewed at the angle of reflection and the fraction of energy received would be that described by Fresnel's Law. In actuality this is never obtainable since the radiant energy is scattered by impurities that form on the surface (dust, oxides, etc.).

In general, surfaces of interest are not smooth but exhibit some form of waviness or irregularity. This irregularity results in a spreading of the reflected energy distribution. At this point, a statement need be made which is based on experimental evidence about the size of the irregularities as compared to the wavelength of the incident radiation. This rule is generally stated as follows: if the irregularities are very small compared to the wavelength of the incident radiation, the majority of the reflected energy will be of the regular form and as the relative size of irregularities increases, the spreading of the reflected energy will increase. Thus in a practical sense all irregularities need not be removed before a surface will exhibit strong regular reflection characteristics.

When radiant energy is incident on a surface that may be characterized as irregular (usually referred to as a matt surface), the incident energy is scattered in all directions to varying degrees and in the case

of appropriately sized irregularities, very little or no trace of the
regular component may be found. This is usually referred to as "diffuse
reflection", that is, all the incident radiation is reflected and re-
fracted in all directions.

In the discussion that follows, this circumstance will be re-
ferred to as non-regular reflection and the word "diffuse" will be
reserved for a special case of non-regular reflection. Note this ter-
minology eliminates the requirement that all interaction need take place
at the surface. Thus when non-regular reflection is observed, the energy
received may result from reflections and refractions of the energy with-
in the material as well as regular reflection between the surface irregu-
larities. This statement assumes the emitted energy is negligible.

The word "diffuse", when used in this discussion, will refer to
the non-regular reflection condition when the surface exhibits reflected
flux characteristics that are independent of the angles of observation
(the surface appears equally bright in all directions). To be explicit,
assume uniform, unidirectional irradiance, H', incident upon a surface
element dA. Thus the energy interacting with the surface in dA is

$$dE = H' \cos \psi \; dA \; .$$

The radiant intensity upon reflection is

$$dJ = \frac{R}{\pi} dE \cos \theta$$

where R is a reflection coefficient.

So $dJ = \frac{RH'}{\pi} dA \cos \psi \cos \theta \, ,$

Thus the apparent radiance is

$$Q = \frac{dJ}{dA'} = \frac{dJ}{dA \, \cos \theta} = \frac{RH'}{\pi} \cos \psi$$

dA' is the projected area in the direction of θ. This result is usually
referred to as Lambert's Law (4). The surface that exhibits this
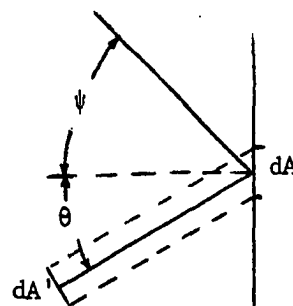
characteristic is called diffuse, Lambertian, or Lambertonion. The deceptive simplicity of this relation has resulted in its widespread use and general acceptance.

No real surface has been found to exhibit an intensity or flux pattern in accordance with predictions bases on this law. In fact the radiation reflected from most matt surfaces deviates considerably from such predictions, except for very limited ranges of ψ and θ (5 - 20). Recognizing the failure of Lambert's Law, some investigators have considered the use of more complicated expressions which contained a number of parameters to be determined experimentally (21- 31). As a consequence, these expressions can be made to agree with actual measured reflected energy data under restricted conditions. The major drawback to this approach is that these models are not based upon firm physical grounds and if the physical model is adequate, it does not fit experimental data well.

Thus there appears to be no such thing as diffuse reflection in the strict sense and no simple theoretical basis for the Lambert Law hypothesis. Its general acceptance has been due to the fact that it describes the reflected intensity pattern from matt surfaces (i.e. no perceivable regular component) as well as any other of the more complicated expressions as yet reported. Therefore, diffuse reflection is just one limit of non-regular reflection.

Surfaces of engineering interest exhibit a superposition of regular and non-regular reflection characteristics to varying degrees depending upon small scale roughness, wavelength, etc. Experimental investigation of such surfaces are extremely difficult to reproduce and

analyze due to instrumentation complication. That is, there is a need

for the existence of, 1) an infinitesimal, high intensity, unpolarized

radiation source, 2) perfect collimators, and 3) infinitesimal but ex-

treme fast and sensitive detectors. Attempts to standardize reflection

measurement procedures and classify reflection characteristics of a sur-

face with only one optical measurement have been undertaken for sometime

(32 - 35) but with little success. The physicists refer to measurements

of this type as determinations of mirror efficiencies while the psycholo-

gist considers the perceptual attributes of surfaces. Some engineers

refer to these measurements as gloss determination, where gloss is defined

as a property of surfaces which causes them to have a shiny or mirror-

like appearance. Therefore, gloss is the degree to which a surface

simulates a perfect mirror in its capacity to reflect incident radiation.

Actually this approach is not truly satisfactory because the distribution

of the reflected radiation in and adjacent to the mirror direction is

too complicated and varied to be compared by a single measurement. In

fact even under the above definition of gloss, several different types

of gloss could exist, for example, objective (specular) - the ratio of

radiation reflected by the test surface in the specular direction to

that of some standard surface under the same condition, and subjective

(contrast) - the ratio of radiation scattered in the specular direction

to that scattered in some other specified direction.

Ament (36) used the statistics of noise theory to rigorously

formulate the problem of predicting the specular (regular) reflection

coefficient of a perfectly conducting surface. Mathematical complexities

prevented him from obtaining an exact solution. Feinstein (37) combined

physical optics and a stochastic process analysis to investigate surface reflections. He obtained the approximate solution of Ament plus some higher order terms. Computational difficulties would preclude the use of his result. Spetner (38) approached the problem in a statistical fashion by assuming the rough surface consists of a large number of independent point scatterers. This theory is restricted to forward scattering.

The most physically appealing approach to the problem of determining a general equation to describe the reflected intensity pattern has been with the use of diffraction theory. The three approaches most generally discussed in the literature are those of Davies (39), Porteus (40) and Beckmann (41). The theories of these three investigators result in the expressions for the far field disturbance due to the two type of reflection characteristics discussed previously. Theoretical investigations of the near field disturbance have also been considered (42 - 44) but will not be discussed in this work.

These are just a few of the approaches taken in the study of surface reflection. But these do not, by a long way, exhaust the models and methods used in attempts to solve the problem of reflection of radiation from a rough surface.

CHAPTER II

BACKGROUND

Definitions

Let us digress to consider definitions that are used in the literature and will be used in the following discussion. Figure 2-1 will be helpful in defining parameters of interest. To define a reflectance, care must be taken to recognize the character of the incident and reflected radiation. Consider first the classical or ideal situation of a uniform, monodirectional incident flux F. In the specular case the reflectance would be defined as

$$\rho_s = \frac{F_r (\theta, \varphi)}{F_i (\psi)} \quad , \quad \theta = \psi, \varphi = 0$$

$$= 0 \quad , \quad \text{elsewhere,}$$

assuming the detector aperture was at least the size of the specimen. The subscripts denote reflection (r) and incidence (i). In the non-regular case

$$\rho_d = \frac{\int I_r (\theta, \varphi) \cos \theta \, d\omega_r}{F_i (\psi)}$$

where I_r represents the intensity and $d\omega_r$ is the solid angle of observation. In both cases ψ is the angle of incidence, θ is the polar angle of reflection and φ is the azimuthal angle of reflection (measured from the plane of incidence).

7
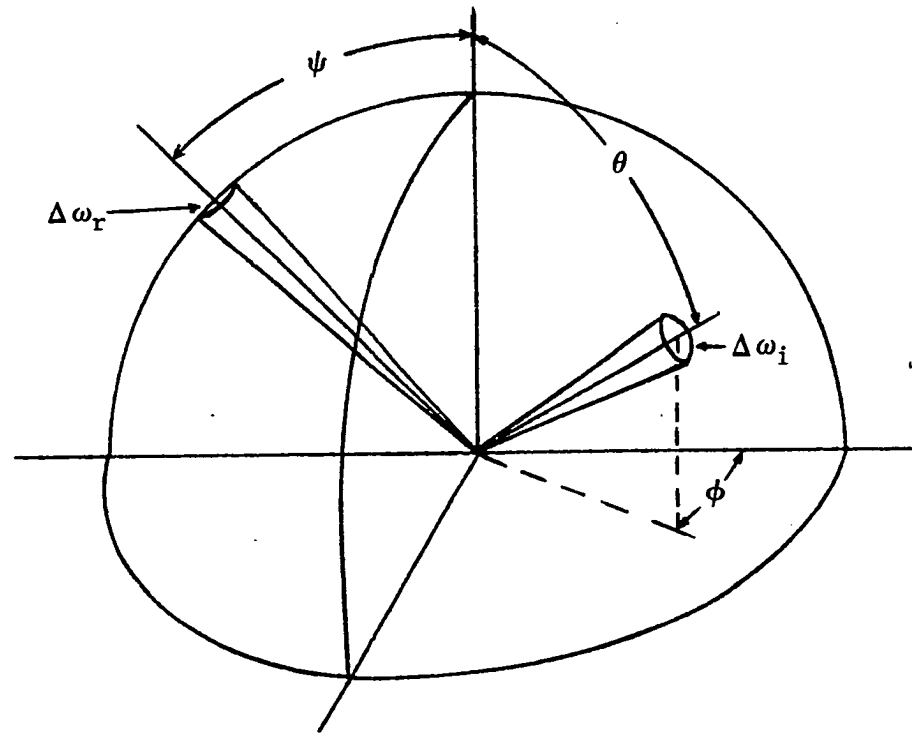
Figure 2-1. Geometry Used in Reflectance Measurements

Most of the experimental apparatus reported in the literature does not deal with the monodirectional situation. In fact the radiation is focused upon the test specimen. Thus the incident intensity is defined as

$$I_i(\psi) = \frac{\Delta F_i}{\cos \psi \, \Delta \omega_i}$$

where $\Delta \omega_i$ is the solid angle of the incident pencil of radiation. When considering the reflected radiation intensity, care must be taken to distinguish between regular and non-regular type surfaces. For the non-regular case,

$$I_r(\psi; \theta, \varphi) = \frac{\Delta F_r(\psi; \theta, \varphi)}{\cos \theta \, \Delta \omega_r} .$$

Note the flux variable and thus the intensity is much smaller than the corresponding terms would be in the regular type situation. In the case of the regular type surface

$$I_r(\psi; \psi, 0) = \frac{\Delta F_r(\psi; \psi, 0)}{\cos \psi \, \Delta \omega_r} .$$

Thus the regular reflectance is usually defined as

$$\rho_s(\psi) = \frac{I_r(\psi; \psi, 0)}{I_i(\psi)} .$$

The non-regular reflectance is referred to as biangular reflectance in the literature and thus connotes the strict dependence of this coefficient upon the angles involved. Thus the biangular reflectance is defined as

$$\rho_{ba} = \frac{I_r(\psi; \theta, \varphi)}{\Delta F_i(\psi)}$$

$$= \frac{I_r(\psi; \theta, \varphi)}{I_i(\psi) \cos \psi \, \Delta \omega_i} .$$

This definition of biangular reflectance leads to certain important

reciprocity relations discussed in references (45 - 48).

Note that under these conditions, the biangular reflectance may be related to the regular reflectance from a non-regular surface by

$$\rho_s \, (\psi) = \rho_{ba} \, (\psi; \, \psi, \, 0) \, \cos \psi \, \Delta\omega_r \; .$$

Three possibilities are apparent for the presentation of the evaluation of reflectances: 1) absolute reflectance measurements, 2) regular reflectance measurements of a specimen relative to a specular reflectance measurement from a highly polished similar specimen or a standard, and 3) biangular reflectance measurements of a specimen relative to the biangular reflectance measurement in a specified direction. Method 1) may be accomplished, but has associated with it an extremely large error. Methods 2) and 3) are popular in the literature with 3) being the usual presentation (e.g. 14).

Approach of Davies

The approach of Davies is based on the diffraction integral theorem of Helmholtz and Kirchhoff (see Appendix A) and lists as its assumptions

1. the surface is not so precipitous that some parts of the surface are shielded from the incident radiation,

2. the surface is made from a perfect conductor,

3. multiple scattering is neglected, and

4. the distribution of the heights of the surface irregularities is Gaussian.

In this work Davies considers only two limiting cases; $\bar{\sigma}/\lambda << 1$ and $\bar{\sigma}/\lambda >> 1$, where $\bar{\sigma}$ is the RMS height and λ is the wave-

length of the incident radiation. In the case of $\bar{\sigma}/\lambda << 1$, Davies obtained expressions for the regular and non-regular components (his words were coherent and incoherent components). The non-regular component is of the form

$$\pi^3 \left(\frac{a'}{\lambda}\right)^2 \left(\frac{\bar{\sigma}}{\lambda}\right)^2 \frac{(\cos\theta + \cos\psi)^4}{\cos\theta\cos\psi} \exp\left\{-\left(\frac{\pi a'}{\lambda}\right)^2 [(\sin\theta\cos\varphi - \sin\psi)^2 + \sin^2\theta\sin^2\varphi]\right\}$$

where a' is a statistical factor which aids in the description of the surface and is called the autocorrelation or autocovariance parameter. The regular component is of the form

$$\exp\left[-\left(\frac{4\pi\,\bar{\sigma}\,\cos\psi}{\lambda}\right)^2\right] .$$

The regular component expression form was determined experimentally in 1916 (49, 50). For the large optical roughness case ($\bar{\sigma}/\lambda >> 1$), Davies obtained the same expression for the regular component, but the non-regular component was of the form

$$\frac{1}{16\pi} \left(\frac{a'}{\bar{\sigma}}\right)^2 \frac{1}{\cos\theta\cos\psi} \exp\left[-\left(\frac{a'}{\bar{\sigma}}\right)^2 \frac{(\sin\theta\cos\varphi - \sin\psi)^2 + \sin^2\theta\sin^2\varphi}{2(\cos\theta + \cos\psi)^2}\right] .$$

This last expression is the final form for the non-regular component after a correction by Spetner (51).

Approach of Porteus

The approach of Porteus is similar to that of Davies and is an attempt to extend the restriction to shorter wavelengths (i.e. $\bar{\sigma}/\lambda < 1$). Porteus begins his work with the Fresnel diffraction integral (see

Appendix A) and lists essentially the same assumptions as Davies. Under

the section which Porteus states as "Normal Surfaces" he arrived at the

same expression for the regular (coherent) component but the non-regular

(incoherent) component has a different form. It is

$$\left\{ 1 - \exp\left[1 - \left(\frac{4\pi\,\bar{\sigma}\,\cos\,\psi}{\lambda}\right)^2 \right] \right\} \left\{ 1 - \exp\left[- \left(\frac{\pi\,a'\,\alpha}{\lambda}\right)^2 \right] \right\}$$

where α is the angle of acceptance of the detector. This equation is

strictly true only for normal incidence ($\psi = 0$).

Approach of Beckmann

Beckmann started his approach with the most general form of the

Helmholtz - Kirchhoff diffraction integral. Because of the more exact

approach of Beckmann, an additional assumption must be added to the list

used by the other two approaches previously discussed. The assumption is

that the field at any point of the surface may be approximated by the

field that would be present on the tangent plane at that point. That is

the field at any point of the surface is expressed as the sum of the

incident and reflected fields on that straight line. This assumption is

exactly correct for an infinite plane and will obviously be quite good

when the radius of curvature of the irregularity is large compared to the

wavelength (i.e. locally flat). But if the irregularities consist of

sharp edges and points, this theory breaks down.

The generality of the approach of Beckmann yields a general

solution that would be exact, within the limit of the assumptions, if

the surface contour was known exactly. Simple forms may be handled, but

actual surface irregularities become mathematically unwieldy. An alter-

nate approach is to use statistics in a fashion similar to the approaches

discussed previously. Thus an almost mathematically manageable solution

may be obtained by assuming a randomly rough surface. In fact for the

case of a normally distributed surface, Beckmann's approach yields the

same expression for the regular component as obtained by Davies and

Porteus. The non-regular (incoherent) component is considerably more

complicated and has the form

$$\frac{e^{-g} \, T^2 \, F^2}{4\pi \cos\theta \cos\psi} \sum_{m=1}^{\infty} \frac{g^m}{m! \, m} \, e^{-v_{xy}^2 \, T^2/4m}$$

where $\quad g = \left[2\pi \frac{\bar{\sigma}}{\lambda} (\cos\psi + \cos\theta) \right]^2$

$$F = \left[\frac{1 + \cos\psi \cos\theta - \sin\psi \sin\theta \cos\varphi}{\cos\theta + \cos\psi} \right]$$

$$T = 2\pi \frac{a'}{\lambda}$$

$$v_{xy}^2 = \sin^2\psi + \sin^2\theta - 2\sin\psi \sin\theta \cos\varphi .$$

Beckmann also presents an equation for the large optical roughness case.
The form is

$$\frac{T^2}{4\pi \, g^2} \, F^2 \exp\left[- \frac{T^2}{4g^2} \, v_{xy}^2 \right]$$

for the non-regular component with no contribution due to the regular

component (i.e. $\bar{\sigma}/\lambda >> 1$). This non-regular component is only an

approximation and it is independent of the wavelength of incident

radiation.

Comparison of the Three Approaches

A fine discussion of the models of Davies and Beckmann appears

in reference (52). In this paper the authors determine the approximate

regions for which these two models would apply by accounting for all the

reflected energy. That is, they numerically integrated the non-regular

components and added the contribution of the regular components for the

small optical roughness case. Theoretically this directional-hemispher-

ical reflectance should be unity. By their calculations this quantity is

not unity in general. The deviations are less than a few percent for

both models for $\bar{\sigma}/\lambda \leq 0.04$, $1 \leq a'/\lambda \leq 100$, and $0° \leq \psi \leq 80°$. For larger

values of $\bar{\sigma}/\lambda$, the Davies equations are very much in error while the

Beckmann values are still acceptable. But for values of $\bar{\sigma}/\lambda \geq 0.1$, both

models are markedly in error with the Davies model by far the worst. The

large optical roughness case of Beckmann was subjected to the same inves-

tigation and found to be greatly in error for values of $a'/\sigma < 10$.

Comprehensive non-regular reflectance measurements were carried

out by Birkebak (53). In his work, he used metal samples as specimens

and discussed the observed trends of the data as compared to the Davies

model. Houchens and Hering (52) analyzed Birkebak's data with the model

of Beckmann and determined the parameters $\bar{\sigma}$ and a'. The results of their

investigation indicated that except for values of very small optical

roughness-wavelength ratioes ($\bar{\sigma}/\lambda \leq 0.16$), a' decreased with increasing

values of this ratio. These investigators believe a' should remain

constant regardless of the wavelength of the incident radiation.

Therefore, it appears that the model of Davies is essentially

restricted to surface irregularities with very small slopes in both cases

discussed. The Beckmann model, though not true in general, is better

than that of Davies; that is, the unit directional-hemispherical reflec-

tance criterion is satisfied over a wider range of variables.

Surface Characteristics

As have been discussed in the previous sections, the experimental approaches to determining the interrelations of the various variables involved for accurate prediction of reflected energy distributions are not satisfactory. At most, one can only fit the data from experiments conducted on a test specimen. A change in any of the variables might and usually does require another analysis to fit the data. The approaches using diffraction theory seem to be a step in the right direction. That is, if these theories were correct, only knowledge of the surface parameters would be necessary to predict the far field disturbance. The drawbacks to these theories are one or more of the following assumptions incorporated into the theories:

1. The dimension of the irregularities are taken either to be much smaller than or much greater than the wavelength of the incident radiation;

2. The radius of curvature of the irregularities is taken to be much greater than the wavelength of the incident radiation;

3. Shadowing effects are neglected;

4. Only either the near or the far field situation is considered;

5. Multiple, inter-surface reflections are neglected;

6. The density of irregularities are not considered;

7. The theory is restricted to a particular profile or surface contour;

8. Perfect conductivity is assumed.

Thus as the degree of rigor of the theory increases, its generality is lost. The result is a set of equations which indicate the trends to be expected, but not a quantitative representation.

The near mathematical impossibility of describing a generally encountered irregular surface requires a statistical approach. When using this statistical approach, one must keep in mind not only that this is an averaging process, but in addition to knowing this mean value, the probability distribution about the mean must be specified. Thus the irregular surfaces met in real life would seem best described by at least two parameters which are indicative of the deviation of characteristic surface dimensions from their mean values. The primary dimension usually considered as a surface characteristic is the RMS surface roughness (height of irregularities). Obviously this dimension will not uniquely describe a rough surface for it tells us nothing about the distances between the hills and valleys of the surface. Thus a peak density or asperity function would seem important. In the literature, the second dimension, if discussed, is the autocorrelation or autocovariance length. This length has been shown to be related to the RMS surface roughness and the RMS slope of the surface (54). It is believed by this investigator that great care must be taken to adequately interpret this dimension. In the literature the surface roughness is usually stated by an RMS surface roughness-wavelength ratio. This cannot be an unique description, but the aforementioned theories are based upon this type of partial restriction. Therefore the results may be misleading.

The definition of these two parameters and their associated distributions, plus knowledge of the electrical properties of the material for the wavelength considered and the conditions of irradiation and observation, would hopefully be all that is necessary in order to determine reflected energy distributions in a general fashion.

From the data available and considering the theories presented in their regions of application, a rule may be stated for which any proposed model for the solution of this problem should adhere. The trends of variations of the reflected distribution as the parameter is varied would seem to go according to the following statement:

> The regularly reflected energy depends upon the angle
> of incidence and a roughness-wavelength ratio $(\bar{\sigma}/\lambda)$.
> Similarly, the non-regularly reflected energy would
> depend on these parameters. Thus the parameter $\bar{\sigma}/\lambda$
> determines the apportionment of the energy between these
> two modes of reflection. That is, for very small values
> of $\bar{\sigma}/\lambda$, the majority of the reflected energy is of the
> regular type. As $\bar{\sigma}/\lambda$ increases, the distribution be-
> comes increasingly non-regular. This statement has
> been fairly well justified by experiment.

A similar statement concerning the other discussed surface defining parameter has not been sufficiently investigated by experiment and the theories presently available do not emphasize its importance. An analytical treatment of the region $\bar{\sigma} \sim \lambda \sim a'$ has not as yet been published. Thus the apparently very complicated interrelation of the parameters $\bar{\sigma}$, a' and λ in this region is completely unknown.

CHAPTER III

DISCUSSION OF STATISTICS

There are a large number of fine texts (55, 56) and short write-
ups (57) which discuss the various rules of probability analysis.   Thus
most of these basics will be assumed. The purpose of this section is to
state the terminology used in the following work so there will be no mis-
understanding.

"Random Variable" is a real number value determined by the out-
come of a random experiment. It may be discrete or continuous.

"Random Experiment", when conducted under a given set of circum-
stances, results in different outcomes which may be characterized by a
number from 0 to 1 and represents the relative frequency that that event
may occur in a large number of trials.

"Random Event" is one result of a large number of random experi-
ments. The "probability" of a random event is the limiting value of the
frequency of occurence.

The "cumulative distribution function" or just distribution
function, F, gives the probability of obtaining a random variable equal
to or less than some specified value X_i. Clearly

$$0 \leq F(X_i) \leq 1 \quad \text{for all } X_i.$$

The "probability density function" or just density function (f)
is related to the distribution function by the rule

18

$$f(x) = \frac{dF(x)}{dx} .$$

Thus $f(x)$ dx is the probability that the random variable is obtained. Therefore

$$F(x) = \int_{-\infty}^{x} f(x)dx .$$

A Monte Carlo simulation is used in this research to investigate the reflectance problem heretofore discussed. This approach is also referred to as synthetic sampling or empirical sampling and has resulted in successful analyses of other physical phenomena (57 - 62). In applying this simulation, a large number of imaginary random experiments are conducted. In each experiment an energy bundle is followed as it is forced to obey predetermined rules. As noted previously, a very large number of experiments must be conducted for the results to be stable. That is, because Monte Carlo simulations involve random numbers, the results are subject to statistical fluctuations. Thus the results are subject to an associated error. The larger the number of trials, the smaller the error.

Determination of the number of trials that will result in an acceptable error band may present some difficulty. The approach used in this research will be using a Bernoulli trials analysis. That is for repeated independent trials, there are only two possible outcomes for each trial and the probability of success (p) and failure (1 - p) (collected in a particular region or not) is constant. Thus the maximum allowable error in estimating p, ϵ, must be specified as well as C the desired probability or confidence level that the estimate value of p, $\bar{p}$, does not differ from p by more than $\pm$ ϵ, where $\bar{p}$ is the result

of a large number of trials and p is the exact value. So

$$| \bar{p} - p | \leq \epsilon$$

as n, the number of trials, becomes large. Thus the following relation based on the normal approximation to the binomial distribution is the probability that the above inequality is true:

$$C = erf(t \; / \; \sqrt{2})$$

where $\quad t = \epsilon \sqrt{\dfrac{n}{p(1 - p)}} \quad .$

Note $\epsilon = p \; B$ where B is the error. This approximation is adequate in general as long as n p or n(1 - p) is greater than 5.

It must be noted that the true probability, p, is not known. It is assumed that a good estimate of p is the ratio of the number of hits in a particular region to the number of trials.

Intimately related to the Monte Carlo simulation is random number generation. Scofield (57) discusses the uniform random number generator subroutine recommended by IBM. In this discussion, he indicates that this subroutine exhibits the appropriate uniform randomness for rather finite sample sizes. This same subroutine was used in this research when a uniformly distributed random number was required.

In addition to uniform random numbers, another form of random number was needed in this research for the distributions of the surface roughness and the density or asperity. As discussed previously, the usual assumption is that these quantities are distributed according to a Gaussian distribution. For the model used in this research (to be discussed in the next chapter), this assumption was not feasible. Instead a distribution derived from the normal distribution was used.

This distribution, usually referred to as Rayleigh distribution, has not been used in reflectance analyses reported in the literature. One statement could be found and that by Beckmann (41). He casts doubt on the possibility that such a distribution exists for real surfaces, but goes on to say that non-symmetrical distributions probably do exist in nature. In Appendix B this distribution is discussed. Also included in this appendix is a discussion of the random number generator used for the production of the height (peak to valley dimension) and density (peak to peak dimension) numbers used in the model of this research.

CHAPTER IV

ANALYTICAL MODEL

This chapter is a general discussion of the model investigated in
this research. The discussion will begin with the presentation of partic-
ular points of the analytical model composition, thus illustrating the
assumptions made. This chapter will conclude with illustrations of the
effect of variations of the important parameters involved.

Surface Construction

Surfaces which yield what has generally been described as non-
regular reflection, are "rough" in nature. The exact character of this
"roughness" cannot be stated in a general form due to the differences in
the physical properties of different materials (ductility, malleability,
conductivity, etc.) and even the same materials after exposure to different
external conditions. This investigation attempts to agree with other
investigators (30, 31) by assuming the general character of the roughness
is that of a V-groove. In addition, it is assumed that the tops of these
grooves are rounded. Both the rounded and V-groove portions reflect in a
mirror-like fashion.

The approach of this investigation is to use a Monte Carlo method.
This approach automatically implies long run times of a digital computer.
Accordingly, this investigation considers only the action of energy bun-

les in the plane of incidence. To do this, the assumption is that the plane of incidence is the most interesting since this plane exhibits all the possible peculiarities of reflection encountered experimentally. As a co-assumption, it is asserted that the vast majority of the energy received in the plane of incidence is the result of inter-reflection within the rounded V-groove whose sides are generally perpendicular to the plane of incidence.

Experimentally, the surface parameters usually used to describe a surface are an RMS peak to valley dimension $(\bar{\sigma})$ and an autocovariance function, a'. Because of the aforementioned lack of experimentally verified information concerning a', this investigator prefers instead to consider a parameter indicative of the peak density. This parameter will be an RMS peak to peak dimension $\bar{a}$. Whether this dimension is even related to the autocovariance length will not be considered.

To make this model essentially similar to reality, the surface heights σ will be distributed in a Rayleigh distribution with $\bar{\sigma}$ as the defining parameter. The peak to peak dimension, a, will also be distributed according to a Rayleigh distribution, but with $\bar{a}$ as the defining parameter. The apex of this V-groove (X_o) is assumed to be selected in a uniform random fashion (see Figure 4-1). For each individual energy bundle σ, a, and X_o will be selected from the appropriate random distribution, thus defining the surface. The energy bundle is followed in this geometry up to four reflections unless it escapes this geometry to the hemisphere above, is refracted at a surface or is trapped by reflecting four times.

The surface is constructed in the following fashion. Figure 4-1
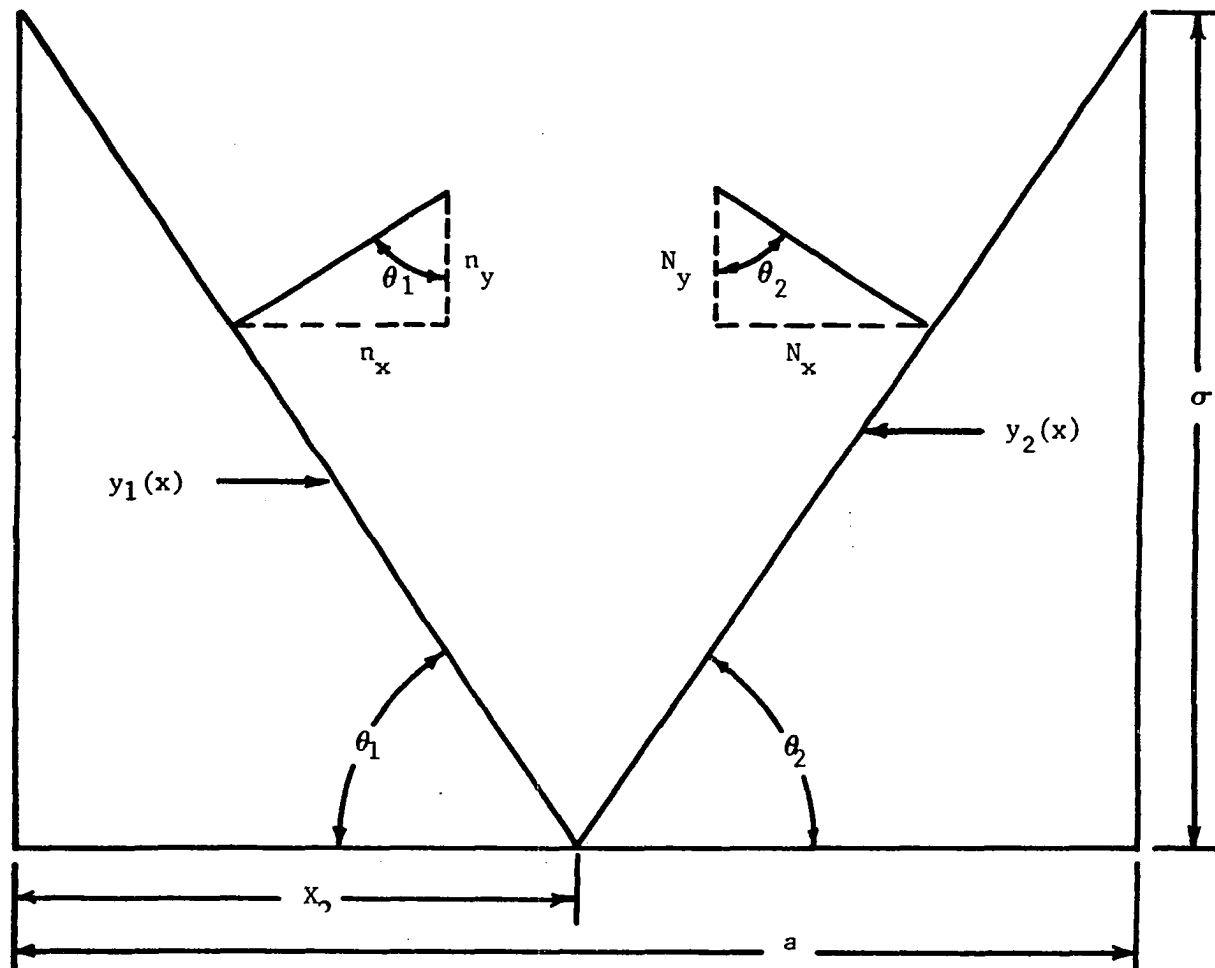
Figure 4-1. Basic V-groove Geometry

represents the geometry from which the energy bundle is either reflected or refracted. The equations for the sides of the V-groove are

$$y_1 = - \left(\frac{\sigma}{X_o}\right) x + \sigma \qquad \text{and}$$

$$y_2 = \left(\frac{x - a}{a - X_o}\right) \sigma + \sigma \; . \qquad (4\text{-}1)$$

Thus the components of the normals of these surfaces are

$$n_y = \cos \theta_1$$

$$n_x = \sin \theta_1$$

$$N_y = \cos \theta_2$$

$$N_x = \sin \theta_2 \qquad (4\text{-}2)$$

where $\quad \theta_1 = \tan^{-1} \dfrac{\sigma}{X_o}$

$$\theta_2 = \tan^{-1} \frac{\sigma}{a - X_o} \; .$$

The assumed circular cap on the upper left point of the V-groove has the equation

$$y_3 = H_1 + \sqrt{b_1^2 - x^2} \; .$$

Note from Figure 4-2, $y_3(x)$ is the equation for the surface up to $x = \bar{x}_1$ and $y = \bar{y}_1$. At this point the equation makes a smooth transition to the straight line $y_1(\bar{x}_1)$.

At the point $(\bar{x}_1, \bar{y}_1,)$

$$\frac{dy_3(\bar{x}_1)}{dx} = \frac{dy_1(\bar{x}_1)}{dx} = -m_1 = \frac{\bar{x}_1}{\bar{y}_1 - H_1} \; , \; m_1 = \tan \theta$$

or $\quad \bar{x}_1 = m_1(\bar{y}_1 - H_1) = m_1(-m_1\bar{x}_1 + \sigma - H_1)$
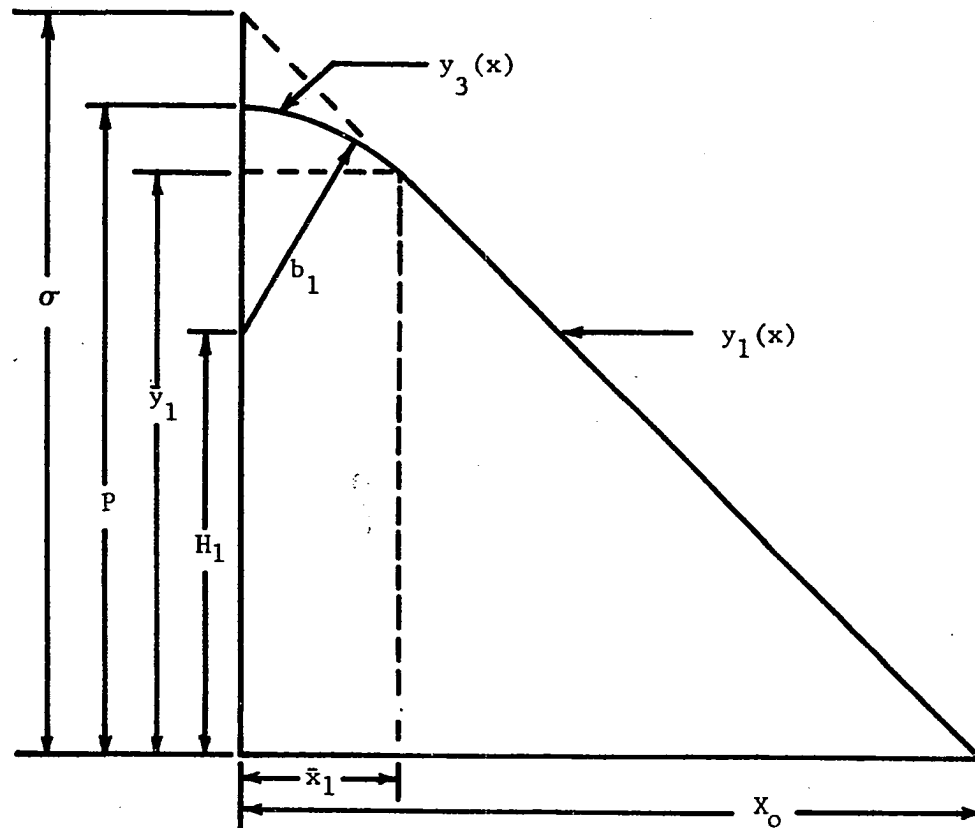
Figure 4-2. Geometry of Left Side of the Rounded V-groove

$$\bar{x}_1 = \frac{m_1(\sigma - H_1)}{1 + m_1^2} \quad . \tag{4-3}$$

Requiring that $y_1(\bar{x}_1) = y_3(\bar{x}_1)$ results in

$$\bar{x}_1 = \frac{m_1(\sigma - H_1)}{1 + m_1^2} + \frac{\left[b_1^2(1 + m_1^2) - (\sigma - H_1)^2\right]^{\frac{1}{2}}}{1 + m_1^2} \quad . \tag{4-4}$$

Note that equation (4-3) must equal equation (4-4).

Thus $\quad b_1 \sqrt{1 + m_1^2} = (\sigma - H_1) \quad .$

So $\quad \bar{x}_1 = \dfrac{m_1 b_1}{\sqrt{1 + m_1^2}}$

$$\bar{y}_1 = H_1 + \frac{b_1}{\sqrt{1 + m_1^2}} \quad .$$

Further requiring that $H_1 + b_1 = P < \sigma$ yields

$$b_1 = \frac{\sigma - P}{\sqrt{1 + m_1^2} - 1} \text{ and } H_1 = \frac{P\sqrt{1 + m_1^2} - \sigma}{\sqrt{1 + m_1^2} - 1} \quad . \tag{4-5}$$

The components of the normal to $y_3(x)$ are

$$n_x = x/b_1$$

$$n_y = \sqrt{1 - (x/b_1)^2} \quad , \quad x \le \bar{x} \quad . \tag{4-6}$$

The assumed circular cap on the upper right point of the V-groove (Figure 4-3) has the equation

$$y_4(x) = H_2 + \sqrt{b_2^2 - (x - a)^2} \quad .$$

$y_4(x)$ is the equation for the surface from $x = \bar{x}_2$ and $y = \bar{y}_2$ to $x = a$ and $y = P$. The smooth transition from the straigh line $y_2(x)$ to $y_4(x)$ is at the point $(\bar{x}_2, \bar{y}_2)$. At this point $\dfrac{dy_4(\bar{x}_2)}{dx} = m_2$ yielding
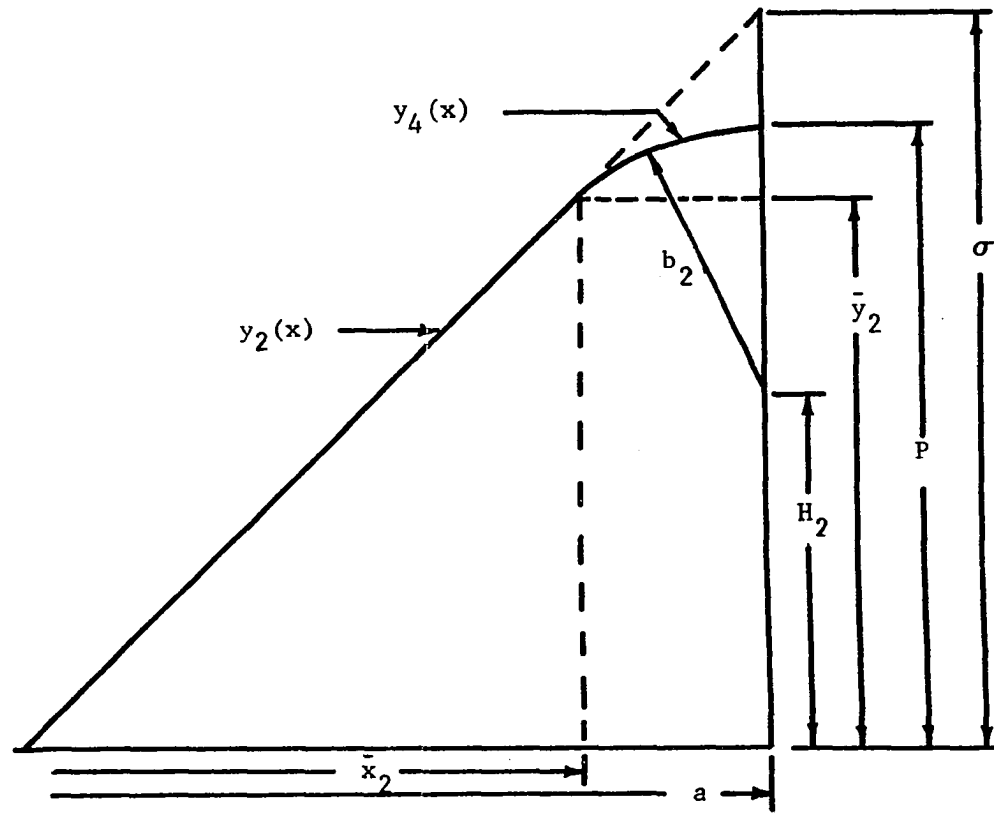
Figure 4-3. Geometry of Right Side of the Rounded V-groove

$$\bar{x}_2 = a - \frac{m_2(\sigma - H_2)}{1 + m_2{}^2} \quad , \quad m_2 = \tan\theta_2 \quad . \tag{4-7}$$

Setting $y_2(\bar{x}_2) = y_4(\bar{x}_2)$ results in

$$\bar{x}_2 - a = \frac{-m_2(\sigma - H_2)}{1 + m_2{}^2} + \frac{\sqrt{m_2{}^2(\sigma - H_2)^2 - (1 + m_2{}^2)[(\sigma - H_2)^2 - b_2{}^2]}}{1 + m_2{}^2} \quad . \tag{4-8}$$

Notice equation (4-7) equals equation (4-8) or

$$b_2\sqrt{1 + m_2{}^2} = \sigma - H_2 \quad .$$

So $\quad \bar{x}_2 = a - \dfrac{m_2 b_2}{\sqrt{1 + m_2{}^2}} \quad$ and $\quad \bar{y}_2 = H_2 + \dfrac{b_2}{\sqrt{1 + m_2{}^2}} \quad .$

Again requiring the $H_2 + b_2 = P < \sigma$ yields

$$b_2 = \frac{\sigma - P}{\sqrt{1 + m_2{}^2} - 1}$$

$$H_2 = \frac{P\sqrt{1 + m_2{}^2} - \sigma}{\sqrt{1 + m_2{}^2} - 1} \quad . \tag{4-9}$$

The components of the normal to $y_4(x)$ are

$$N_x = -(a - x) / b_2$$

$$N_y = \sqrt{1 - \frac{(a - x)^2}{b_2{}^2}} \quad . \tag{4-10}$$

It may be noted that the surface shape is very much dependent on the roundness parameter P. At P = 1, the surface is triangular. As P decreases, the radius of the round portion, required for continuity, increases until for a particular value of P, given σ and a, the transition point is superimposed on X_o. The value of P which produces this geometri-

cal configuration for the particular case of $X_o = a$ is defined as P(LIM)
(see Figure 4-4). From geometrical consideration, the following expression
relating P(LIM), σ, and a may be derived. The result is

$$P(LIM) = \frac{a}{\sigma} \left[\sqrt{1 + \left(\frac{a}{\sigma}\right)^2} - \frac{a}{\sigma} \right] \quad .$$

(4-11)

Figure 4-5 illustrates the variation of P(LIM) versus σ/a. Notice P(LIM)
is never greater than 0.5 and decreases monotonically to zero as σ/a
approaches infinite. Thus for given values of σ and a various cases must
be considered. Figure 4-6 illustrates three of the six possible cases
when $P < P(LIM)$ which are included in this analysis. The other three
cases are related similarly but on the left side of X_o.

The relations discussed in this section are embodied in sub-
routines SURF1 and SURF2 (appendix C).

Penetration

Quantum mechanics indicates that the localization of a radiation
quantum or energy bundle to a region less than the wavelength of the
radiation quantum before a collision or interaction is impossible (63).
In an attempt to analytically reproduce experimental results of other
investigators and utilize the aforementioned statement, a quantum mechani-
cal wavepacket, in which the energy bundle is positioned, is assumed to be
approximated by a sphere, or a circle in the two-dimensional model used in
this research. This "billiard-ball" model is used to indicate an initial
maximum depth of penetration of the radiation quantum into the rounded V-
groove by means of a geometric calculation. That is, the point of first
incidence cannot be deeper than this maximum depth. This calculation
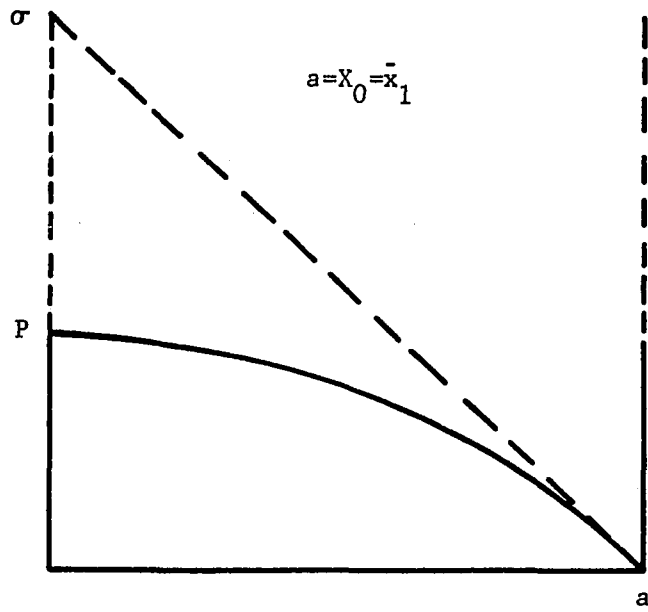
Figure 4-4. Geometry Used in the Definition of P(Lim)
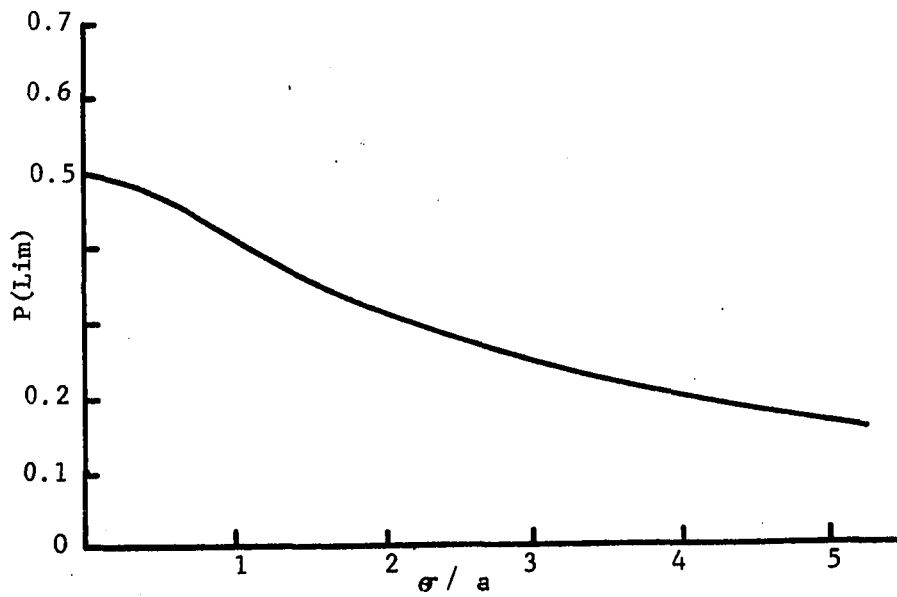
Figure 4-5. Relation of P(Lim) and σ/a
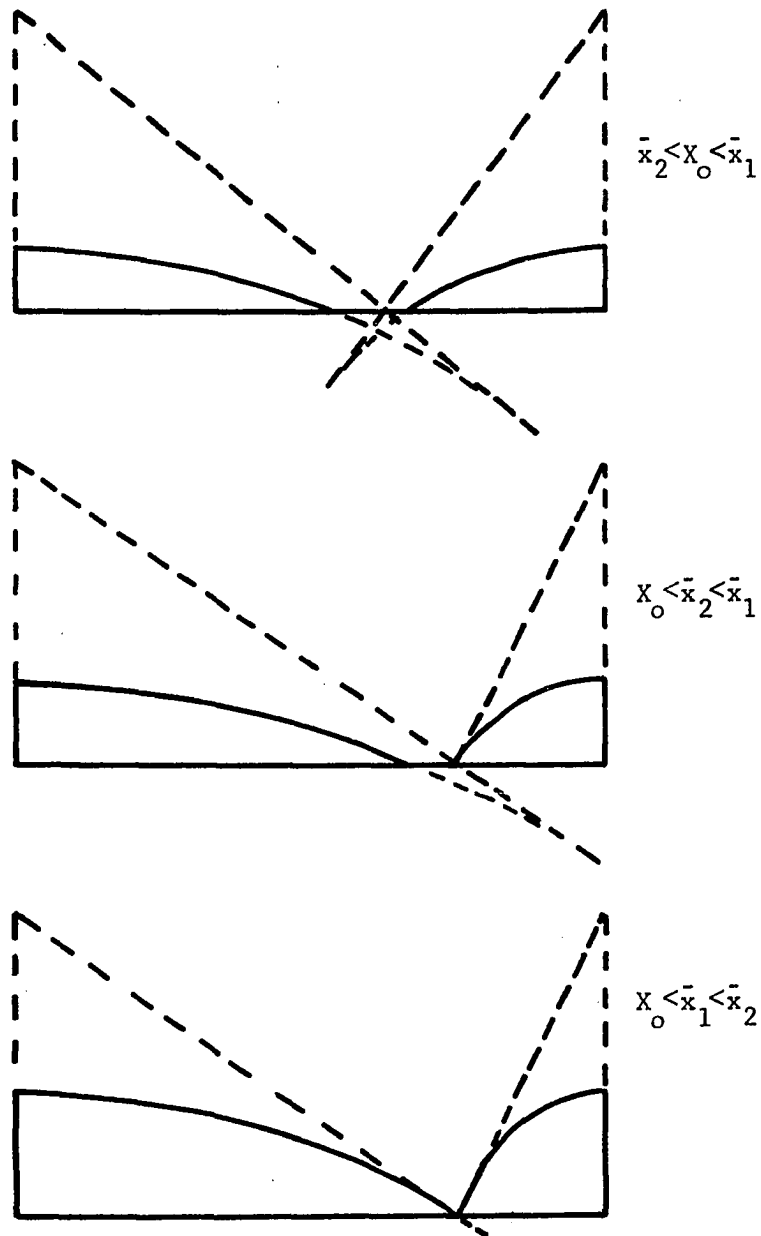
Figure 4-6. Illustration of Various Unusual Geometries
Encountered When $P < P(Lim)$

assumes a "localization circle" of radius λ and depends on the ratioes σ/a and σ/λ.

Since this is an approximation, the rounded V-groove is approximated by a symmetric V-groove of height σ and width a. The apex of the V-groove is the origin for this calculation with the X axis along a, while σ is in the Y direction. There are five regions or interrelations of σ, λ, and a. Case I: $\psi \leq \frac{\pi}{2} - \theta_1$, $\lambda \leq \lambda_{max}$ (see Figure 4-7)

The equation for the "localization circle" is

$$x^2 + (y - \bar{b})^2 = \lambda^2 \ .$$

Note that $\bar{b} = \lambda \sec \theta = \frac{2\lambda}{a}\sqrt{\sigma^2 + \left(\frac{a}{2}\right)^2}$

$$h = \bar{b} - \lambda = \lambda\left[\sqrt{1 + 4\left(\frac{\sigma}{a}\right)^2} - 1\right] \ . \tag{4-12}$$

To determine the region of validity of this equation, i.e. determination of λ_{max}, the circle is positioned at the top of the V-groove so that the radius is perpendicular to the sides of the V-groove at the points $\left(\frac{a}{2}, \sigma\right)$ and $\left(-\frac{a}{2}, \sigma\right)$. So

$$\lambda_{max}^2 = \frac{a^2}{4} + (\sigma - \bar{b})^2.$$

Using the above expression for $\bar{b}$

$$\frac{\lambda_{max}}{\sigma} = \frac{1}{4}\left(\frac{a}{\sigma}\right)^2 \sqrt{1 + 4\left(\frac{\sigma}{a}\right)^2} \ . \tag{4-13}$$

Case II: $\psi \leq \frac{\pi}{2} - \theta_1$, $\lambda \geq \lambda_{max}$ (see Figure 4-8)

Again the equation for the "localization circle" is

$$x^2 + (y - \bar{b})^2 = \lambda^2 \ .$$

Note that from the cosine law
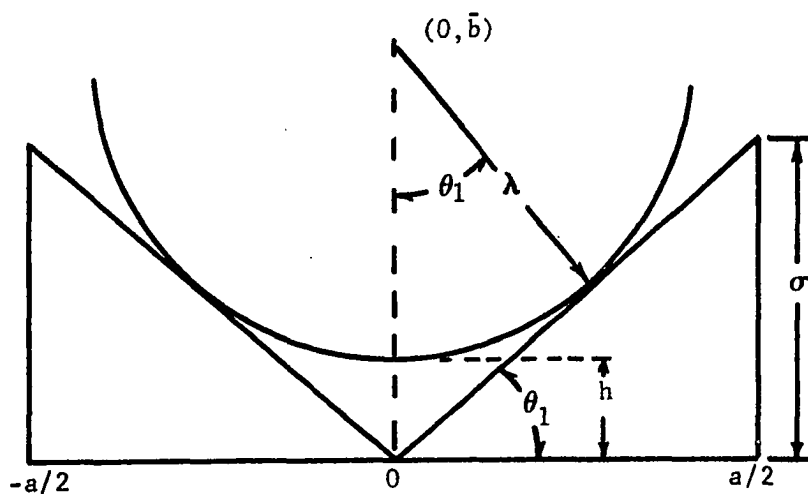
Figure 4-7. Geometry Used in Defining the Penetration Depth for $\psi \leq \frac{\pi}{2} - \theta_1$ and $\lambda \leq \lambda_{max}$
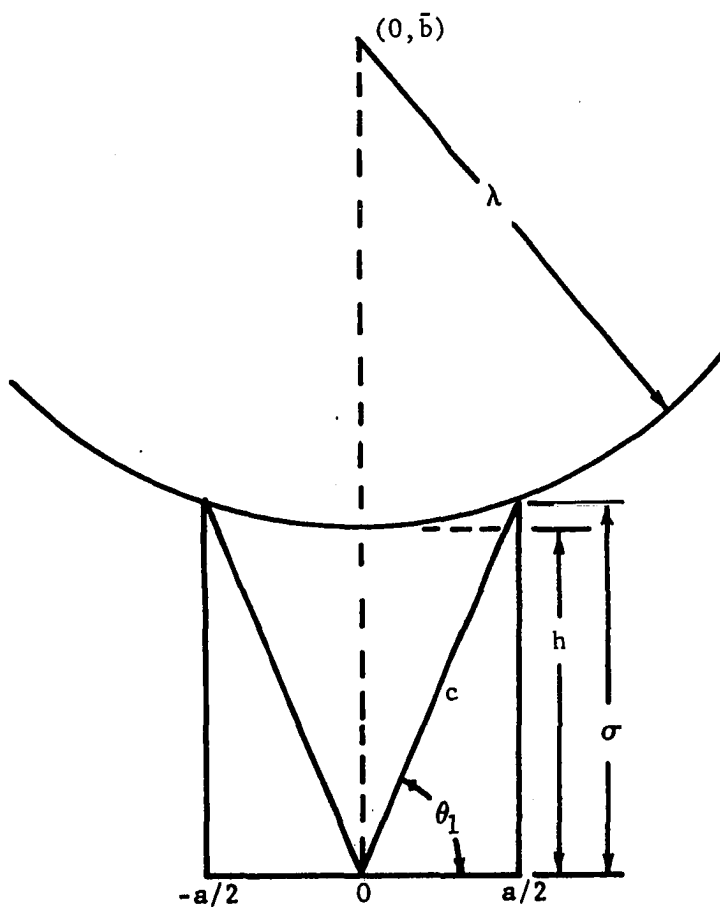
Figure 4-8. Geometry Used in Defining the Penetration Depth for $\psi \leq \frac{\pi}{2} - \theta_1$ and $\lambda \geq \lambda_{max}$

$$\lambda^2 = \bar{b}^2 + c^2 - 2bc \cos\left(\frac{\pi}{2} - \theta_1\right)$$

$$= \bar{b}^2 + c^2 - 2bc \sin\theta_1$$

or $\quad \bar{b}^2 - (2c \sin\theta_1)\,\bar{b} + (c^2 - \lambda^2) = 0$.

Thus $\quad \bar{b} = c \sin\theta_1 \overset{+}{-} \sqrt{c^2 \sin^2\theta_1 - (c^2 - \lambda^2)}$.

But $\quad \sin\theta_1 = \sigma/c$ and $\cos\theta = a/2c$.

So $\quad \bar{b} = \sigma + \sqrt{\lambda^2 - \left(\frac{a}{2}\right)^2}$ and

$\quad\quad h = \bar{b} - \lambda$

or $\quad \dfrac{h}{\sigma} = 1 - \dfrac{\lambda}{\sigma} + \sqrt{\left(\dfrac{\lambda}{\sigma}\right) - \left(\dfrac{a}{2\sigma}\right)^2}$ where $\lambda > \lambda_{max}$. $\hspace{2em}$ (4-14)

Case III: $\psi \geq \dfrac{\pi}{2} - \theta_1$, $\lambda < \lambda_{max}$ (see Figure 4-9)

This situation is somewhat more complicated than either cases I or II. λ_{max} is not as defined as case I, and notice that the center of the "localization circle" is at $(\bar{c}, \bar{b})$ due to the non-symmetry resulting from the geometric shadowing. The shadow boundary on the right side of the V-groove is at the point

$$X'_o = \frac{a}{2}\left(\frac{\tan\theta_1 - \cot\psi}{\tan\theta_1 + \cot\psi}\right)$$

$$y_o = \sigma\left(\frac{\tan\theta_1 - \cot\psi}{\tan\theta_1 + \cot\psi}\right) = h_{min} \; .$$

Thus $\quad \bar{b} = \dfrac{2\sigma\bar{c}}{a} + \lambda\sec\theta,$

$$= \lambda\sec\theta_1 + \frac{2\sigma\bar{x}_o}{a} - \frac{2\sigma\bar{b}}{a}\tan\beta$$

since $\quad \bar{c} = \bar{x}_o - \bar{b}\tan\beta$

where $\quad \bar{x}_o = \left(\tan\beta + \dfrac{a}{2\sigma}\cot\beta\right)h_{min}$

Figure 4-9. Geometry Used in Defining the Penetration Depth for
$\psi \geq \frac{\pi}{2} - \theta_1$ and $\lambda \leq \lambda_{max}$

Figure 4-10. Geometry Used in Defining the Penetration
Depth for $\psi \geq \frac{\pi}{2} - \theta_1$ and $\lambda_{max2} > \lambda > \lambda_{max}$

Thus $\quad \bar{b} = \dfrac{\lambda \sec \theta_1 + \dfrac{2\sigma}{a} \bar{x}_o}{1 + \dfrac{2\sigma}{a} \tan \beta}$.

Recall $\quad h = \bar{b} - \lambda$

$$= \dfrac{\lambda \sec \theta_1 + (1 + \dfrac{2\sigma}{a} \tan \beta)\, h_{min}}{1 + \dfrac{2\sigma}{a} \tan \beta} \qquad (4\text{-}15)$$

where $\quad \beta = \dfrac{1}{2}\left[\psi - \left(\dfrac{\pi}{2} - \theta_1\right)\right]$.

To obtain an expression for λ_{max} in this situation, the procedure is the same as in Case I ($x = a/2$, $y = \sigma$ and λ is perpendicular to the side of the V-groove at that point). After algebraic manipulation,

$$\left(\dfrac{\lambda}{\sigma}\right)_{max} = -\dfrac{G}{2F\sigma} + \dfrac{\sqrt{G^2 + 4FH}}{2F\sigma} \qquad (4\text{-}16)$$

where $\quad H = D - BE^2 + B^2 \sec^2 \beta$

$\quad G = AE - 2AB \sec^2 \beta$

$\quad F = 1 - A^2 \sec^2 \beta$

$\quad E = 2\sigma + \tan \beta\, (2\bar{x}_o - a)$

$\quad D = \left(\bar{x}_o - \dfrac{a}{2}\right)^2 + \sigma^2$

$\quad C = \bar{x}_o - b \tan \beta$

$\quad B = h_{min}$

$\quad A = \dfrac{\sec \theta_1}{1 + \dfrac{2\sigma}{a} \tan \beta}$.

Case IV: $\psi > \dfrac{\pi}{2} - \theta_1$, $\lambda_{max\,2} > \lambda > \lambda_{max}$ (see Figure 4-10)

λ_{max} is as defined as in case III. Again

$$(x - \bar{c})^2 + (y - \bar{b})^2 = \lambda^2 \ .$$

This is the most complicated arrangement in that the "localization circle" is pinned at $x = a/2$, $y = \sigma$ and is tangent to the shadow line at (x', y'). After a great deal of algebra,

$$\bar{b} = \lambda \sin \psi + \sigma - a \cos \psi \sin \psi$$

$$+ \cos \psi \ \sqrt{a^2 \cos \psi (2\lambda/a - \cos \psi)}$$

and $h = \bar{b} - \lambda$.   (4-17)

The imposed restriction on the upper limit of this case is $x' = -a/2$, $y' = \sigma$. This is used to define $\lambda_{max\ 2}$. Notice that for this condition, $\bar{c} \equiv 0$ and the "localization circle" is perpendicular to the shadow line at $(-a/2, \sigma)$ and pinned at $x = a/2$, $y = \sigma$. The geometry yields

$$\lambda_{max\ 2} = \frac{a}{2} \sec \psi .$$ (4-18)

Case V: $\psi > \frac{\pi}{2} - \theta_1$ and $\lambda > \lambda_{max\ 2}$

$\lambda_{max\ 2}$ is as defined in case IV. For this situation, case II is used if ψ is less than ψ_{crit} where

$$\tan \psi_{crit} = \frac{(h + \lambda - \sigma)}{a/2} .$$

If ψ is greater than ψ_{crit}, case III is used.

The interpretation of this depth of penetration is the following: The intersection of this height with the sides of the V-groove for the $\psi \le \frac{\pi}{2} - \theta_1$ case and the right side of the V-groove in the $\psi > \frac{\pi}{2} - \theta_1$ case defines a forbidden zone, in which the energy bundle cannot strike the V-groove for <u>first</u> incidence, as illustrated in Figure 4-11. The basis for the assumption of the "localization circle" is the experimental evidence of many investigators that if the relationship of λ and σ are such that
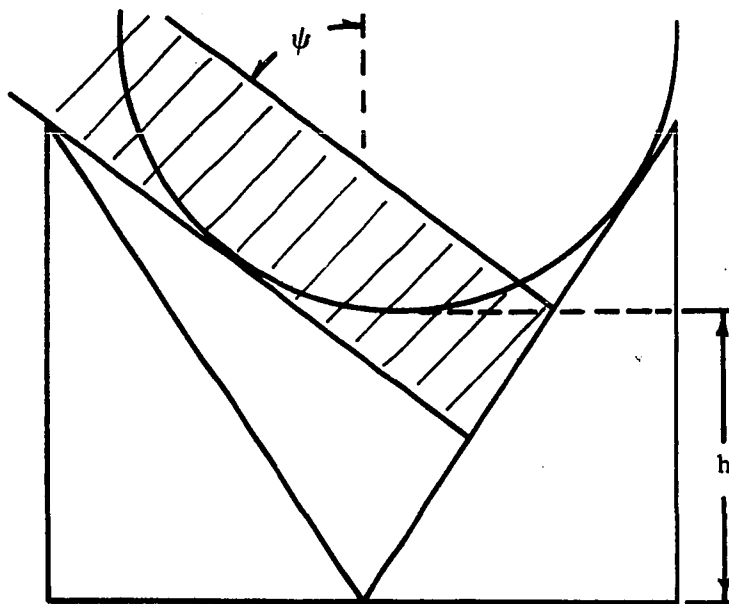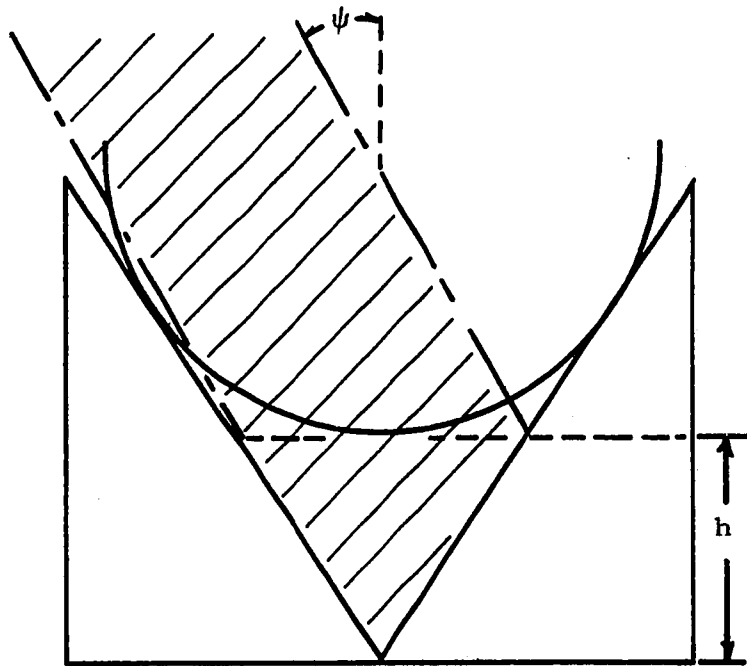
/// Represents The Forbidden Zone

Figure 4-11. Illustration of Forbidden Regions

essentially non-regular reflection is obtained, increasing the wavelength will eventually result in a large regular reflection component (i.e. σ/λ approaches zero implies a large regular component and σ/λ large implies essentially no regular component). Thus for this model, as λ increases, the first incidence point of the energy bundle is closer to the top of the V-groove. The tops of the V-groove are rounded, being exactly flat at $(\overset{+}{\underset{-}{}} a/2, \sigma)$. So the model follows the experimental evidence in a gross fashion. The equations discussed in this section are used in subroutine PENET (appendix C).

First Incidence Probability

The decision must be made as to which side of the rounded V-groove the energy bundle strikes first. This decision must depend on σ, a, λ and the penetration depth.

The hypothesis of a penetration depth introduced the idea of a forbidden zone in which the energy bundle could not strike the surface for first incidence. It would seem to follow that the probability to determine the side of the first incidence would depend on the relative area available for incidence or in this two-dimensional model - line available.

In addition, there is an assumed smoothness factor, which depends in some complicated fashion upon the incidence angle and the average deviation of the roughness peaks from the mean roughness σ. Figure 4-12 illustrates the situation. For an angle of incidence, ψ_1, the second peak is completely masked from the source. For an angle of incidence, ψ_2, the second peak sees the source. Note as ψ approaches zero, the effect of $\bar{\varepsilon}$ should decrease. In the ψ_1 case, the energy bundle may only strike the
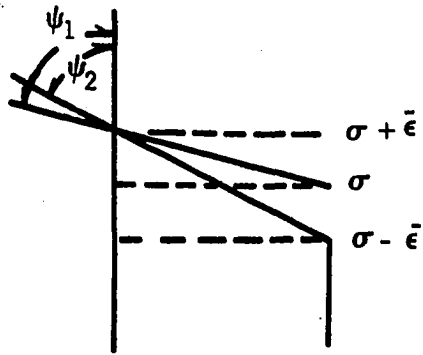
Figure 4-12.   Illustration of Shadowing
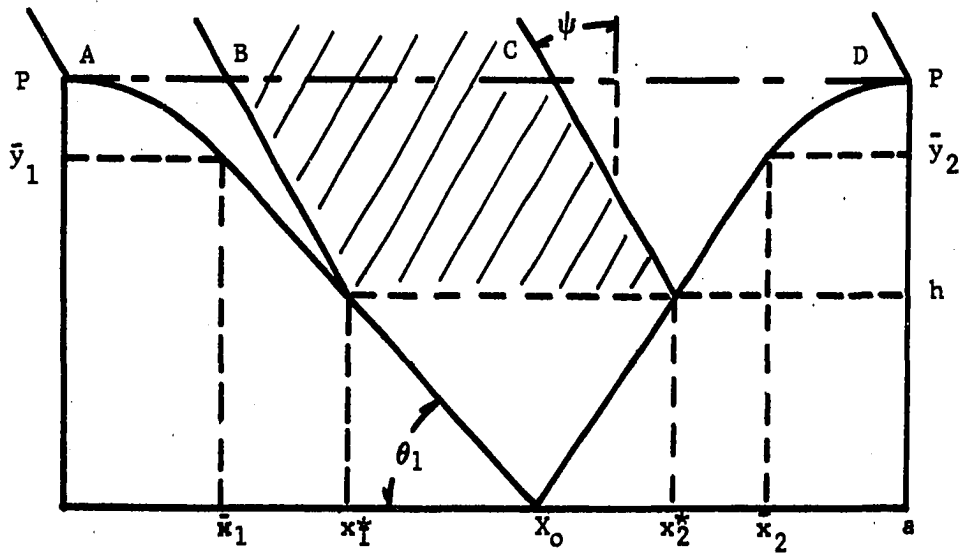
Figure 4-13.   Geometry Used for Definition of the Side of
First Incidence Probability for $\psi \leq \frac{\pi}{2} - \theta_1$

first peak. In the ψ_2 case interreflections are allowed. Not knowing

the form of this function, a postulated function was used: Its form is

$$\bar{F} = \exp(\bar{A} \tan^2 \psi)$$

where $\bar{A}$ is an unknown function of σ, a, λ, and $\bar{\epsilon}$. Note $\bar{F}$ goes to 1 as

$\bar{A}$ approaches zero or ψ approaches 0°, and as $\bar{A}$ approaches infinity or ψ

approaches 90°, $\bar{F}$ becomes very large.

Let us consider the situation when $\bar{F} = 1$ such that $\bar{A} = 0$. There

are two cases.

Case I: $\psi \leq \frac{\pi}{2} - \theta_1$ (see Figure 4-13)

Notice the forbidden region of first incidence and the penetration

depth h defines the corresponding intersection with the sides of the

rounded V-groove   (x_1^* and x_2^*). Thus any energy bundle which would strike

the left side of the V-groove, must do so between 0 and x_1^*, having first

crossed the line $\overline{AB}$. Similarly any energy bundle which would strike the

right side of the V-groove would have first crossed the line $\overline{CD}$ and would

strike the V-groove between x_2^* and a. Assuming the incident radiant ener-

gy is uniform, a simple area (line) ratio would be an adequate probability.

Thus the probability that the energy bundle would strike the left side of

the rounded V-groove first is

$$P(\text{left}) = \overline{AB} \ / \ (\overline{AB} + \overline{CD})$$

$$= \frac{x_1^* - (P - h) \tan \psi}{x_1^* - (P - h) \tan \psi + (a - x_2^*) + (P - h) \tan \psi} \quad (4\text{-}19)$$

$$= \frac{x_1^* - (P - h) \tan \psi}{a - (x_2^* - x_1^*)} \quad .$$

Case II: $\frac{\pi}{2} > \psi \geq \frac{\pi}{2} - \theta_1$

There are two subcases to be considered: 1. $h \leq \bar{y}_1$ and 2. $h \geq \bar{y}_1$. Figure 4-14 is representative of subcase 1. Note that we must define a new upper limit (for x_1^*) for incidence on the left side of the rounded V-groove. The point (x', y') is the shadow boundary line (point). Thus the upper limit is not x_1^* but x'. The probability of first incidence on the left side is as in Case I. Thus

$$P(\text{left}) = \frac{x' - (P - y') \tan \Psi}{x' - (P - y') \tan \Psi + (a - x_2^*) + (P - h) \tan \Psi}$$

$$= \frac{x' + (P - y') \tan \Psi}{a - x_2^* + x' + (y' - h) \tan \Psi} \quad .$$

Subcase 2 has two parts

(a) $\Psi_c > \Psi > \frac{\pi}{2} - \theta_1$

(b) $\Psi > \Psi_c$

where Ψ_c represents tangential incidence at the depth of penetration.

Part (a) is representative of the situation in which the depth of penetration is less than the shadow boundary (see Figure 4-15).

This is then just Case I, since the shadow boundary is in the forbidden zone (x_1^* to x_2^*) (i.e. $x_1^* \leq x' \leq x_2^*$).

Part (b) is representative of this situation in which the depth of penetration is greater than the shadow boundary but above the surface transition point $\bar{y}_1$ (see Figure 4-16). This is then just Case II (i.e. the shadow boundary is outside of the forbidden zone - $x' < x_1^*$).

Figures 4-17 illustrate the variation of $P(\text{left})$ for various σ/a, σ/λ, P and X_o/a situations.

In the case of the situations for which $\bar{F} > 1$, the probability
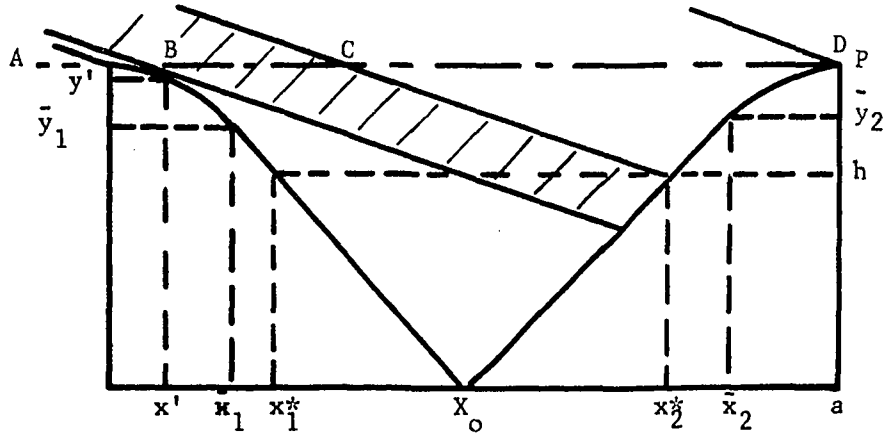
Figure 4-14. Geometry Used for the Definition of the Side of First Incidence Probability for $\psi \geq \frac{\pi}{2} - \theta_1$
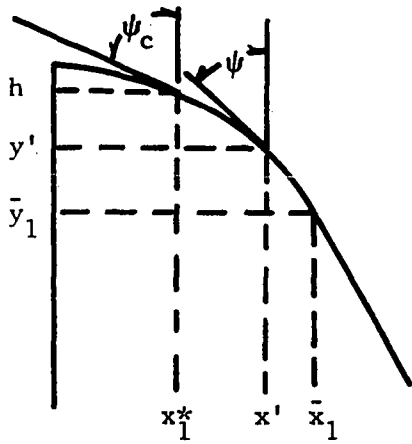
Figure 4-15. Illustration of the Geometry Involved When There is a Shadow Boundary and $\psi_c > \psi$
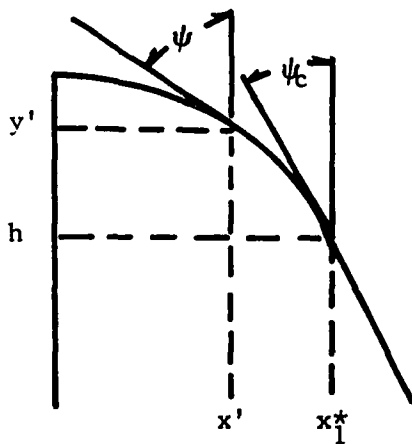
Figure 4-16. Illustration of the Geometry Involved when There is a Shadow Boundary and $\psi_c < \psi$

$\sigma / a = 1.5$
$X_o / a = 0.45$
$P = 0.9$

$\sigma / \lambda = 1.0$
$X_o / a = 0.45$
$P = 0.9$
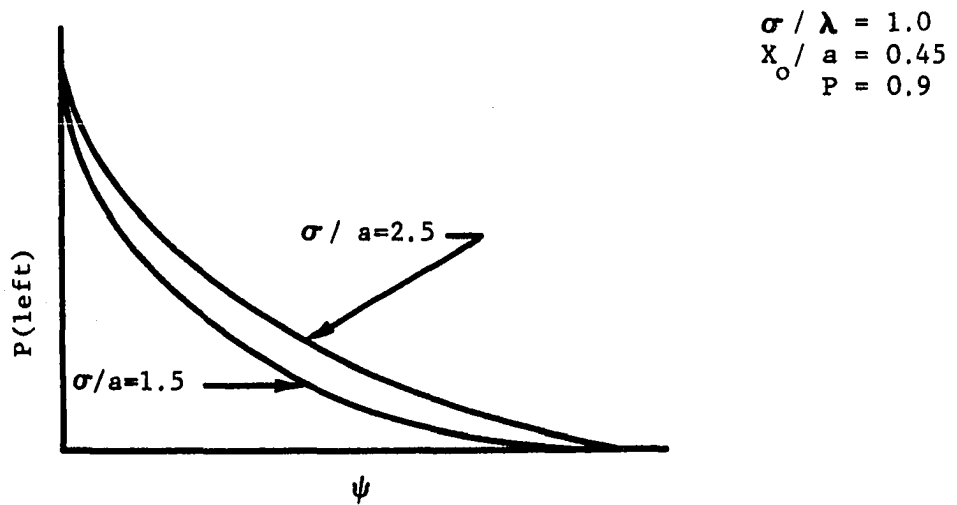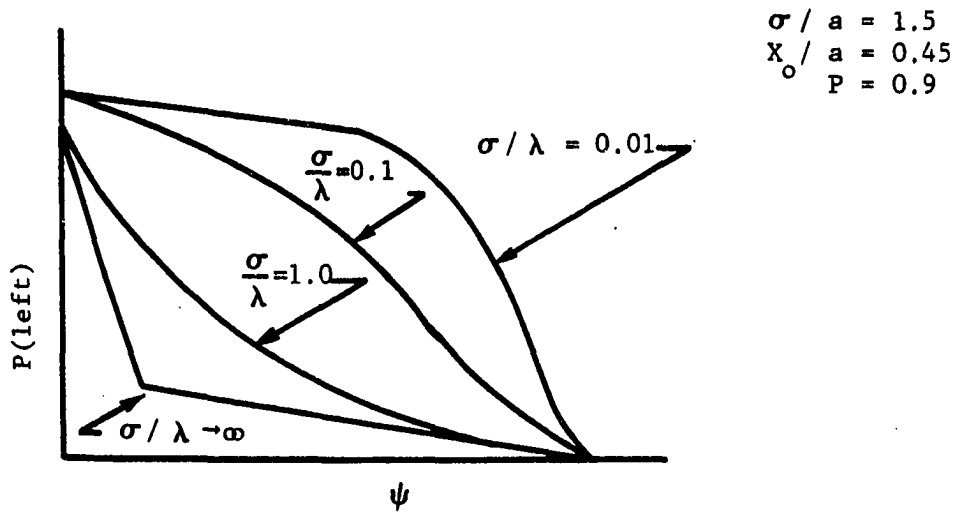
Figure 4-17. P(left) versus ψ with σ / a and σ / λ as Parameters

will be defined in an analogous fashion. That is

$$P(\text{left}) = \overline{AB}\ \bar{F}\ /\ (\overline{AB}\ \bar{F} + \overline{CD})\ .\tag{4-21}$$

Since this could not be derived, this statement has nothing but a basic heuristic indication of correctness.

Note as $\bar{F}$ approaches infinite, $P(\text{left}) = 1$ and if $\bar{F} = 1.000$, $P(\text{left}) \leq 1$.

The computation of first incidence probability is made in subroutine APROB (appendix C).

First Incidence Point

To determine the first point of incidence on either the right or left side of the rounded V-groove, the basic assumption is that the incident energy bundles are uniformly distributed. The probability is uniform across the beam between lines along the incident direction intersecting the surface at $x = x_2^*$ and $x = a$ for the right side and intersecting the surface at $x = 0$ and $x = x_1^*$ for the left side.

An illustration of the pertinent geometry for the determination of the first incidence point on the right side appears as Figure 4-18. Let $A = \cot \Psi$, where Ψ is the angle of incidence. Then

$$\textcircled{y_1} = A(x_2^* - x) + y_2^*$$

$$\textcircled{y_2} = A(a - x) + P\ \ .$$

At $x = 0$, we may define a uniformly distributed random number

$$R_a = \frac{e}{\textcircled{y_2} - \textcircled{y_1}}\ ,\quad 0 \leq e \leq \textcircled{y_2} - \textcircled{y_1}\ .$$

The assumed line of flight of the energy bundle is then

$$y_? = \textcircled{y_1} + e$$
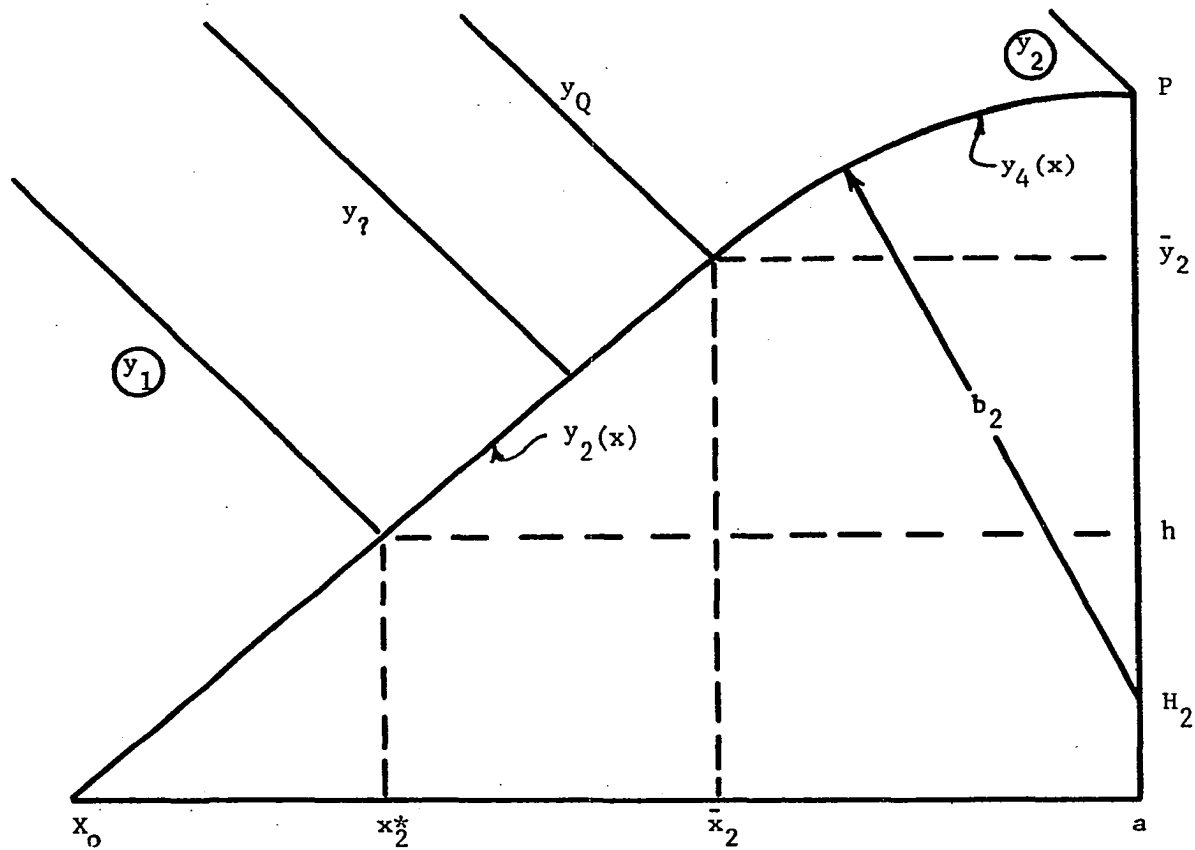
Figure 4-18.   Geometry Used in Defining the First Point of Incidence
on Right Side of Rounded V-groove

$$y_? = A(x_2^* - x) + y_2^* + Ra[A(a - x_2^*) + (P - y_2^*)] .$$

Notice the line of flight of the energy bundle incident at the transition

point $(\bar{x}_2, \bar{y}_2)$ is

$$y_Q = A(\bar{x}_2 - x) + \bar{y}_2 .$$

So at $x = 0$,

$$y_Q - \widehat{y_1} = A(\bar{x}_2 - x^*_2) + (\bar{y}_2 - h) .$$

Thus the particular uniformly distributed random number which would pro-

duce $y_? = y_Q$ would be

$$\bar{R} = (y_Q - \widehat{y_1}) / (\widehat{y_2} - \widehat{y_1}) .$$

To select, in a random fashion, the point of first incidence, two cases

must be considered.

Case I: $R_a \leq \bar{R}$

In this case $y_?(x)$ and $y_2(x)$ must be solved simultaneously for x,

yielding

$$x = \frac{\sigma X_o + (a - X_o) \left| Ax_2^* + y_2^* + R_a[A(a - x_2^*) + (P - y_2^*)] \right|}{\sigma + A(a - X_o)} . \qquad (4\text{-}22)$$

Thus for $R_a = 0$, $x = x_2^*$ and for $R_a = \bar{R}$, $x = \bar{x}_2$.

Case II: $R_a \geq \bar{R}$

In this case $y_?(x) = y_4(x)$ results in

$$x = \frac{(AC + a)}{1 + A^2} - \frac{[(AC + a)^2 - (1 + A^2)(C^2 + a^2 - b_2^2)]^{\frac{1}{2}}}{1 + A^2} \qquad (4\text{-}23)$$

where $C = y_2^* - H_2 + Ax_2^* + R_a[A(a - x_2^*) + (P - y_2^*)] .$

To compute the point of first incidence on the left side of the

rounded V-groove two cases must be considered.

Case I : $\psi < \frac{\pi}{2} - \theta_1$ (see Figure 4-19)

As in the preceding case

$A = \cot \psi$

$\textcircled{$y_1$} = -Ax + P$

$\textcircled{$y_2$} = -A(x - x_1^*) + y_1^*$

$y_Q = -A(x - \bar{x}_1) + \bar{y}_1$

$y_? = -Ax + P + R_a (Ax_1^* + y_1^* - P)$

$$R_a = \frac{e}{\textcircled{y_2} - \textcircled{y_1}}$$

$$\bar{R} = \frac{y_Q - \textcircled{y_1}}{\textcircled{y_2} - \textcircled{y_1}}$$

at $x = 0$.

Subcase (a) $R_a \geq \bar{R}$

For this situation, $y_? = y_1$, resulting in

$$x = \frac{P - \sigma + R_a(Ax_1^* + y_1^* - P)}{A - m_1} \tag{4-24}$$

where $m_1 = \sigma/X_o$.

Thus for $R_a = 1$, $x = x_1^*$ and for $R_a = \bar{R}$, $x = \bar{x}_1$.

Subcase (b) $R_a \leq \bar{R}$.

Thus $y_? = y_3$ resulting in

$$x = \frac{AC}{1 + A^2} - \frac{[b_1^2(1 + A^2) - C^2]^{\frac{1}{2}}}{1 + A^2} \tag{4-25}$$

where $C = P - H_1 + R_a(Ax_1^* + y_1^* - P)$.

Case II: $\psi > \frac{\pi}{2} - \theta_1$ (see Figure 4-20)

In this particular case, the point (x_1^*, y_1^*) may be shadowed.   If

Figure 4-19. Geometry Used in Defining First Point of Incidence on Left Side of Rounded V-groove $\psi < \frac{\pi}{2} - \theta_1$

Figure 4-20. Geometry Used in Defining First Point of Incidence on Left Side of Rounded V-groove $\psi > \frac{\pi}{2} - \theta_1$

so, we must define a new point of maximum penetration for this side. This may be accomplished easily by noting that the shadow boundary is determined by $\vec{I} \cdot \vec{N} = 0$. Thus the shadow boundary point is

$$x' = b_1 \cos \psi$$

$$y' = y_3(x') .$$

Thus $x_1^* = x'$ and $y_1^* = h = y'$. With these definitions the computation of case I, subcase (b) yields the first incidence point. If (x_1^*, y_1^*) is not shadowed, the procedure is to use case I, subcase (b) with the original (x_1^*, y_1^*).

Point (x, y) is computed in subroutine XYLFT or XYRIT (appendix C).

Reflected Direction

The law of reflection may be used to determine the reflected direction in general form given the incident direction, the equation of the surface, and the point of incidence.

Consider the determination of the reflected direction. Recall that for regular reflection the angle of incidence ψ equals the angle of reflection θ. Thus

$$\cos \psi = \cos \theta$$

and $\qquad \sin \psi = \sin \theta .$

In vector form these equations are

$$\vec{N} \cdot \vec{R} = - \vec{N} \cdot \vec{I} \tag{4-26}$$

and $\qquad \vec{I} \times \vec{N} = \vec{R} \times \vec{N} . \tag{4-27}$

Operating on equation (4-27) by $\vec{N} \times$ yields

$$\vec{N} \times (\vec{I} \times \vec{N}) = \vec{N} \times (\vec{R} \times \vec{N})$$

or $\quad \vec{I} - (\vec{N} \cdot \vec{I}) \vec{N} = \vec{R} - (\vec{N} \cdot \vec{R}) \vec{N}$.

Thus $\quad \vec{R} = \vec{I} - [(\vec{N} \cdot \vec{I}) - (\vec{N} \cdot \vec{R})] \vec{N}$

$$= \vec{I} - 2 (\vec{N} \cdot \vec{I}) \vec{N} \text{ from equation (4-26)}.$$

And in Cartesian coordinate matrix form $\vec{R} = M \vec{I}$

where $\quad M = \begin{pmatrix} 1 - 2n_x^2 & - 2n_x n_y & - 2n_x n_z \\ - 2n_x n_y & 1 - 2n_y^2 & - 2n_y n_z \\ - 2n_x n_z & - 2n_y n_z & 1 - 2n_z^2 \end{pmatrix}$

and n_x, n_y, and n_z are the components of the normal to the surface at the point of incidence. For the model reported herein $n_z = 0$.

So $\quad \begin{pmatrix} R_x \\ R_y \\ R_z \end{pmatrix} = \begin{pmatrix} 1 - 2n_x^2 & - 2n_x n_y & 0 \\ - 2n_x n_y & 1 - 2n_y^2 & 0 \\ 0 & 0 & 1 \end{pmatrix} \begin{pmatrix} I_x \\ I_y \\ I_z \end{pmatrix}$

And if $I_x = \sin \psi$ and $I_y = - \cos \psi$

$$R_x = (1 - 2n_x^2) I_x - 2n_x n_y I_y$$

$$R_y = - 2n_x n_y \ I_x + (1 - 2n_y^2) I_y .$$

These coefficients are determined in subroutine REFLT (appendix C).

Model Characteristics

Now that the basic assumptions of the analytical model have been discussed, it would seem advisable to put the whole picture together. It may be recalled from the previous sections that the analysis of this research was conducted using a Monte Carlo method. Thus each energy bundle

considered requires the construction of a new rounded V-groove. So height

σ, width a, and V-groove vertex point, X_o are all different for each ener-

gy bundle. Therefore the lobing effects of periodically rough surfaces

will not be observed (41).

This analysis was programmed for the IBM-360-40 system, available

at the University of Oklahoma, under the code name MCR. The program is

listed in Appendix C. Primary requirements to initiate a run are an angle

of incidence, ψ, RMS height, $\bar{\sigma}$, RMS width, $\bar{a}$, wavelength, λ, and the com-

ponents of the index of refraction. With this information, surfaces are

constructed in the previously indicated random fashion. A penetration

depth is computed as well as the first incidence probability. Comparison

of this probability to a uniformly distributed random number makes the

decision as to whether the first incidences is on the left or right side

of the rounded V-groove. Recall the penetration depth limits how deeply

the energy bundle may go for first incidence. Having determined this

point, the Fresnel reflection coefficient for unpolarized light (64) is

computed. As before, a random number comparison with this coefficient

determines if the energy bundle is refracted or reflected. If refracted,

that bundle is lost and a new surface is constructed. If reflected, it

does so obeying the laws of geometrical optics for regular (specular) re-

flection. The determination is now made as to whether the bundle escapes

the rounded V-groove or strikes the other side. If the bundle escapes

this geometry, its angle is categorized into one of 36 - five degree in-

tervals and counted. If the bundle does not escape the geometry, a

straight line trajectory is used to determine the point of incidence on

the other side of the rounded V-groove. Note, the depth of penetration

restriction is not used; that is, the energy bundle may strike any line of sight position on the rounded V-groove after first incidence. When the point of second incidence is determined, the Fresnel coefficient is computed and the reflected-refracted decision is made, with the same alternatives. This procedure may continue up to four times. If the energy bundle does not escape by the fourth reflection, it is defined as trapped and a new surface is constructed.

The output of these runs are presented in two forms. The first is just an accumulative count of the number of energy bundles which escape into the various five degree intervals. Also a count is made as to the number which escape in one degree intervals on either side of the regular reflection angle (i.e. $\psi - 5^\circ \le \theta \le \psi + 5^\circ$). The second listing of the data is a ratio of the number in a five degree interval and the maximum number in any interval.

A run consists of at most 10,000 energy bundles with an execution time of 4 to 5 minutes per 1,000 energy bundles.

The number of energy bundles received is proportional to the energy and thus the intensity. Recall from chapter II that reflectances are ratioes of intensities. Thus the biangular reflectance of any test specimen in the direction (θ, φ), with ψ being the angle of incidence, relative to the biangular reflectance of the sample in the specular direction under the same irradiation conditions and receiving acceptance angle, is just the ratio of the corresponding numbers of energy bundles. Therefore

$$\frac{\rho_{ba}(\psi;\theta,\varphi)}{\rho_{ba}(\psi;\psi,0)} = \frac{N(\psi;\theta,\varphi)}{N(\psi;\psi,0)} \tag{4-28}$$

where $N(\psi,\theta,\varphi)$ is the number of energy bundles received about the direction (θ,φ) when ψ is the angle of incidence. Notice equation (4-28) is just representation (3) of data, discussed in chapter II, and the second mode of MCR data presentation. All data presented from this research will be based on this equation.

The changes of reflected distributions with the variation of the discussed parameters may be seen in Figures 4-21 to 4-24. In Figures 4-21 to 4-23 the second form of MCR data presentation is plotted while in Figure 4-24 the first mode is illustrated. Figure 4-21 indicates this model follows the appropriate trend for $\bar{\sigma}/\lambda$. That is as $\bar{\sigma}/\lambda$ increases, the reflected distribution becomes more non-regular. Figure 4-22 illustrates the spread of the distribution with the ratio of $\bar{\sigma}/\bar{a}$. This is consistent with the assumption that if the energy bundle gets into the V-groove, a more non-regular characteristic will result. Thus the larger the ratio $\bar{\sigma}/\bar{a}$, all else being equal, the higher the first incidence point is on the rounded V-groove. Included on part a of this figure is the Ideal or Lambert distribution. Figure 4-23 illustrates the effect of variation of parameter P. Recall that as P approaches one, the amount of roundness at the peaks decreases. Notice that increasing the parameter P has a similar effect as decreasing the $\bar{\sigma}/\bar{a}$ ratio. The difference is that the change in P more drastically effects the curvature of the peak. Figure 4-24 is presented to indicate the actual difference the change in the angle of incidence has on the distribution shape and maximum magnitude. Notice that the distribution becomes more slender and tall as the angle of incidence increases. This is consistent with experimental observation.
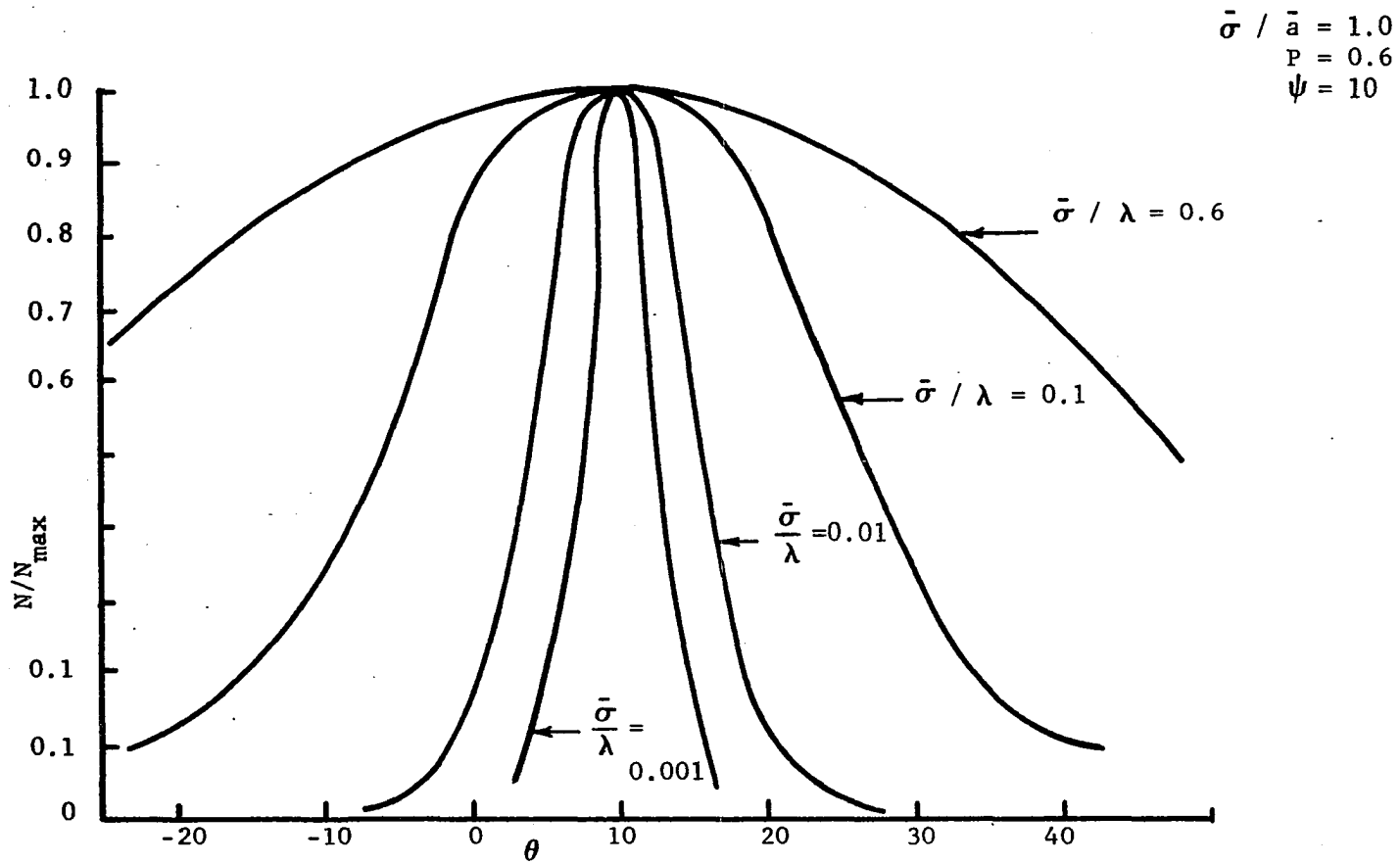
Figure 4-21. Illustration of Variation of Reflected Distribution as a
Function of $\bar{\sigma} / \lambda$
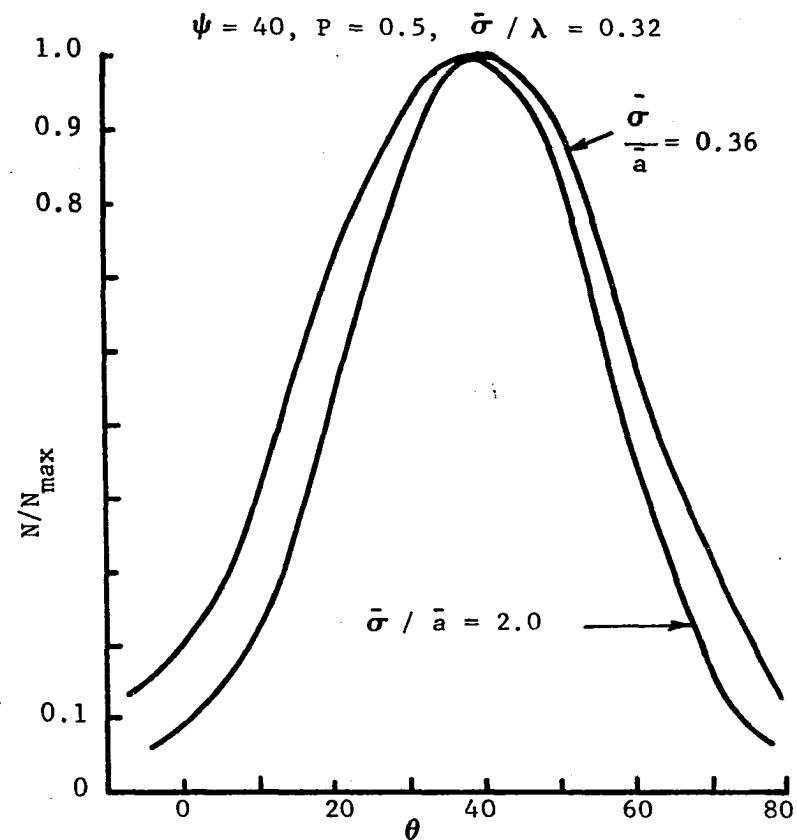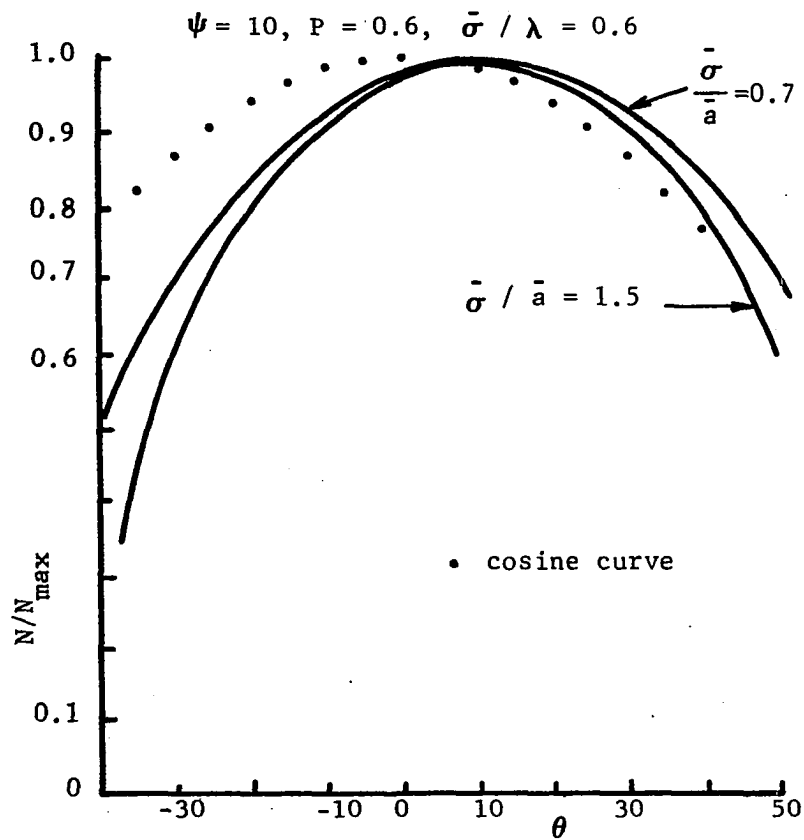
Figure 4-22.   Illustration of Variation of Reflected Distribution as a Function of $\bar{\sigma} / \bar{a}$
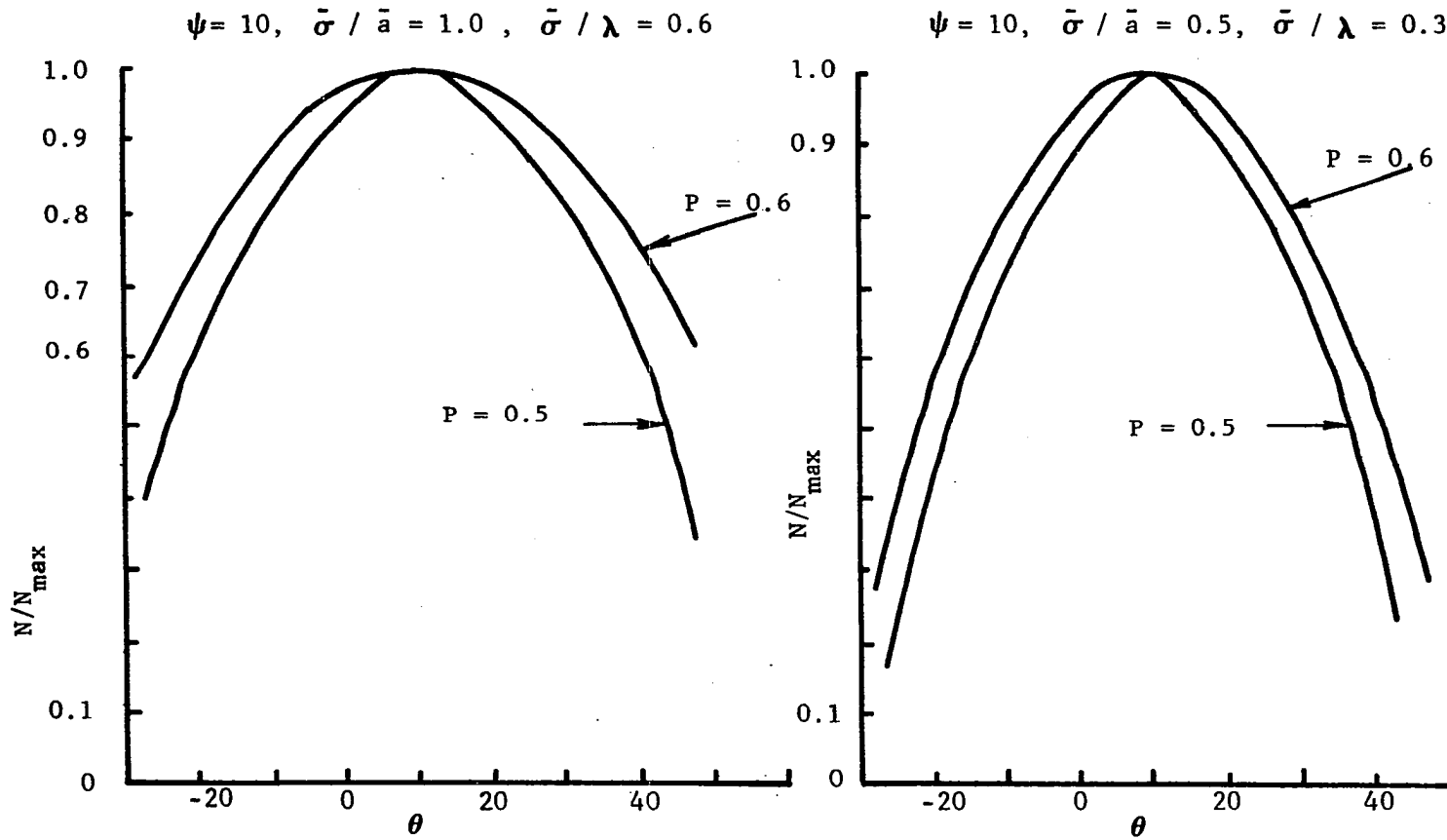
Figure 4-23.   Illustration of Variation of Reflected Distribution as a
Function of P

58
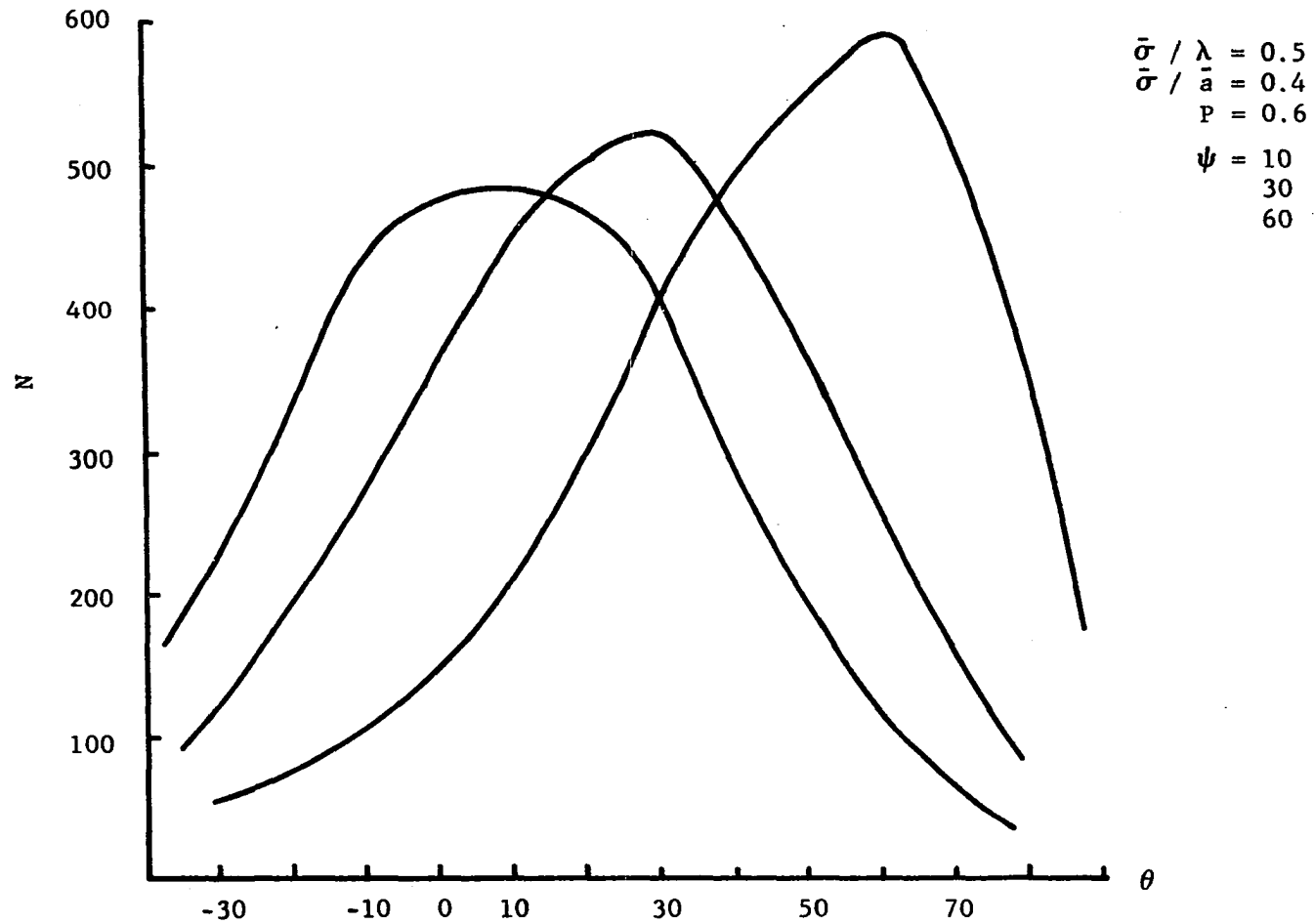
Figure 4-24. Illustration of Variation of Reflected Distribution
as a Function of Angle of Incidence

Closure

It must be remembered that this model represents only an artificial resemblance to the actual fact. It is an attempt to make progress in understanding how and why rough surfaces reflect as they do and in particular to look at the region not explicitly covered by the more appealing diffraction theory, that is the region $\sigma/\lambda \sim 1$. The results will hopefully yield suggestions as to what surface parameters might be measured for accurate prediction of the reflected energy distribution for all wavelengths.

CHAPTER V

COMPARISON OF MODEL TO EXPERIMENTAL RESULTS

Chapter IV has been used to develop the model, thus setting the
stage to consider its usefulness. Before actually considering a compar-
ison of the model with published experimental data, a brief statement of
the purpose for this will be made.

All theories and models for whatever physical phenomena they are
supposed to describe must face the test of conforming to reality. Thus
by fitting the output of the MCR digital computer program to experimental
data, statements may be made concerning the parameters vital to a thorough
understanding of the effect of rough surfaces on the reflected distribu-
tion. Heretofore the only surface characteristic actually presented in
a reflectance measurement was the RMS roughness, $\bar{\sigma}$. This dimension has
been used in the model. In addition, an RMS peak to peak dimension, $\bar{a}$,
has been used in lieu of the autocovariance length introduced in the
theories available. Also a peak roundness parameter, P, has been intro-
duced. The usefulness of these parameters in describing the reflected
energy distribution must be examined.

Experimental Considerations

Before attempting to match the experimental data, consideration
must be given to the set-up of the apparatus and what the resultant data

from this apparatus truly represents. Three points must be discussed. They are 1) the conditions of surface illumination and viewing, 2) detected distribution distortion due to finite aperture sizes and 3) optical roughness.

1) All experimental methods use combinations of collimated and focused beams for the incident and reflected energy. It is important to determine if the surface under investigation is totally or partially covered by the field of view of the incident and/or viewing optics. If the surface is totally covered by the incident beam, it is said to be over-illuminated; otherwise it is said to be under-illuminated. Similarly if the area viewed by the receiving optics is larger than the surface under examination, it is said to be over-detected, otherwise under-detected. In either of the "over" cases, the corresponding projected area varies as the cosine of the angle between the surface normal and the direction of interest. In either of the "under" cases, the area viewed is varied, but the surface always intercepts the total area viewed by the corresponding optics. The Figure (5-1) illustrates the commonly used experimental situations. The interpretation of the detector output depends upon which combination is used in the experimental situation. For example, in the over-illuminated, under detected situation for a diffuse surface, if ψ is fixed, the detector output would be constant as θ is varied. If θ is fixed and ψ is varied, the detector output will vary as the cosine of ψ.

2) Since finite angles of acceptance are necessary in actual experimental apparatus, a certain degree of distortion will be exhibited (13, 65). The angle of acceptance, as used in this discussion, is the generating
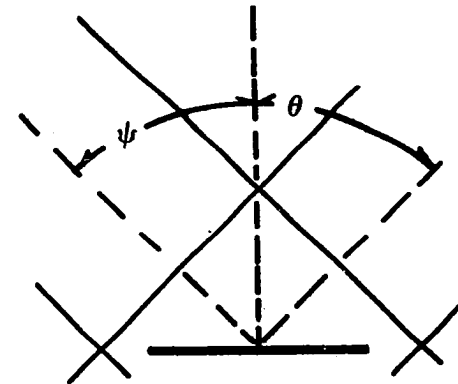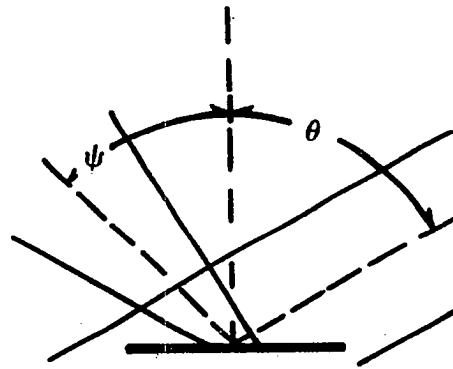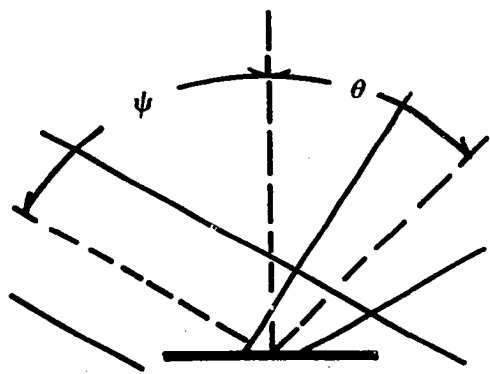
Figure 5-1. Illustration of Detection-Illumination Conditions

angle of the solid angle cone of radiation, incident or received. This
is particularly evident when the reflected energy distribution displays a
sharp increase such as would be encountered with a large regular compo-
nent. A simple model may be constructed in an attempt to account for this.
Assume that the area viewed by the detector is circular and of radius c.
Also for simplicity, assume the sensitivity is uniform across this area.
Assume the reflected beam is also uniform and circular of radius b. The
output of this detector will be directly proportional to the area common
to both the beam and the detecting area. Figure 5-2 illustrates the geom-
etry, with the shaded area representing the area in common.

If $u = y/c$, then

$$\eta = \tan^{-1}\sqrt{\frac{c^2 - y^2}{y^2}} = \tan^{-1}\left[\frac{\sqrt{1 - u^2}}{u}\right]$$

$$\xi = \tan^{-1}\left[\sqrt{\frac{c^2 - y^2}{x^2}}\right] = \tan^{-1}\left[\frac{c\sqrt{1 - u^2}}{x}\right]$$

Thus the shaded area is

$$S = (\eta c^2 - c^2 u \sqrt{1 - u^2}) + (\xi b^2 - cx\sqrt{1 - u^2})$$

Normalizing S to the detecting area yields

$$F_N = \frac{S}{\pi c^2} = \frac{1}{\pi}\left[\eta + \xi\left(\frac{b}{c}\right)^2\right] - \frac{\sqrt{1 - u^2}}{\pi}\left[u + \frac{x}{c}\right]$$

$$= \frac{1}{\pi}\left[\cos^{-1}u + \left(\frac{b}{c}\right)^2 \cos^{-1}\left(\frac{x}{b}\right)\right] - \frac{\sqrt{1 - u^2}}{\pi}\left[u + \frac{x}{c}\right]$$

where $\quad x = c\sqrt{\left(\frac{b}{c}\right)^2 - 1 + u^2}$

Notice if $c = b$, $x = y$ and

$$F_N = \frac{2}{\pi}\left[\cos^{-1}u - u\sqrt{1 - u^2}\right]$$
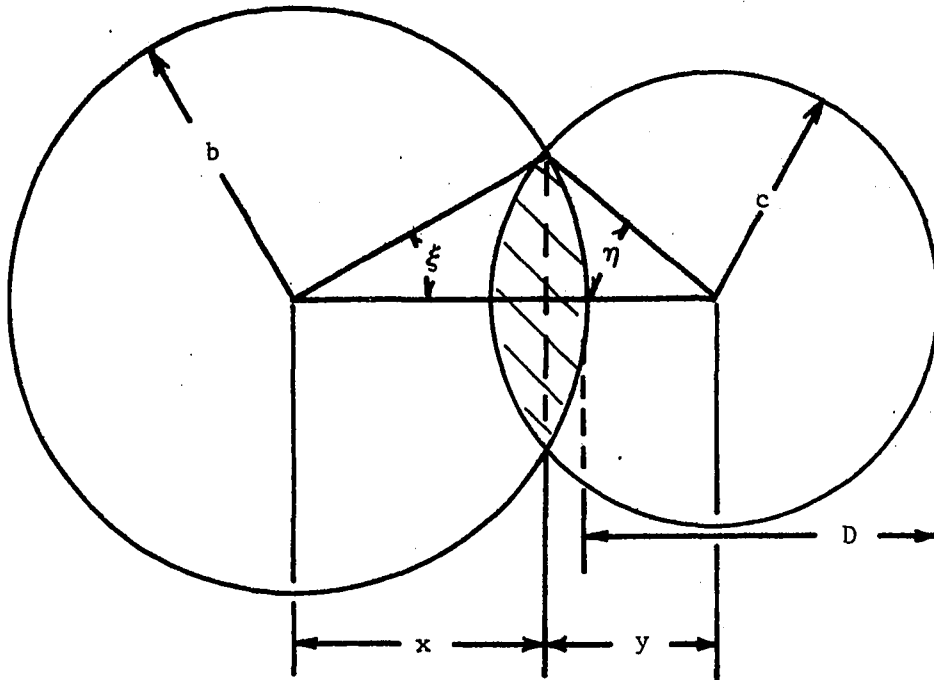
Figure 5-2. Geometry Used in Uniform Beam-Finite Receiving Aperture Distortion Calculation

I: $c = 0$
II: $c = 0.1c$
III: $c = b$
IV: $c = 2b$

$0 < D < 2c$
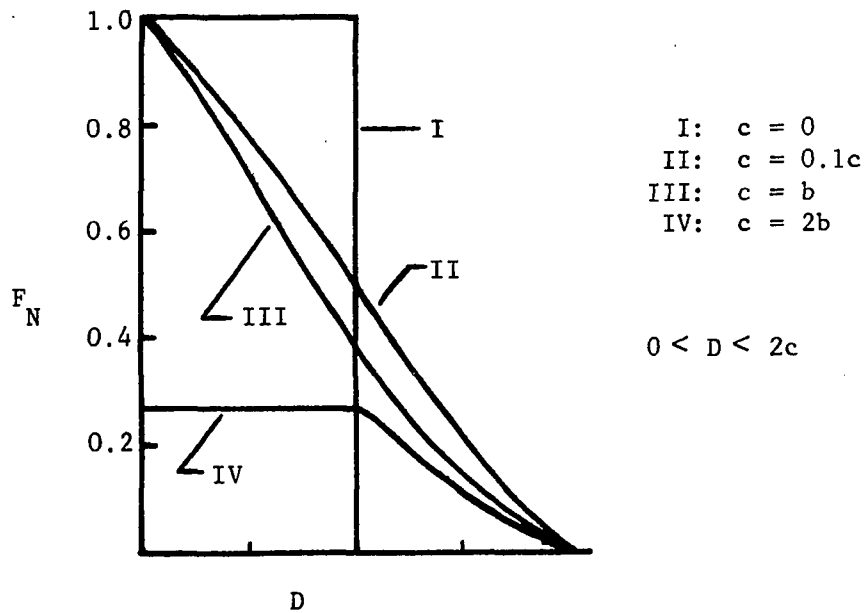
Figure 5-3.   Ideal Detector Responses Due to Finite Apertures

Figure 5-3 illustrates the various expected responses for various combinations of c and b.

Both of these items will be used in the discussions that follow.

3) When reflectance experiments are conducted, attempts are made to measure the RMS roughness. Recall that roughness as used in this investigation indicates a statistical description for an isotropic randomly rough surface. Other surface descriptions such as waviness, tool markings, and relatively infrequent minute cracks or flaws are considered so big or widely spaced as to be excluded from the roughness measurements of interest here. Also the surfaces are considered free of contamination. Profilometry is the most common method used for evaluating the roughness of a surface. Other methods are available (66). If the surface irregularities are very deep or closely spaced or the material of the surface is soft, this method yields very unreliable results. That is, the physical dimension of the tipped stylus cannot actually follow the surface, or its weight destroys the actual contour. Therefore, as would be expected, great difficulty has been experienced in attempts to fit the regular component of the theory of Davies, for example, to data in the regions when this theory should be valid. As an alternative, the theory is used to determine another roughness measurement. This dimension is termed "RMS optical roughness" σ_o and is obtained by measuring the reflectance at very long wavelengths and small angles of acceptance (13, 14, 65 and 54). As could be expected, these numbers are larger than are obtained by mechanical means by from 1.2 to 3 times. In the analysis of this investigation, the optical RMS roughness will be used.

Example for Comparison

In order to determine the usefulness of this model, it was compared to experimental data published by other investigators.

The first data considered were that presented in reference (13). Birkebak used the under-illuminate, over-detect method with angles of acceptance of approximately two degrees. The two test samples considered were aluminum coated ground glass and roughened nickel. The data are presented as a ratio of two biangular measurements similar to the second output listing of the MCR digital computer program discussed previously in Chapter IV. The only usable surface characteristic stated by Birkebak is the RMS optical roughness. Thus decisions had to be made as to the magnitudes of $\bar{\sigma}/\bar{a}$ and P. Figures 5-4 to 5-8 illustrate the comparisons for various pieces of data. The data of Figure 5-4 was taken on an aluminum coated ground glass sample with $\sigma_o/\lambda = 0.58$. The MCR output for $\bar{\sigma}/\bar{a} = 0.5$, $\bar{\sigma}/\lambda = 0.6$ and P = 0.4 fits quite well. Similarly for a nickel sample and $\sigma_o/\lambda = 0.6$, the MCR output of $\bar{\sigma}/\bar{a} = 0.5$, $\bar{\sigma}/\lambda = 0.6$ and P = 0.5 is in good agreement (Figure 5-5). Figure 5-6 is an illustration of the direct superposition of the regular and non-regular components. For the angles of acceptance given by Birkebak, the regular response function was fitted to the spiked portion. The output of MCR was fitted to the remainder of the figure. This figure is plotted for a test sample of nickel with σ_o/λ equal to 0.32 and MCR output of $\bar{\sigma}/\lambda = 0.3$, $\bar{\sigma}/\bar{a} = 0.5$ and P = 0.5. A similar procedure was used to fit the regular response function and the MCR output to another nickel sample as illustrated in Figure 5-7. Figure 5-8 is the final piece of data presented by Birkebak in which the output of MCR and the regular response was fitted.

Al-coated grd. glass: $\sigma_0 / \lambda = 0.58$

MCR: $P = 0.4$, $\bar{\sigma} / \lambda = 0.6$, $\bar{\sigma} / \bar{a} = 0.5$
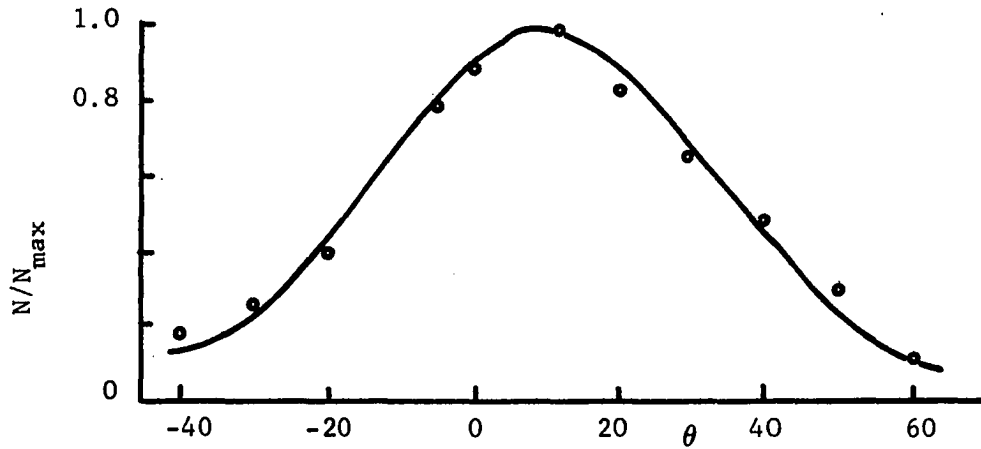
Figure 5-4. Graphical Comparison of Raw Data of Birkebak and MCR Output

Nickel: $\sigma_0 / \lambda = 0.6$

MCR: $P = 0.5$, $\bar{\sigma} / \lambda = 0.6$, $\bar{\sigma} / \bar{a} = 0.5$
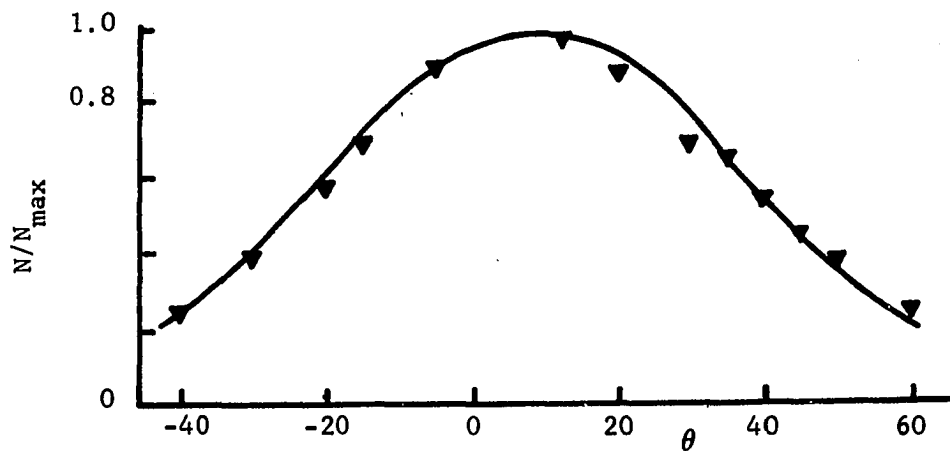
Figure 5-5. Graphical Comparison of Raw Data of Birkebak and MCR Output

■   Nickel: σ_0 / λ = 0.32

—   MCR: P = 0.5, $\bar{\sigma} / \lambda$ = 0.3, $\bar{\sigma} / \bar{a}$ = 0.5
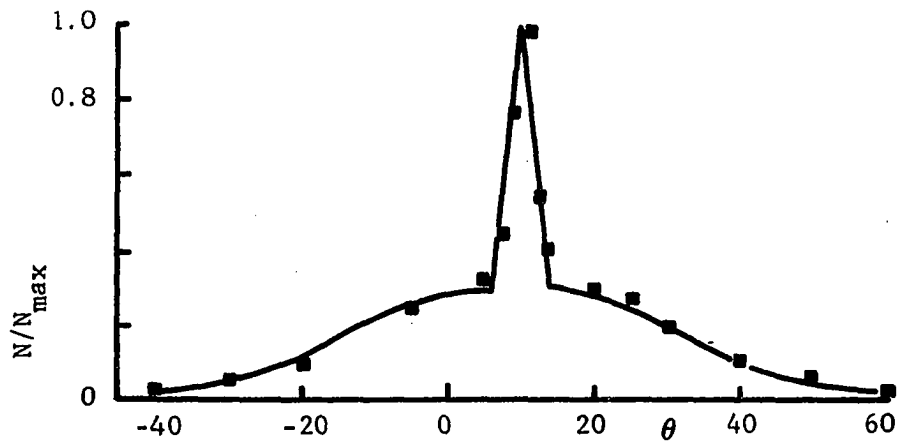
Figure 5-6. Graphical Comparison of Raw Data of
Birkebak and MCR Output

▼   Nickel; σ_0 / λ = 0.23

—   MCR: P = 0.6, $\bar{\sigma} / \lambda$ = 0.3, $\bar{\sigma} / \bar{a}$ = 0.5
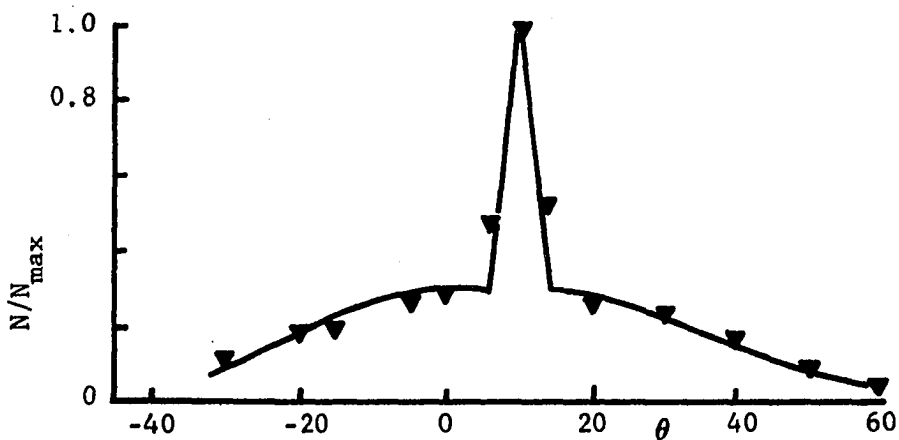
Figure 5-7. Graphical Comparison of Raw Data of
Birkebak and MCR Output
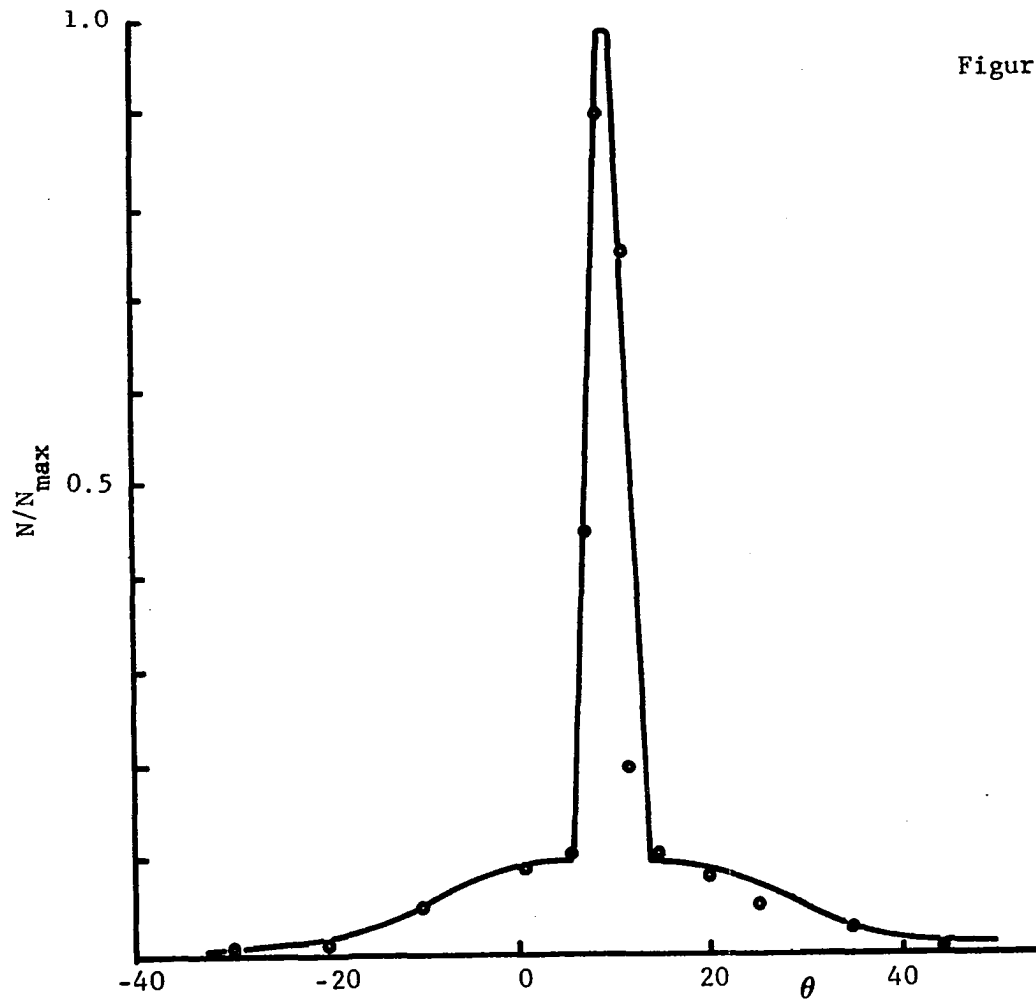
Figure 5-8. Graphical Comparison of
Raw Data of Birkebak and
MCR Output

● Al-coated grd. glass:
$0.11 < \sigma_o / \lambda < 0.19$

— MCR:
$\bar{\sigma} / \lambda = 0.15$
$\bar{\sigma} / a = 0.5$
$P = 0.5$

N/N_{max}

θ

70

Again the fit is quite good.

The second set of data considered for comparison was that pre-
sented in reference (14). The material used in the experiments of these
investigators, Torrance and Sparrow, was a nonconductor, fused polycrys-
talline magnesium-oxide ceramic. The acceptance angles of approximately
two degrees in an under-illuminate, under-detect experimental set-up was
used.

The analysis for non-conducting material is somewhat more com-
plicated than for a conductor. The reason for this is that there is a
contribution to the received energy due to a volume effect. This effect
is available when considering reflection from metals but the magnitude
of this component is quite small due to the large absorption coefficients
associated with metals. In the case of dielectrics, this contribution
may be sizeable. In agreement with other investigators (24, 31), it is
assumed that this volume contribution is diffuse for the analysis used
in this work.

As in the previous case, the data are presented as a ratio of bi-
angular reflectances. A graphic comparison may be made from Figures 5-9
and 5-10. These data were taken on the same sample at two angles of in-
cidence and two different wavelengths. The conditions of the surface and
the variables used in the MCR digital computer program appear in the
figures. In Figure 5-9, the volume effect is represented by a constant
value. The difference between 5-9 a and b is only the angle of incidence.
In Figure 5-10, in addition to the volume effect and the rough surface
effect, a sizeable regular component may be noted. This component was
fitted exactly as was done in the preceding examples. The difference
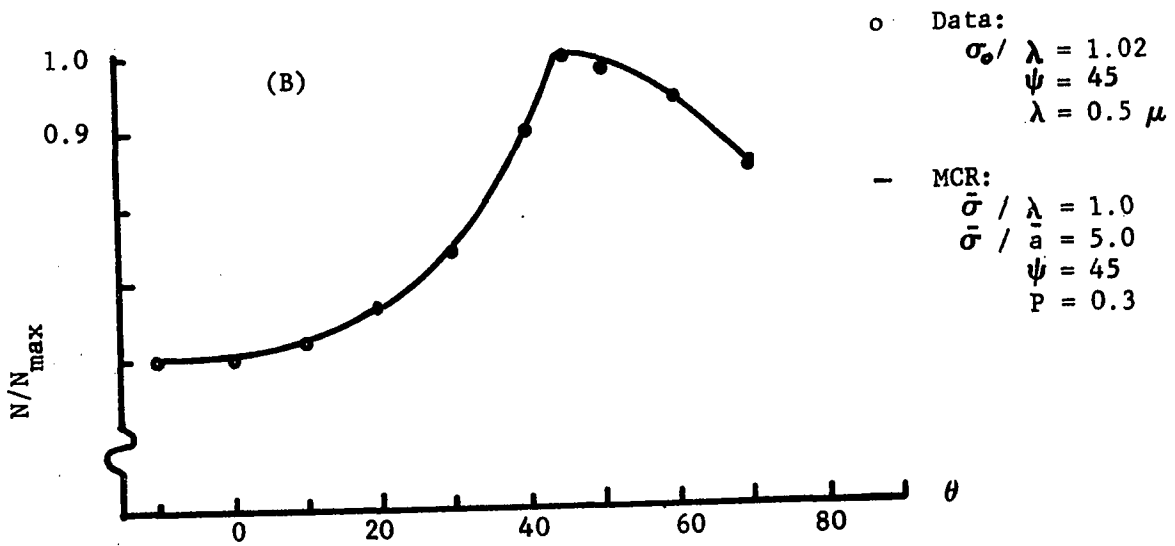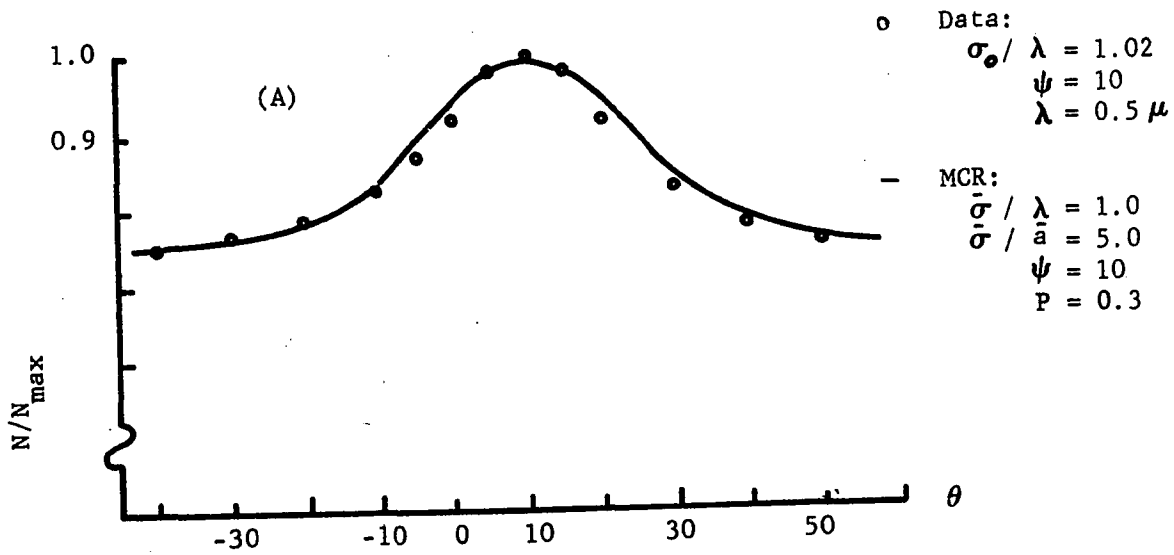
Figure 5-9. Graphical Comparison of Raw Data of Torrance and Sparrow and MCR Output
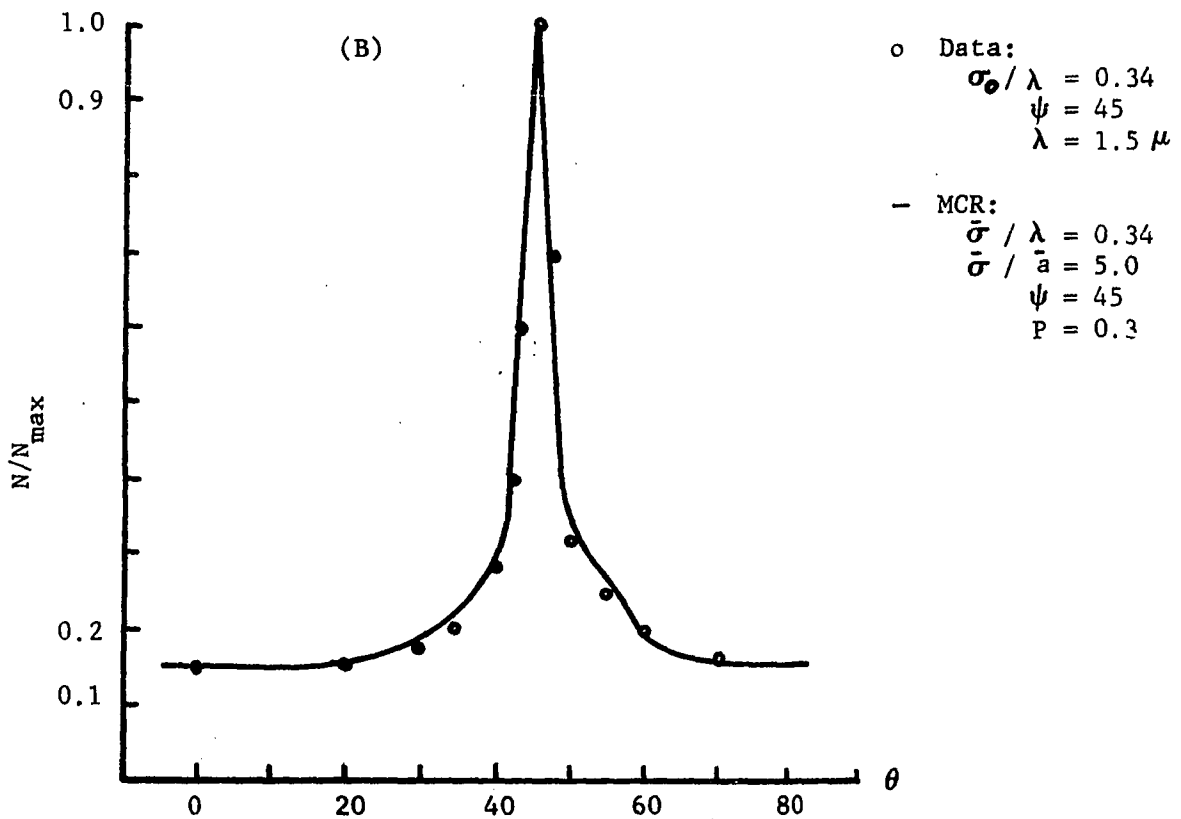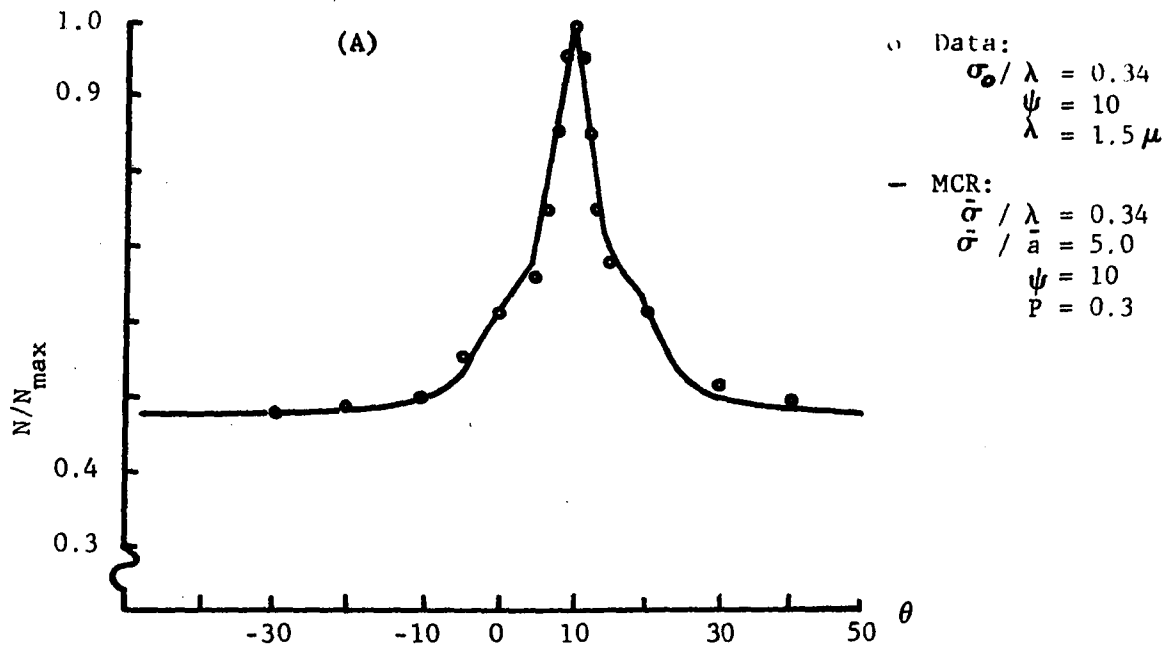
Figure 5-10. Graphical Comparison of Raw Data of Torrance
and Sparrow and MCR Output

between Figures 5-9 and 5-10 is that the wavelength was increased from

0.5μ to 1.5μ and the difference between 5-10 a and b is the angle of

incidence. It may be noted that the values used in MCR were chosen in

accordance with the data available from this publication and that the

fit is quite good.

A portion of the data presented in reference (16), by Herold and

Edwards, was considered next. These investigators used an under-illumi-

nate, over-detect method with very large angles of acceptance: incident

3.4°, emergence 4.7° shadowed to 4.1°. With acceptance angles of this

size and in particular with the receiving angle larger than the incidence

angle, the resultant detected distribution will not be truly representa-

tive of the actual distribution. Data were taken on six samples of which

only the F-40 sample of aluminum coated sintered bronze and sandblasted

aluminum were used for comparison. For the F-40 sample, these investiga-

tors did not state any surface characteristics other than that it was

"very diffuse and highly reflective". Therefore no information was avail-

able concerning the surface parameters. The best fit of these data is

presented in Figure 5-11. As in the preceding examples, once a close fit

was made for one set of parameters, only the parameter that was experi-

mentally varied, in this case the angle of incidence, was altered. As

can be seen in this figure, the fit is not as good as in the preceding

examples, but still indicates an appropriate general trend.

By far the worst fit was made with the sandblasted aluminum sam-

ple. Herold and Edwards correlated the "specular" component with the

theory of Davies using an RMS optical roughness of 0.8μ. The incident

wavelength was 5.0μ yielding a σ_o/λ of 0.16. A graphical comparison can
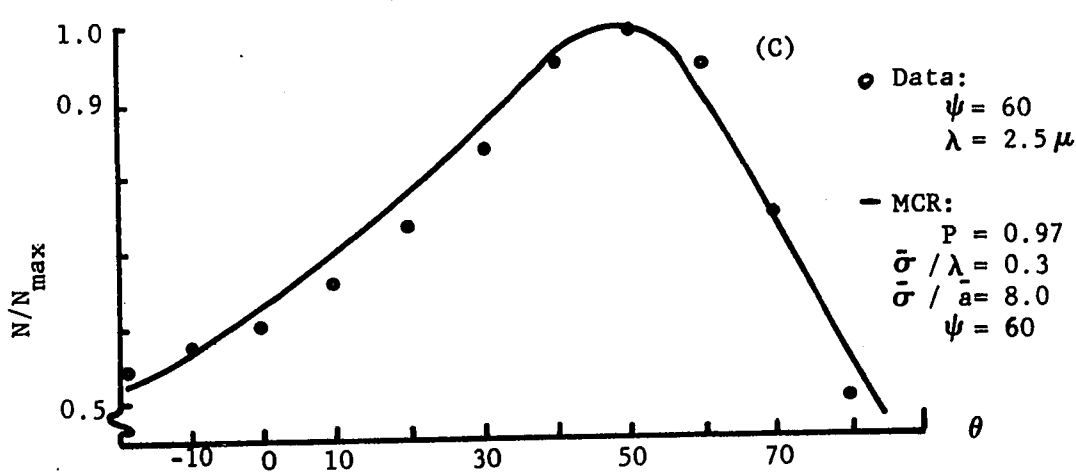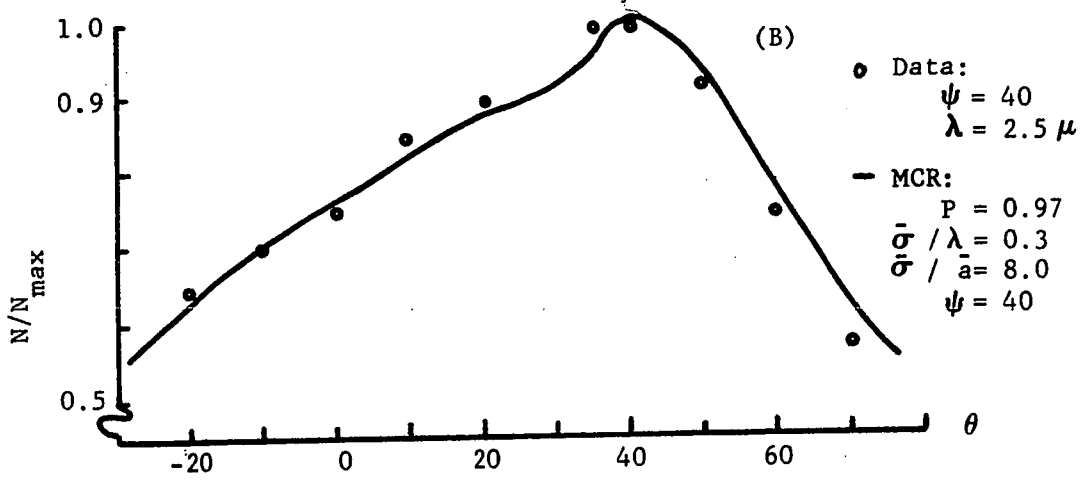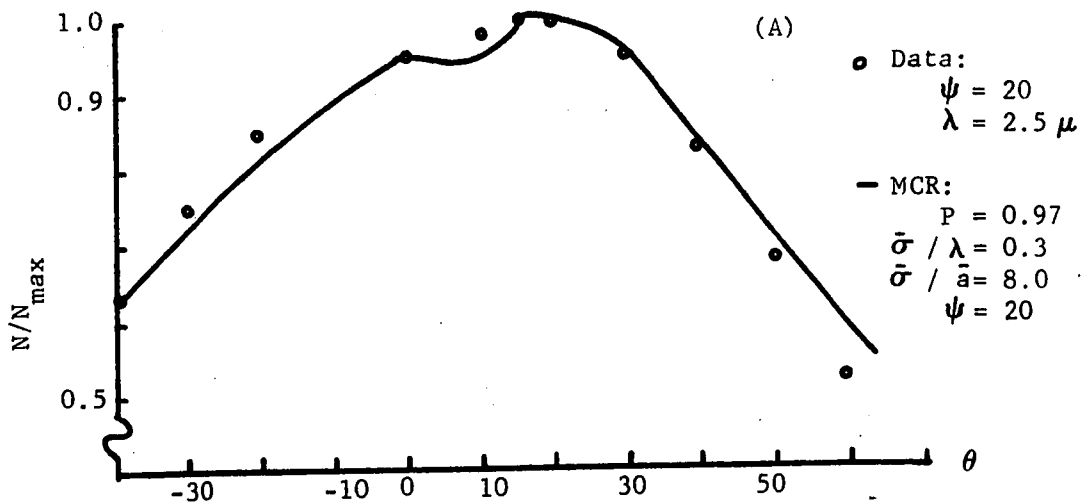
Figure 5-11. Graphical Comparison of Raw Data of Herold
and Edwards and MCR Output

1.0

N/N$_{max}$

0.2

-40   -20   0   20   40   60   80 θ

Data:

$\sigma_0 / \lambda = 0.16$

$\lambda = 5.0 \mu$

○ $\psi = 20$

▼ $\psi = 40$

■ $\psi = 60$

MCR:

$P = 0.95$

$\bar{\sigma} / \lambda = 0.16$

$\bar{\sigma} / \bar{a} = 8.0$

—— $\psi = 20$

– – $\psi = 40$

–·– $\psi = 60$
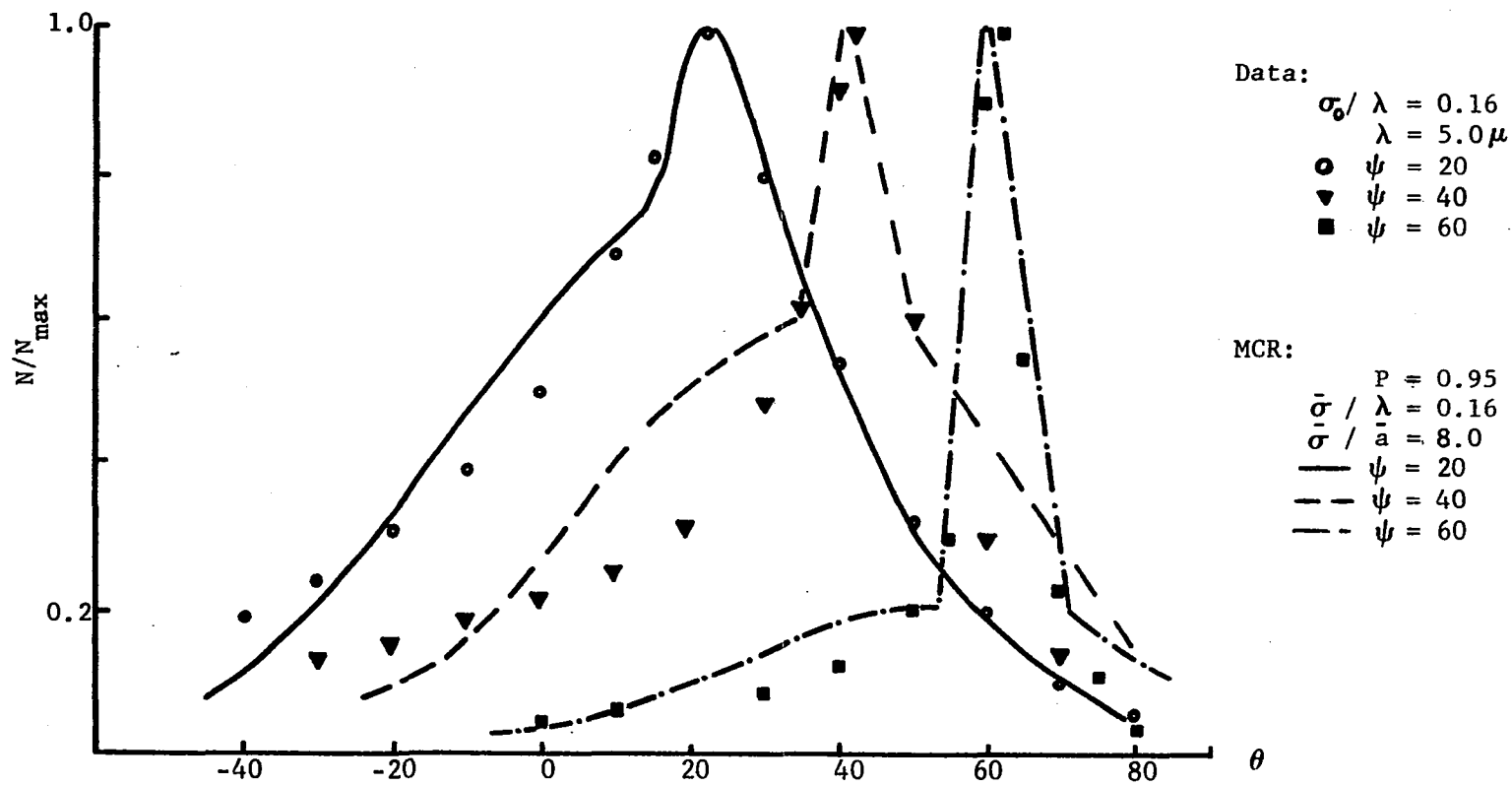
Figure 5-12.   Graphical Comparison of Raw Data of Herold
and Edwards and MCR Output

be made with Figure 5-12. Notice that the regular component was fitted as before, and except for the 20° incident case, the fit is generally poor.

As a final example, the data presented in reference (65) was considered. Francis used an under-illuminate, under-detect method with extremely large angles of acceptance of 6.4° incident and 5.3° receiving. The sample for consideration was sandblasted stainless steel (type 302). The results of the comparison are presented in Figures 5-13 to 5-16. The RMS optical roughness and the wavelength considered appear on the figures. The parameters $\bar{\sigma}/\bar{a}$ and P were determined for the 30° angle of incident case illustrated in Figure 5-13. These numbers were then used throughout the remainder of tne calculations. The regular components were of course included.

Closure

A smoothness factor was introduced in Chapter IV which was an assumed strong function of the angle of incidence and weakly dependent on the surface characteristics. For the examples considered, this function was not necessary. That is, to fit the data, $\bar{A}$ of 0.15 was used, thus $\bar{F}$ was approximately equal to one.

A word must be said concerning the error involved in this type of analysis. As was discussed in Chapter III, the error must be stated with a confidence level. As a representative example, a 90% confidence level was chosen and the data used for Figure 5-5 was considered. The results appear in Table 5-1.
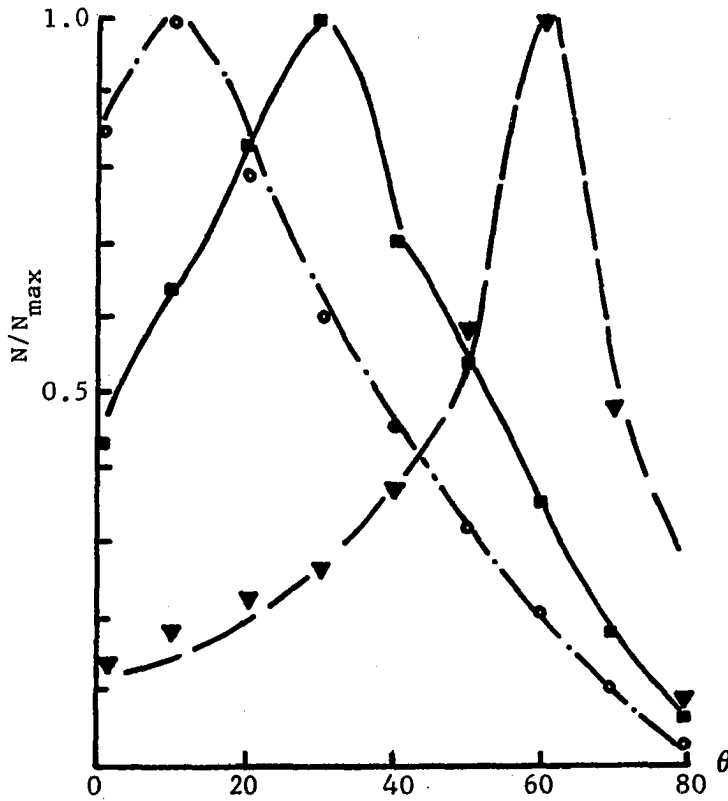
Figure 5-13. Graphical Comparison of Raw Data of Francis and MCR Output

Data: $\sigma_0/\lambda = 0.282$
$\lambda = 5.0\,\mu$

MCR: $P = 0.62$
$\bar{\sigma}/\lambda = 0.282$
$\bar{\sigma}/\bar{a} = 0.4$

MCR		Data
——·——	10	◯
————	30	■
— — —	60	▼
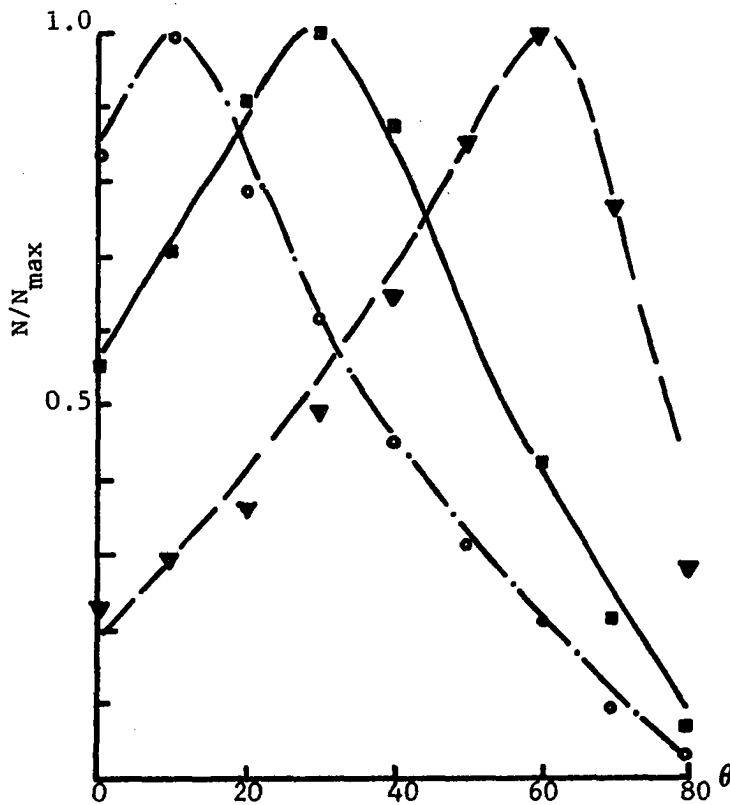
Figure 5-14. Graphical Comparison of Raw Data of Francis and MCR Output

Data: $\sigma_0/\lambda = 0.47$
$\lambda = 3.0\,\mu$

MCR: $P = 0.62$
$\bar{\sigma}/\lambda = 0.47$
$\bar{\sigma}/\bar{a} = 0.4$

MCR		Data
——·——	10	◯
————	30	■
— — —	60	▼
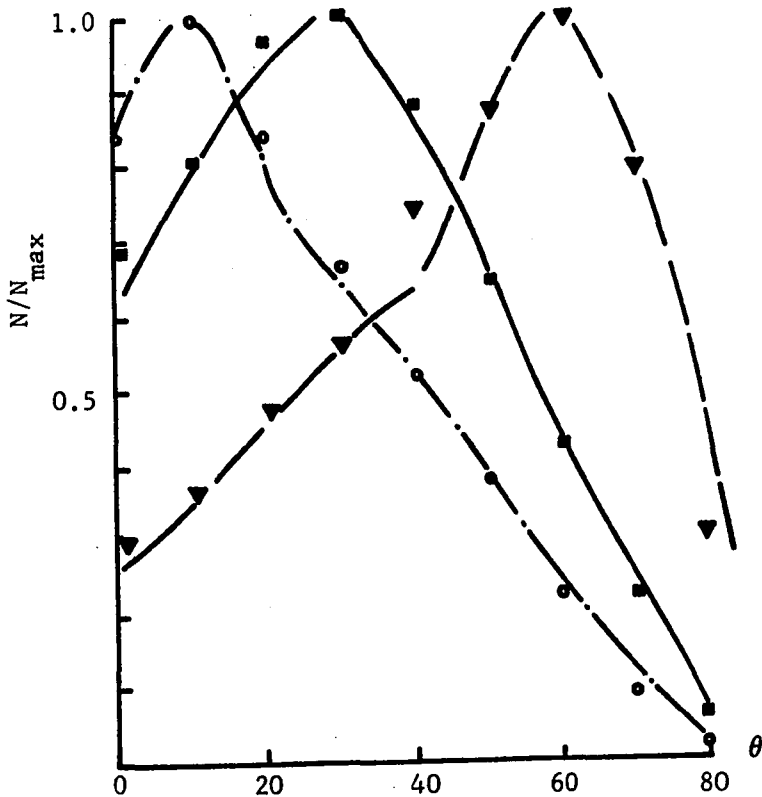
Figure 5-15. Graphical Comparison of Raw Data of Francis and MCR Output

Data: σ_0 / λ = 0.705
λ = 2.0 μ

MCR: P = 0.62
$\bar{\sigma} / \lambda$ = 0.705
$\bar{\sigma} / \bar{a}$ = 0.4

MCR		Data
—·—·—	10	◉
———	30	■
— — —	60	▼
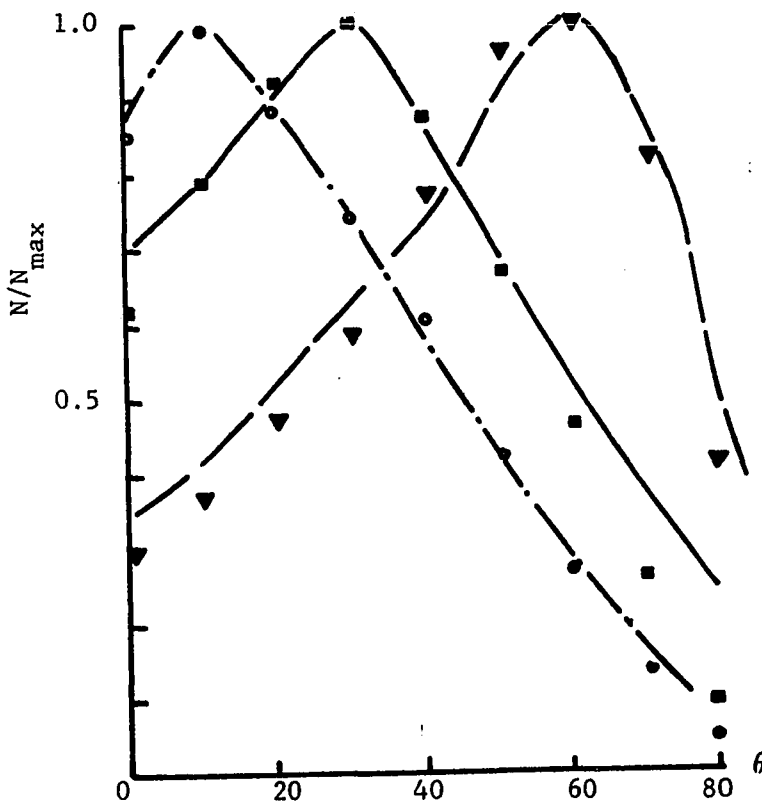
Figure 5-16. Graphical Comparison of Raw Data of Francis and MCR Output

Data: σ_0 / λ = 0.94
λ = 1.5 μ

MCR: P = 0.62
$\bar{\sigma} / \lambda$ = 0.94
$\bar{\sigma} / \bar{a}$ = 0.4

MCR		Data
—·—·—	10	○
———	30	■
— — —	60	▼

TABLE 5-1

EXAMPLE ERROR BAND OF MCR FOR 90% CONFIDENCE
LEVEL AND 10,000 SAMPLES

θ	Hits	Error
10	670	±3.0%
20	650	±3.2%
30	580	±3.4%
40	410	±4.0%
50	270	±4.6%
60	150	±7.0%

Thus there is 90% confidence that the position of the points on the solid curve are true to within the stated error bands. These error bands are at least as good as the experimental error.

CHAPTER VI

FINAL STATEMENTS

This research has been an attempt to contribute to the solution
of the problem of understanding the effects of rough surface characteris-
tics upon reflected distributions.   In doing so, the artifice of a pene-
tration depth for first incidence was introduced.   The localization circle
(used to determine this penetration depth and whose radius is the wave-
length of the incident radiation) was quite unique and basic to this
research and when associated with this model of the surface is seemingly
adequate.   A theoretical analysis using this assumption may be fruitful.

Table 6-1 is a compilation of the experimental and MCR parameters
used.   It may be seen from this table that a wide range of surface charac-
teristics have been investigated.   And since the MCR output fit these
data quite well, except for one case, it may be inferred that not only a
peak to valley dimension be measured, but also peak to peak dimension.
In addition, another in-surface parameter seems essential for an accurate
description of the total reflected distribution.   This dimension is in
the plane of the surface and is representative of the portion of the surface
that is contributing to the regularly reflected component.   Though not an
object of this investigation or an output of MCR, some general statements
may be made concerning this parameter:

TABLE 6-1

EXPERIMENTAL AND MCR PARAMETERS

Sample	$\psi \, (^{\circ})$	$\lambda \, (\mu)$	σ_0/λ	$\bar{\sigma}/\lambda$	$\bar{\sigma}/\bar{a}$	P
Al-g.g. (1)	10	1.0	0.58	0.60	0.5	0.40
Nickel (1)	10	1.0	0.60	0.60	0.5	0.50
Nickel (1)	10	1.5	0.32	0.30	0.5	0.50
Nickel (1)	10	6.0	0.23	0.30	0.5	0.60
Al-g.g. (1)	10	4.0	0.15	0.15	0.5	0.50
MgO (2)	10	0.5	1.02	1.00	5.0	0.30
MgO (2)	45	0.5	1.02	1.00	5.0	0.30
MgO (2)	10	1.5	0.34	0.34	5.0	0.30
MgO (2)	45	1.5	0.34	0.34	5.0	0.30
A.S.B. (3)	20	2.5		0.30	8.0	0.97
A.S.B. (3)	40	2.5		0.30	8.0	0.97
A.S.B. (3)	60	2.5		0.30	8.0	0.97
Al (3)	20	5.0	0.16	0.16	8.0	0.95
Al (3)	40	5.0	0.16	0.16	8.0	0.95
Al (3)	60	5.0	0.16	0.16	8.0	0.95
Al (4)	10	5.0	0.282	0.282	0.4	0.62
Al (4)	30	5.0	0.282	0.282	0.4	0.62
Al (4)	60	5.0	0.282	0.282	0.4	0.62
Al (4)	10	3.0	0.47	0.47	0.4	0.62
Al (4)	30	3.0	0.47	0.47	0.4	0.62
Al (4)	60	3.0	0.47	0.47	0.4	0.62
Al (4)	10	2.0	0.705	0.705	0.4	0.62

TABLE 6-1 (continued)

Sample		$\psi(^o)$	$\lambda(\mu)$	σ_0/λ	$\bar{\sigma}/\lambda$	$\bar{\sigma}/\bar{a}$	P
Al	(4)	30	2.0	0.705	0.705	0.4	0.62
Al	(4)	60	2.0	0.705	0.705	0.4	0.62
Al	(4)	10	1.5	0.94	0.94	0.4	0.62
Al	(4)	30	1.5	0.94	0.94	0.4	0.62
Al	(4)	60	1.5	0.94	0.94	0.4	0.62

Al-g.g.(1) - Aluminum Coated Ground Glass - From Birkebak

Nickel (1) - Roughened Nickel - From Birkebak

MgO   (2) - Magnesium Oxide Crystal - From Torrance & Sparrow

A.S.B. (3) - Aluminum Coated Sintered Bronze - From Herald & Edwards

Al   (3) - Sandblasted Aluminum - From Herold & Edwards

Al   (4) - Sandblasted Aluminum - From Francis

1) That portion of the surface that would be represented

by this parameter is effectively flat.

2) This portion of the surface must effectively increase

as the wavelength increases.

Neither of these parameters have received much attention experimentally

and to this investigator, these parameters are vital information when

presenting reflectance data. An analysis similar to that presented in

Appendix D might be used to determine $\bar{a}$ and this flatness parameter by

one experimental measurement.

Evidently the state of the surface must be specified in a statis-

tical manner. In an attempt to establish a Monte Carlo model for reflec-

tion, it was assumed that the surface roughness, σ, and the density length, a, were Rayleigh distributed random numbers. The assumed Rayleigh distribution for the roughness parameter, σ, is apparently not too bad. This may not have been an accurate assumption for the density length, since to fit experimental data a portion of the surface has to be assumed flat. Experimental effort must be exerted in an attempt to measure these in-surface parameters such that a more accurate distribution function may be considered. Also it may be noted that the reflected energy distribution is dependent upon the curvature of the surface near the peaks as indicated by the variation of the parameter P. Though an extremely difficult task, the development of a method to estimate this type of parameter, even in a statistical fashion, would be a great help in further study and theoretical analysis of the problem of predicting the reflected energy distribution.

By examination of the graphical illustrations of the examples considered, it is evident that the model presented in this research can be made to represent experimental data. In fact, if the σ_o/λ ratio is known and the $\bar{\sigma}/\bar{a}$ ratio and P can be determined from one set of data, the wavelength and angle of incidence of the radiation may be varied and MCR will yield a close approximation to the contribution of the reflection from the rough portion of the surface. Thus this theory is regarded as suffciently justified since it can predict a qualitative picture.

LIST OF REFERENCES

1. Love, T. J., Radiative Heat Transfer, Charles Merrill Books Inc.,
    Columbus, Ohio, 1968.

2. Rossi, B., Optics, Addison-Wesley Publishing Company Inc., Reading,
    Massachusetts, 1957.

3. Dante, "La Divina Commedia, Purgatoric XV", 16-24.

4. Lambert, J. H., "Photometria sive de mensura et gradibus luminis,
    colorum et umbrae", Part I, Cap 2. Sections 53, 72, 77-81,
    Ausburg (1760).

5. Worthing, A. G., "Deviation From Lambert's Law and Polarization of
    Light Emitted By Incandescent Tungsten, Tantalum and Molybdenum
    and Change In the Optical Constants of Tungsten With Tempera-
    ture", Journal of the Optical Society of America, 13, 635 (1926).

6. Harrison, V. G. W., "The Light-Diffusing Properties of Magnesium
    Oxide", The Printing and Allied Trades Research Association,
    London, p. 408, 1946.

7. Hill, A. J., "A First-Order Theory of Diffus Reflecting and Trans-
    mitting Surfaces", Journal of the Society of Motion Picture
    Technical Engineers, 61, 19 (1953).

8. Middleton, W. E. K., "An Improved Sphere Paint", Illuminating En-
    gineering, 48, 254 (1953).

9. Agnew, J. T. and McQuistan, R. B., "Experiment Concerning Infrared
    Diffuse Reflectance Standards in the Range 0.8 to 20.0 Microns",
    Journal of the Optical Society of America, 43, 999 (1953).

10. Budde, W., "Standards of Reflectance", Journal of the Optical Society
    of America, 50, 217 (1960).

11. Rambauske, W. R. and Roettele, D. L., "Investigation of Optical Cross-
    Sections for Laser-Radar", Technical Documentary Report No.
    ASD -TDR - 62 - 726, Navigation and Guidance Laboratory, Aero-
    nautical Systems Division, Wright-Patterson Air Force Base,
    Ohio, March, 1962.

12. Hapke, B. W. and Horn, H. W., "Photometric Studies of Complex Surfaces with Applications to the Moon", Journal of Geophysical Research, 68, #15, 4545 (1963).

13. Birkebak, R. C. and Eckert, E. R. G., "Effect of Roughness of Metal Surfaces on Angular Distribution on Monochromatic Reflected Radiation", Journal of Heat Transfer, February, 91 (1965).

14. Torrance, K. E. and Sparrow, E. M., "Biangular Reflectance of an Electric Nonconductor as a Function of Wavelength and Surface Roughness", Journal of Heat Transfer, May, 283 (1965).

15. Look, D. C., "Diffuse Reflection from a Plane Surface", Journal of the Optical Society of America, 55, 1628 (1965).

16. Herold, L. M. and Edwards, D. K., "Bidirectional Reflectance Characteristics of Rough, Sintered-Metal", 3rd Aerospace Sciences Meeting (AIAA), 24-26, Jan., 1966.

17. Brandenberg, W. M. and Neu, J. T., "Unidirectional Reflectances of Imperfectly Diffuse Surfaces", Journal of the Optical Society of America, 56, 97 (1966).

18. Torrance, K. E. and Sparrow, E. M., "Off-Specular Peaks in the Directional Distribution of Reflected Thermal Radiation", Journal of Heat Transfer, May, 1966.

19. Torrance, K. E., Sparrow, E. M. and Birkebak, R. C., "Polarization, Directional Distribution, and Off-Specular Peak Phenomena in Light Reflected from Roughened Surfaces", Journal of the Optical Society of America, 56, 916 (1966).

20. Miller, E. R. and Von Kannon, R. S., "Development of a Bidirectional Spectroreflectometer", Thermo-physics of Spacecraft and Planetary Bodies, Vol. 20, 219 Academic Press, New York, 1967.

21. Grabowski, L., "On the Theoretical Photometry of Diffuse Reflection", Astrophysics Journal, 39, 299 (1914).

22. Russell, H. N., "On the Albedo of Planets and Their Satellites", Astrophysics Journal, 43, 173 (1916).

23. Berry, E. M., "Diffuse Reflection of Light From a Matt Surface", Journal of the Optical Society of America, 7, 627 (1923).

24. Pokrowski, G. I., "Zur Theorie der Diffusen Lichtrefexion", Z. Phys.,
    Part I : 30 66 (1924)
    Part II : 35, 34 (1925)
    Part III: 35, 390 (1926)
    Part IV : 36, 472 (1926).

25. Barkas, W. W., "Analyses of Light Scattered from a Surface of
        Low Glass Into Its Specular and Diffuse Components", Proceedings,
        of the Physical Society, 51(2), 274 (1939).

26. Middleton, W. E. K. and Mungall, A. G., "The Luminous Directional
        Reflectance of Snow", Journal of the Optical Society of America,
        42, 572 (1952).

27. Melamed, N. T., "Optical Properties of Powders - Part I. Optical
        Absorption Coefficients and the Absolute Value of Diffuse
        Reflectance - Part II. Properties of Luminescent Powders",
        Journal of Applied Physics, 34, 560 (1963).

28. Hapke, B. W., "A Theoretical Photometric Function for the Lunar
        Surface", Journal of Geophysical Research, 68, #15, 4571 (1963).

29. Schatz, E. A., "Reflectances of Compacted Powder Mixtures",
        Journal of the Optical Society of America, 57, 941 (1967).

30. Nelson, H.F. and Goulard, R., "Reflection from a Periodic Dielectric
        Surface", Journal of the Optical Society of America, 57, 760
        (1967).

31. Torrance, K. E. and Sparrow, E. M., "Theory for Off-Specular
        Reflection From Roughened Surfaces", Journal of the Optical
        Society of America, 57, 1105 (1967).

32. Hammond, H. K. (III) and Nimeroff, I., "Measurement of Sixty-
        Degree Specular Gloss", Journal of Research of the National
        Bureau of Standards, 44, 585 (1950).

33. Hunter, R. S., "Gloss Evaluation of Materials", A S T M Bulletin,
        T P 190, 48 (1952).

34. Nimeroff, I., "Analyses of Goniophotometric Reflection Curves",
        Journal of the Optical Society of America, 42, 579 (1952).

35. Middleton, W. E. K., and Mungall, A. G., "An Instrument for
        the Measurement of Distinctness-of-Image Gloss", Canadian
        Journal of Technology, 31, 60 (1953).

36. Ament, W. S., "Toward a Theory of Reflection by a Rough Sur-
        face", Proceedings of the I.R.E., 41, 142 (1953).

37. · Feinstein, J., "Some Stochastic Problems in Wave Propagation
        Part I" I.R.E. Transactions AP-2, 23 (1954).

38. Spetner, L. M., "A Statistical Model for Forward Scattering of
        Waves Off a Rough Surface", I.R.E. Transactions, Ap-6,
        88 (1958).

39. Davies, H., "Reflection of Electromagnetic Waves From a Rough Surface", Proceedings of the Institute of Electric Engineers, 101, 209 (1954).

40. Porteus, J. O., "Relation Between the Height Distribution of a Rough Surface and the Reflectance at Normal Incidence", Journal of the Optical Society of America, 53, 1394 (1963)

41. Beckmann, P. and Spizzichino, A., The Scattering of Electromagnetic Waves From Rough Surfaces, MacMillan Company, New York, (1963).

42. Oberhettinger, F., "On Asymptotic Series for Function Occurring in the Theory of Diffraction of Waves by Wedges", Journal of Mathematics and Physics, 34, 245 (1956).

43. Oberhettinger, F., "On the Diffraction and Reflection of Waves and Pulses by Wedges and Corners", Journal of Research of the National Bureau of Standards, 61(5), 343 (1958).

44. Lebedev, N. M. and Skal'skaya, I. P., "A New Method for Solving the Problems of Diffraction of Electromagnetic Waves By a Wedge with Finite Conductivity", Soviet Physics - Technical Papers, 7(10), 867 (1963).

45. Clark, J. A., Theory and Fundamental Research in Heat Transfer, Macmillan Company, New York, 1963.

46. McNicholas, H. J., "Absolute Methods of Reflectometry", Journal of Research of the National Bureau of Standards, 1, 29 (1928).

47. Von Fragstein, C., Optik, 12, 60 (1955).

48. Nicodemus, F. E., "Directional Reflectance and Emissivity of an Opaque Surface", Applied Optics, 4(7).767 (1965).

49. Gorton, A. F., "Reflection From, and Transimssion Through, Rough Surfaces,". Physical Review, 7, 66 (1916).

50. Chinmayanandam, T. K., "On the Specular Reflection From Rough Surfaces", Physical Review, 13, 96 (1918).

51. Spetner, L. M. "Discussion of Reference 39", Proceedings of the Institute of Electrical Engineers, 102 (III), 148 (1955).

52. Houchen, A. F. and Hering, R. G., "Bidirectional Reflectance of Rough Metal Surfaces", Thermophysics of Spacecraft and Planetary Bodies, 20, 65 (1967), Academic Press, New York, 1967.

53. Birkebak, R. C., "Monochromatic Directional Distributionaof Reflected Thermal Radiation From Roughened Surfaces", Ph.D. Dissertation, Mechanical Engineering Dept., University of Minnesota, Minneapolis, Minn. (September 1962).

54. Bennett, H. E. and Porteus, J. O., "Relation Between Surface Roughness and Specular Reflectance at Normal Incidence", Journal of the Optical Society of America, 51, 123 (1961).

55. Arley, N. and Buch, K. R., Introduction to the Theory of Probability and Statistics, John Wiley and Sons, Inc., New York (1950).

56. Feller, W., Introduction to the Theory of Probability and Its Applications, Vol I., John Wiley and Sons, Inc., New York, 1950.

57. Scofield, G. L., "Radiative Heat Transfer From An Arbitrary Plane Source to a Semi-Infinite Aerosol", Ph.D. Dissertation, Aerospace and Mechanical Engineering, University of Oklahoma, Norman, Oklahoma, (May, 1968).

58. Stockham. L. W., "Radiative Heat Transfer From a Finite Cylindrical Particle Cloud:, Ph.D. Dissertation, Aerospace and Mechanical Engineering, University of Oklahoma, Norman, Oklahoma (May 1967).

59. Howell, J. R. and Perlmutter, M., "Monte Carlo Solution of Thermal Transfer Through Radiant Media Between Gray Walls", Transactions of the ASME, February 1964, pp. 169.

60. Perlmutter, M. and Howell, J. R., "Radiant Transfer from Gray Gas Between Concentric Cylinders Using Monte Carlo", Journal of Heat Transfer, 4(4). 669 (1965).

61. Corlett, R. C., "Direct Monte Carlo Calculation of Radiative Heat Transfer in Vacuum", Transactions of the ASME, November, 1966, pp. 519.

62. Campbell, P. M., "Monte Carlo Method for Radiative Transfer", International Journal of Heat and Mass Transfer, 10 (4) 519 (1967).

63. Bohm, D., Quantum Theory, Prentice-Hall, Inc., Englewood Cliffs, New Jersey, 1951).

64. Menzel, D. H. (editor), Fundamental Formulas of Physics, Volume II, Dover Publications, Inc., New York, 1960.

65. Francis, R. E., "The Experimental Determination of Reflectance Functions for Type 302 Stainless Steel", Masters Thesis. Aerospace and Mechanical Engineering Department, University of Oklahoma, Norman, Oklahoma (May, 1967).

66. Funai, A. I. and Rolling, R. E., "Inspection Techniques for the Characterization of Smooth, Rough, and Oxidized Surfaces", Thermophysics of Spacecraft and Planetary Bodies, 20, 41 (1967), Academic Press, New York, 1967.

67. Born, M. and Wolf, E., Principles of Optics, Electromagnetic Theory of Propagation, Interference and Diffraction of Light, Pergamon Press, London, 1959.

68. Poincare', H., "Theorie Mathe'matique de la lumiere', Paris, George Carre', II, 187 (1892).

69. Kaplan, W., Advanced Calculus, Addison Wesley Publishing Company, Inc., Reading, Massachusetts, 1952.

APPENDIX A

DIFFRACTION THEORY (67)

Huygens - Fresnel

Huygen, the first proponent of the wave theory of electromagnetic

radiation, described propagation of wave disturbances in the following

fashion: Every point on a wavefront propagating from a source is a

source of secondary wavelets and the wavefront at any instant of time

later is the result of the superposition (envelope) of these secondary

wavelets. Fresnel accounted for diffraction by assuming that these

secondary wavelets mutually interfere.   This combination is generally

referred to as the Huygens-Fresnel Principle. To understand this state-

ment, consider the spherical, monochromatic wavefront of radius r_o at

some instant in time, propagating from P_o to P'.

Deleting the time variation, the disturbance at Q may be re-

presented by $(A \exp (ikr_o))/r_o$. Using the Huygens-Fresnel principle,

this point (Q) is now the source of a secondary wavelet and its contri-

bution to the total disturbance at P' is

$$du = K(\alpha) \frac{Ae^{ikr_o}}{r_o} \frac{e^{ikr}}{r} dS$$

where $K(\alpha)$ is called an inclination or obliquity factor which describes

the variation with direction of the amplitude of the secondary wavelet.

Thus the total disturbance at P' is

91
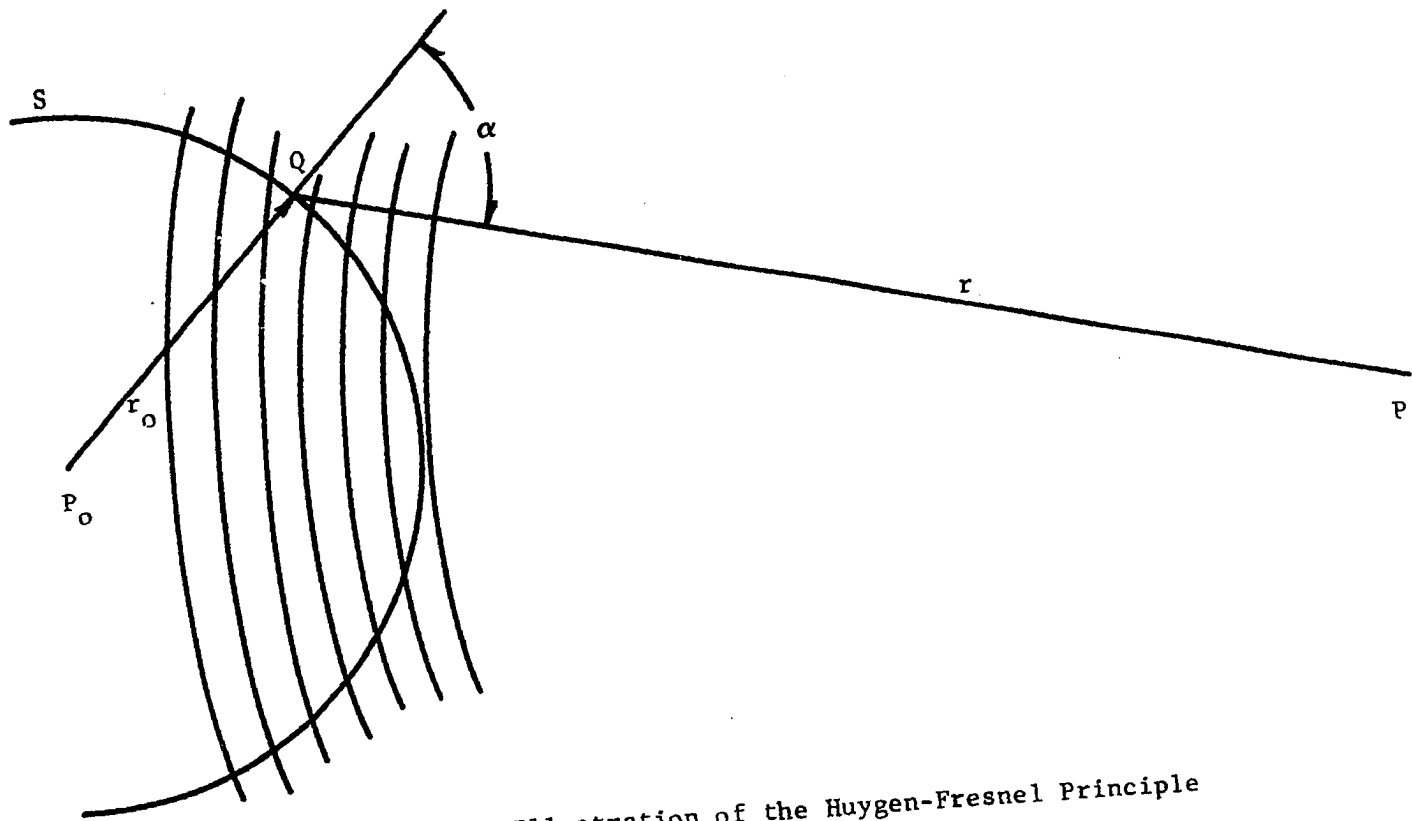
Figure A-1.   Illustration of the Huygen-Fresnel Principle

$$u = \frac{Ae^{ikr_0}}{r_0} \int \int \frac{e^{ikr}}{r} K(\alpha) \, dS \quad .$$

Kirchhoff

Kirchhoff put the Huygens-Fresnel theory on sounder mathematical grounds and showed that this principle yields an approximate form of an integral solution to the homogeneous wave equation.

Consider a monochromatic scaler wave

$$V(x,y,z,t) = U(x,y,z)e^{-iwt}$$

where $\omega = k \, c$. In a vacuum the space dependent portion satisfies the time-independent wave equation

$$(\nabla^2 + k^2)u = 0 \quad . \tag{A-1}$$

This equation is usually referred to as the Helmholtz equation.

Now assuming U and any other function U' have continuous first and second partial derivatives within and on the surface, we may invoke Greens' Theorem to obtain

$$\int \int \int (u\nabla^2 u' - u'\nabla^2 u) \, dv = - \int \int \left(u \frac{\partial u'}{\partial n} - u \frac{\partial u}{\partial n} \right) dS. \tag{A-2}$$

Note $\frac{\partial}{\partial n}$ is the derivative along the inward normal. If, in addition U' also satisfies the Helmholtz equation, the left side of (A-2) vanishes, yielding

$$\int \int \left(u \frac{\partial u'}{\partial n} - u' \frac{\partial u}{\partial n} \right) dS = 0. \tag{A-3}$$

Assuming $U' = e^{ikr}/r$, and noting that a singularity exists at $r = 0$, if the fiducial point is within the surface S, the integration must exclude this point due to the aforementioned continuity requirements. Thus equation (A-3) has the form

$$\left\{ \iint_S + \iint_{S'} \right\} \left[u \frac{\partial}{\partial n} \left(\frac{e^{ikr}}{r} \right) - \frac{e^{ikr}}{r} \frac{\partial u}{\partial n} \right] dS = 0, \tag{A-4}$$

where S' is the region around the singular point. Assume S' is a spherical region of radius ϵ. Then equation (A-4) may be put in the form

$$\iint_S \left[u \frac{\partial}{\partial n} \left(\frac{e^{ikr}}{r} \right) - \frac{e^{ikr}}{r} \frac{\partial u}{\partial n} \right] dS$$

$$= - \iint \left\{ u \frac{e^{ik\epsilon}}{\epsilon} \left(ik - \frac{1}{\epsilon} \right) - \frac{e^{ik\epsilon}}{\epsilon} \frac{\partial u}{\partial n} \right\} \epsilon^2 \, \partial\Omega, \tag{A-5}$$

where $\partial\Omega$ is the element of the solid angle. Note in the limit as ϵ approaches zero, the right side of equation (A-5) has the form

$$\lim_{\epsilon \to o} \iint u e^{ik\epsilon} \, \partial\Omega = 4\pi u$$

$$\therefore \quad u = \frac{1}{4\pi} \iint_S \left[u \frac{\partial}{\partial n} \left(\frac{e^{ikr}}{r} \right) - \frac{e^{ikr}}{r} \frac{\partial u}{\partial n} \right] dS. \tag{A-6}$$

This is the integral theorem of Helmholtz and Kirchhoff in general form. Notice that the Kirchhoff approach uses in a general fashion the Huygens-Fresnel Principle, but is not restricted by rules governing the contributions of different elements of the propagating surface of the disturbance. Kirchhhoff went on to show that his theorem may be reduced to an approximate and simpler form which is essentially equivalent to the formulation of Fresnel and yielded additional information about the obliquity factor.

The major drawback to obtaining the Fresnel approximation is in the assumptions made concerning the behavior of U and $\frac{\partial u}{\partial n}$ in the immediate vicinity of the edge of the aperture. These assumptions are

in A $\qquad$ $U = U^{(i)}$ $\qquad$ and $\dfrac{\partial u}{\partial n} = \dfrac{\partial u}{\partial n}^{(i)}$

in B $\qquad$ $U = 0$ $\qquad$ and $\dfrac{\partial u}{\partial n} = 0$ $\qquad\qquad$ (A-7)

where A represents the region of the aperture, B represents the region on the non-illuminated side of the screen in which region A is and $U^{(i)}$ is the incident wave disturbance. Equations (A-7) are known as the Kirchhoff's boundary conditions and are the basis of the Kirchhoff's diffraction theory. The consequences of this assumption have been discussed in the literature and have been found to be in error on the boundaries of the aperture (68).

Nevertheless, the Kirchhoff theory is considered entirely adequate as long as the wavelength of the radiation is quite small in comparison with the size of the aperture or diffracting obstacle. When this last requirement is not true, more refined methods must be used and of the cases considered, only a few have resulted in solutions.

APPENDIX B

RAYLEIGH DISTRIBUTION DISCUSSION

For the model discussed in this research, the height distribution, for example, cannot range from $-\infty$ to $+\infty$. From the mathematical model discussed in Chapter IV, the height distribution can range from 0 to $+\infty$. Thus a nonsymmetrical distribution seems in order. No physical reasoning yields a requirement for the distribution. Thus intuition was the major factor in the decision to use a Rayleigh distribution. This distribution seems adequate when the probability of a perfectly flat surface is zero and any height may be expected. Also the majority of the heights considered should be nonsymmetrically positioned between 0 and ∞.

The Rayleigh distribution may be derived from two normal distributions, both with a mean of zero and the identical variances. Consider the two normal distributions

$$F_1(y_1;0,\sigma) = \frac{1}{\sigma\sqrt{2\pi}} \int_{-\infty}^{y_1} e^{-s^2/(2\sigma^2)} \, dS$$

$$F_2(y_2;0,\sigma) = \frac{1}{\sigma\sqrt{2\pi}} \int_{-\infty}^{y_2} e^{-t^2/(2\sigma^2)} \, dt.$$

Let $G(y_1,y_2,\sigma) = \frac{1}{2\pi\sigma^2} \int_{-\infty}^{y_1} e^{-s^2/(2\sigma^2)} \, dS \int_{-\infty}^{y_2} e^{-t^2/2\sigma^2} \, dt$.

But since s and t are independent

$$G(y_1, y_2, \sigma) = \frac{1}{2\pi\sigma^2} \int_{-\infty}^{y_1} \int_{-\infty}^{y_2} e^{-(t^2 + s^2)/2\sigma^2} \, dt \, dS.$$

Consider the following change of variables:

$$x^2 = S^2 + t^2$$

$$z = \tan^{-1} \frac{S}{t}$$

$$S = x \cos z$$

$$t = x \sin z .$$

Thus the Jacobian of transformation (69) is

$$dSdt = \frac{\partial(S,t)}{\partial(x,Z)} \, dxdZ$$

$$= \begin{vmatrix} \dfrac{\partial S}{\partial x} & \dfrac{\partial S}{\partial Z} \\[2mm] \dfrac{\partial t}{\partial x} & \dfrac{\partial t}{\partial Z} \end{vmatrix} \, dxdZ = xdxdZ.$$

So

$$G(y_1, y_2, \sigma) = \frac{1}{2\pi\sigma^2} \int_0^{y_1} \int_0^{y_2} xe^{-x^2/2\sigma^2} \, dxdZ.$$

Integrating z from 0 to 2π

$$G(y_1, \sigma) = \frac{1}{\sigma^2} \int_0^{y_1} xe^{-x^2/2\sigma^2} \, dx.$$

Thus by definition the probability density function is

$$g(x, \sigma) = \frac{x}{\sigma^2} e^{-x^2/2\sigma^2} \qquad\qquad\qquad \text{(B-1)}$$

where now the random variable x is related to two normally distributed random variables y_1 and y_2 by the relation

$$x = \sqrt{y_1^2 + y_2^2} \qquad . \qquad\qquad\qquad \text{(B-2)}$$

Equation (B-1) is the density function for a Rayleigh distributed random variable. The cumulative Rayleigh distribution follows immediately from the definition:

$$F(x,\sigma) = \int_0^x \left(\frac{y}{\sigma^2}\right) e^{-y^2/2\sigma^2} \, dy = 1 - e^{-x^2/2\sigma^2}, \quad x \geq 0. \tag{B-3}$$

The expected or mean value is

$$E(x,\sigma) = \int_0^\infty \left(\frac{y^2}{\sigma^2}\right) e^{-y^2/2\sigma^2} \, dy = \sigma\sqrt{\frac{\pi}{2}} = \mu.$$

The first moment is zero as it is supposed to be and the second moment or variance is

$$E(x - \mu)^2 = \text{Var } (x) = \int_0^\infty (x - \mu) g(x,\sigma) dx$$

$$= \left(\frac{4 - \pi}{2}\right) \sigma^2 = 0.429 \, \sigma^2.$$

A means to generate numbers distributed in a random fashion according to this Rayleigh law follows immediately from the above derivation. That is, one needs only to have sets of normally distributed random numbers and then using (B-2), the Rayleigh distributed number may be obtained. To generate the normally distributed random numbers, the subroutine, GAUSS, suggested by IBM was used. When these were determined, equation (B-2) yielded the appropriate Rayleigh distributed random variable.

It seemed desirable to check the output of this procedure. It must be remembered that due to the finite number of the random variables considered, exact fit with the actual distribution function is impossible. Thus what is next presented is only an indication that the random variables are distributed correctly.

The computer program which appears at the end of this appendix was used to check the resulting distribution. The outputs of this program were counted as to those between 0 and 0.5σ, 0.5σ and σ, ----, 2.0σ and infinity. Five different starting numbers were considered. The results appear in the following table.

TABLE B-1

CUMULATIVE RAYLEIGH DISTRIBUTION USED IN MCR AND THE IDEAL

IX	1	11	111	1111	11111	AVG	ΔF
0 - 0.5σ	0.124	0.100	0.101	0.112	0.114	0.110	0.1175
0.5σ - 1.0σ	0.258	0.281	0.280	0.255	0.251	0.265	0.2760
1.0σ - 1.5σ	0.278	0.288	0.278	0.285	0.282	0.280	0.2819
1.5σ - 2.0σ	0.210	0.182	0.196	0.202	0.222	0.190	0.1893
2.0σ - ∞	0.130	0.149	0.145	0.146	0.131	0.140	0.1353

Five runs of 1,000 points each were considered. Column 1 exhibits the collection regions of the generated random numbers. Because of the manner of collection (dependent on σ), the only variable is the starting numbers IX. The next five columns are the relative number collected per region. Column seven is the average over the 5,000 points considered. The last column designated, ΔF, is the theoretical relative number that should be in each region. As can be seen, the agreement is quite good considering the sample size. This was deemed acceptable agreement.

CUMULATIVE RAYLEIGH DISTRIBUTION PROGRAM

```
      READ (2,15)  S,    IX

  15 FORMAT (1F10.0,16)
      K1            =   0
      K2            =   0
      K3            =   0
      K4            =   0
      K5            =   0
      AM            =   0
      V2            =   0.0
      IC            =   100
      DO 10 I=1,1000
      DO 20 J=1,2
      CALL GAUSS (IX,S,AM,V)
      V2            =   V2 + V*V
  20 CONTINUE
      SV2           =   SQRT(V2)
      IF (SV2 - 0.5*S) 1,1,2
   1 K1            =   K1 + 1
      GO TO 9
   2 IF (SV2-S)  3,3,4
   3 K2            3   K2 + 1
      GO TO 9
   4 IF (SV2 - 1.5*S) 5,5,6
   5 K3            =   K3 + 1
      GO TO 9
   6 IF (SV2 - 2.*S)  7,7,8
   7 K4            =   K4 + 1
      GO TO 9
   8 K5            =   K5 + 1
   9 V2            =   0.0
      IF (I-IC)  10,25,25
  25 IC            =   IC . 100
      WRITE (3,30) I,SV2,K1,K2,K3,K4,K5
  10 CONTINUE
  30 FORMAT (15, F12.7,515)
      CALL EXIT
      END
```

APPENDIX C

MCR COMPUTER PROGRAM

Legend

The following definitions are provided to clarify the coding in the following computer program.

Code Symbol	Meaning
SOA	Characteristic parameter of the total surface
SOL	Characteristic roughness-wavelength ratio for total surface
P	Degree of roundness
PSI	Angle of incidence
AN	Real portion of the index of refraction
AK	Imaginary portion of the index of refraction
IX	Starting number for random number generators
N	Total number of points for the run
NCO	Number of points run before first data is printed
NCOL	Interval (number of points run) of data printout after NCO
ASF	Smoothness factor
SOL1	Input SOL (see above)
SOA1	Input SOA (see above)
AM	Required mean of Gaussian distributions
PSIM5	Angle of incidence minus five degrees
PSIP5	Angle of incidence plus five degrees

101

Code Symbol	Meaning
PH	Direction in which energy bundle is traveling
PSI1	Angle of incidence in radians
KP(I)	Number of energy bundles in region I, $1 \leq I \leq 36$ (5 degree intervals)
KPP(I)	Number of energy bundles in region I where $1 \leq I \leq 10$ (1 degree interval from PSIM5 to PSIP5)
KLOST	Number of energy bundles lost through the surface by refraction
KTRAP	Number of energy bundles lost on fifth reflection
K1R	Number of energy bundles that escape after one reflection
K2R	Number of energy bundles that escape after two reflections
K3R	Number of energy bundles that escape after three reflections
K4R	Number of energy bundles that escape after four reflections
SOL	Height to wavelength ratio per energy bundle
SOA	Height to width ratio to energy bundle
RSOA	Reciprocal of SOA
HOS	Normalized depth of penetration-height ratio
XOA	Normalized V-groove vertex position
H1	Left hand center of curvature for rounded portion normalized by σ
H2	Right hand center of curvature for rounded portion normalized by σ
B1	Radius of curvature of left hand rounded portion normalized by a
B2	Radius of curvature of right hand rounded portion normalized by a
S1	Slope of left hand side of V-groove
S2	Slope of right hand side of V-groove

Code Symbol	Meaning
X1	Horizontal coordinate of the left hand transition point from rounded portion to V-groove normalized to a
X2	See XOA
X3	Horizontal coordinate of the right hand transition point from rounded portion to V-groove normalized to a
TO	See S1
T2O	TO times TO
ANX	Horizontal component of the unit normal to the left hand portion of the V-groove
ANY	Vertical component of the unit normal to the left hand portion of the V-groove
Y1B	Vertical component of the left hand transition point from rounded portion to V-groove normalized to σ
Y2B	Vertical component of the right hand transition point from rounded portion to V-groove normalized to σ
XSR1	Horizontal coordinate of the intersection of HO with the left side of surface normalized to a
XSR2	Horizontal coordinate of the intersection of HO with the right side of surface normalized to a
XP	Horizontal coordinate of shadow boundary normalized to a
YP	Vertical coordinate of shadow boundary normalized to σ
PROB	Random number selected for PROB1 decision
PROB1	Probability that the energy bundle strikes left hand side of surface first
X	Horizontal coordinate of the intersection of energy bundle with surface normalized to a
Y	Vertical coordinate of the intersection of energy bundle with surface normalized to σ
BNX	Horizontal component of the unit normal to the surface at the point of intersection (X,Y)
BNY	Vertical component of the unit normal to the surface at the point of intersection (X,Y)

Code Symbol	Meaning
RY	Vertical component of the reflected direction
RX	Horizontal component of the reflected direction
PSIR	Angle of reflectance measured from the vertical
CAN	Cosine of the local angle of incidence at the point (X,Y)
SAN	Sine of the local angle of incidence at the point (X,Y)
PSIF	Local angle of reflection
R	Local reflection coefficient
PROBR	Random number selected for R decision
K	Indicates direction of reflectance; that is right to left or left to right
RAT(I)	Ratio of the number of particles in compartment I and the maximum number of particles in a compartment
RSOL	Reciprocal of SOL
T	Slope of symmetrically positioned V-groove
TD	Complement of T
ALOSM	Maximum wave length of energy bundle when the angle of incidence is less than TD normalized to σ
ALOSP	Maximum wavelength of energy bundle when the angle of incidence is greater than TD normalized to σ
Y3(X,H1,B1)	Equation for rounded portion of left side normalized to σ
Y4(X,H2,B2)	Equation for rounded portion of right side normalized to σ
PL	Limiting value of P for regular surface configuration
X1C	Intersection of the left rounded portion and the line Y = 0 (irregular surface configuration) normalized to a
X2C	Intersection of the right rounded portion and the line Y = 0 (irregular surface configuration) normalized to a
YI	Horizontal component of the direction of the local incidence
ZI	Vertical component of the direction of the local incidence
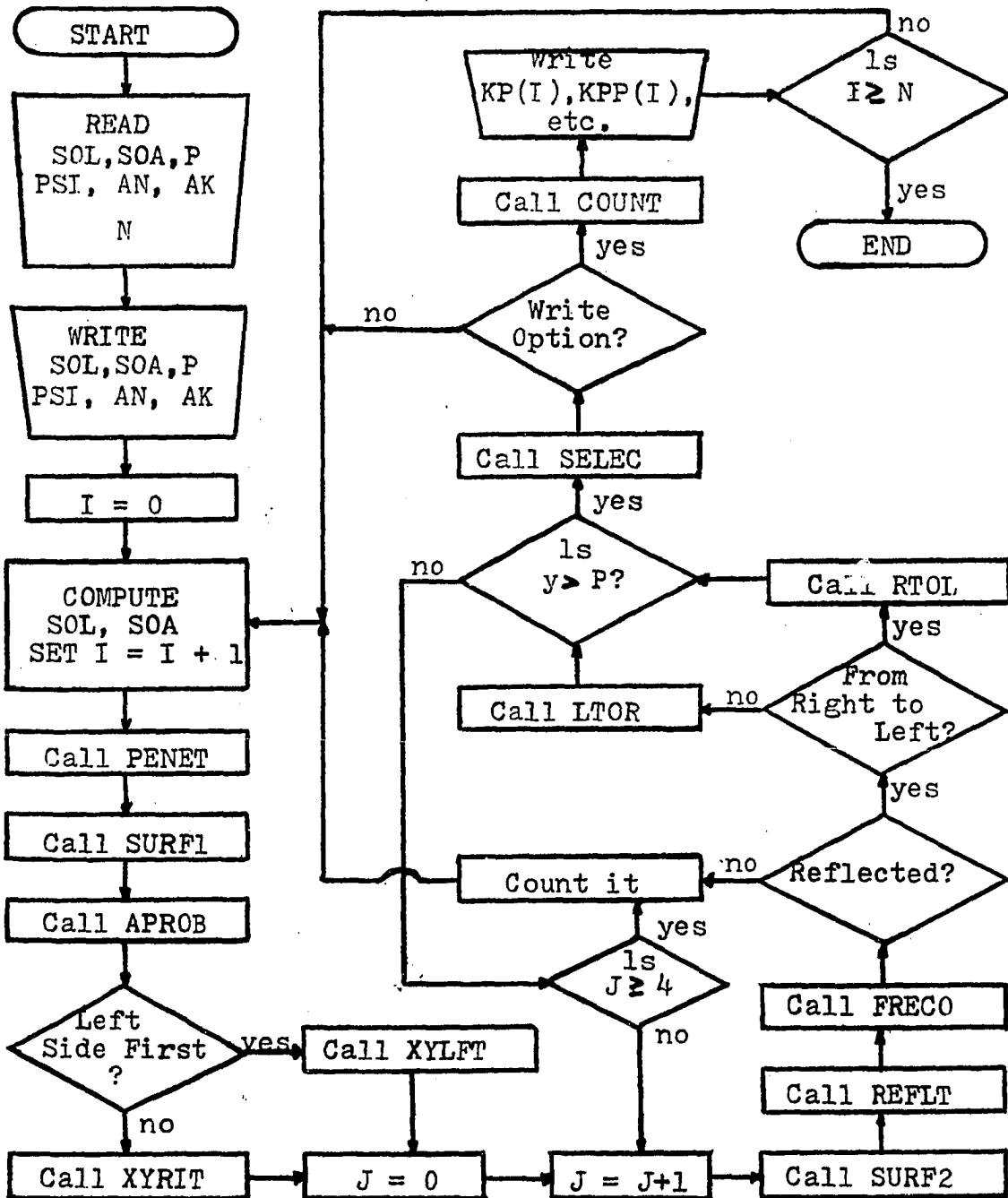
Figure C-1. Flowchart of MCR.

```
      MAIN PROGRAM - - - MCR
      DIMENSION   KP(40) ,RAT(40)   ,KPP(10)
      READ (1,3) SOA,SOL,P,PSI,AN,AK
    3 FORMAT (6F10.0)
      READ (1,2) IX,N,NCO,NCO1 ,ASF
    2 FORMAT (4I6, F6.0)
      WRITE (3,5) SOL, SOA, PSI ,P,AN,AK
    5 FORMAT (1H1, 6X, 'SIGMA / LAMDA  =', 1F12.5, / , 7X, 'SIGMA / A
     1   =', 1F12.5,/,7X,'INC-ANGLE      =', 1F12.5,/,7X,'P
     2 =',1F12.5,/7X,'REF. INDEX     =',1F12.5, /, 7X,'ABS. INDEX    ='
     3, 1F12.5)
      SOL1            =    SOL
      SOA1            =    SOA
      AM              =    0.0
      PSIM5           =    PSI - 5.
      PSIP5           =    PSI + 5.
      PH              =    PSI / 57.29578
      PSI1            =    PH
      DO  1       I =    1,40
      KP(I)           =    0
    1 CONTINUE
      DO 15   J7=1,10
      KPP(J7)         =    0
   15 CONTINUE
      KLOST           =    0
      KTRAP           =    0
      K1R             =    0
      K2R             =    0
      K3R             =    0
      K4R             =    0
      DO   955 I     =    1,N
      VSOL            =    0.
      VSOA            =    0.
      DO 7   III=1,2
      CALL GAUSS (IX, SOL1, AM, V)
      VSOL            =    VSOL + V*V
```

```
      CALL GALSS (IX, SOA1, AM, VP)
      VSOA         =    VSOA + VP*VP
    7 CONTINUE
      SOL          =    SQRT (VSOL)
      SOA          =    SQRT (VSOA)
      RSOA         =    1. / SOA
      CALL PENET (SOA, SOL, PH , HOS)
      HO           =    HOS*P
      CALL        SURF1 (SOA, XOA, IX, H1, H2, B1, B2, S1, S2, X1, X2,
     1 X3, TO, T2C, ANX, ANY, P, Y2B, Y1B, RSOA)
      CALL APFOB (SOA, P, HO, XSR1, XSR2, XP,YP, S1, PH, B1, H1, RSOA,
     1 Y1B, X1, Y2B, B2, H2, X3, S2, PROB1, ASF)
      CALL RANDU (IX, IY, PROB)
      IX           =    IY
      IF (PROB - PROB1) 10,10,20
   10 CALL XYLFT(PH, S1, IX, XP, YP, XSR1, Y1B, P, SOA, X1, H1, HO,
     1 B1, RSCA, X, Y)
      GO TO 30
   20 CALL XYRIT(PH, IX, HO, Y2B, P, RSOA, X3, XSR2, SOA, XOA, H2, B2,
     1 X,Y)
   30 DO 888   J   =    1,4
      CALL SURF2 (X,Y,P, SOA, IX, X1, H1, B1, S1, ANY, ANX, BNY, BNX
     1 , XOA, X3, S2, H2, B2, RSOA)
      CALL REFLT (BNX, BNY,PH , RX,RY,PSIR)
      CAN          =    ABS(RX*BNX + RY*BNY)
      IF (CAN - 1.)  80,81,81
   81 PSIF         =    0.0
      GO TO 53
   80 SAN          =    SQRT(1. - CAN*CAN)
      IF(CAN)      51,52,51
   52 PSIF         =    90.
      GO TO 53
   51 PSIF         =    57.29578 * ATAN(SAN/CAN)
   53 CALL FRECO (AN, AK, PSIF,BNX, BNY, R)
      CALL RANDU (IX, IY, PROBR)
      IX           =    IY
```

```
      IF (R - PROBR)        31,32,32
   31 KLOST           =      KLOST + 1
      GO TO 999
   32 IF (XOA - X)          41,42,43
   41 CALL RTOL ( SOA, P, X, Y, XOA, S1, S2, H1, H2, B1, B2, X1, X3,
     1 PSIR, RSOA, Y1B, Y2B)
      K               =      1
      GO TO 44
   42 KLOST           =      KLOST + 1
      GO TO 999
   43 CALL LTOR ( SOA, P, X, Y, XOA, S1, S2, H1, H2, B1, B2, X1, X3,
     1 PSIR, RSOA, Y1B, Y2B)
      K               =      2
   44 IF (Y - P ) 46,46,45
   45 CALL SELEC  (KP , PSIR,PSIM5, PSIP5, KPP)
      IF (J - 2) 100,101,102
  100 K1R            =       K1R + 1
      GO TO 999
  101 K2R            =       K2R + 1
      GO TO 999
  102 IF (J - 4) 103,104,104
  103 K3R            =       K3R + 1
      GO TO 999
  104 K4R            =       K4R + 1
      GO TO 999
   46 IF (K-1)              47,47,48
   47 PH             =      -(PSIR + 180.) / 57.29578
      GO TO 888
   48 PH             =      (180. - PSIR) / 57.29578
  888 CONTINUE
      KTRAP          =      KTRAP + 1
  999 PH             =      PSI1
      IF (I-N)          943,948,948
  943 IF (I - NCO)          955,945,945
  945 WRITE (3,944)  NCO
  944 FORMAT(////, 5X, 'AFTER', I7,'  BUNDLES, THE REFLECTED DISTRIBUTIO
```

```
      IN IS AS FOLLOWS')
      GO TO 930
  948 WRITE (3,947) N
  947 FORMAT ( /////, 5X, 'AFTER A TOTAL OF', I7, '   BUNDLES THE FINAL D
     1ISTRIBUTICN IS')
      NCO          =    N
  930 WRITE (3,901)
      WRITE (3,900) (KP(JI),JI=1,35,2)
      CALL COUNT (KP,RAT)
      WRITE (3,903) (RAT(II) , II=1,35,2)
      WRITE (3,902)
      WRITE (3,900)  (KP(J2)   , J2 = 2,36,2)
      WRITE (3,903) (RAT(III) , III=2,36,2)
      WRITE (3,961) PSIM5,PSIP5, (KPP(J3), J3=1,10)
  961 FCRMAT (/, 2F10.5, 10I8, /)
      WRITE (3,998) KLOST,K1R, K2R, K3R, K4R, KTRAP
      NCO          =    NCO + NCO1
  955 CONTINUE
  900 FORMAT (7X , 18I6)
  901 FORMAT(' REGIONS',4X,'1',5X,'3',   5X,'5', 5X,'7', 5X,'9',4X,'11'
     1,4X,'13', 4X,'15', 4X,'17', 4X,'19', 4X,'21', 4X,'23', 4X,'25', 4X
     2,'27', 4X,'29', 4X,'31', 4X,'33', 4X,'35')
  902 FORMAT (1H0 ,'REGIONS', 4X,'2', 5X,'4', 5X,'6', 5X,'8', 4X,'10',
     14X,'12', 4X,'14', 4X,'16', 4X,'18', 4X,'20', 4X,'22', 4X,'24', 4X
     2,'26', 4X,'28', 4X,'30', 4X,'32', 4X,'34', 4X,'36')
  903 FORMAT(7X, 18F6.3)
  998 FORMAT (1H0, 3X, 'LOSS NUMBER THROUGH THE SURFACE', I9,/,
     1 4X, 'ESCAPE NUMBER AFTER 1 REFLECTION ', I7, / ,
     2 4X, 'ESCAPE NUMBER AFTER 2 REFLECTIONS', I7, / ,
     3 4X, 'ESCAPE NUMBER AFTER 3 REFLECTIONS', I7, / ,
     4 4X, 'ESCAPE NUMBER AFTER 4 REFLECTIONS', I7, / ,
     5 4X, 'NUMBER TRAPPED IN THE V-GROOVE' , I10)
      CALL EXIT
      END
```

```
      SUBROUTINE PENET   (SOA,SOL,P  , HOS)
      T              =   ATAN(2.*SOA)
      RSOL           =   1. / SOL
      TD             =   1.5707963 - T
      IF (TD - P     )   40,10,10
   10 ALOSM          =   (SQRT(1. + 4.*SOA*SOA)) / (4.*SOA*SOA)
      IF (RSOL-ALOSM)    20,20,30
   20 HOS            =   RSOL * (SQRT(1.0 + 4.*SOA*SOA) - 1.)
      GO TO 90
   30 HOS            =   1. - RSOL + SQRT(RSOL*RSOL - (1./(2.*SOA))
     1     *(1./(2.*SOA)))
      GO TO 90
   40 BETA           =   0.5* (P- (TD))
      A              =   COS(BETA)/((COS(BETA) + 2.*SOA*SIN(BETA))
     1        *   CCS(T)  )
      B              =   - COS(P+T) / COS(P-T)
      XOB            =   B*((SIN(BETA) / COS(BETA)) + 1./(2.*SOA))
      D              =   (XOB - (1./(2.*SOA)))**2 + 1.
      E              =   (SIN(BETA) * (2.*XOB - 1./SOA) / COS(BETA)) + 2.
      F              =   1. -(A*A / (COS(BETA)*COS(BETA)))
      G              =   A*E -2.*(A*B /( COS(BETA)*COS(BETA)))
      H              =   D - B*E + B*B/(COS(BETA)*COS(BETA))
      ROOT           =   G*G + 4.*F*H
      IF (ROOT) 100,100,101
  100 ALOSM          =   -G/(2.*F)
      GO TO 102
  101 ALOSM          =   (-G + SQRT(    ROOT    )) / (2.*F)
  102 IF  (RSOL - ALOSM)  50,50,60
   50 HOS            =   (RSOL*A          )  + B - RSOL
      GO TO 90
   60 Z              =   1. / (2. * SOA)
      ALOSP          =   Z / COS(P)
      IF (RSOL - ALOSP)  70,70,80
   70 HOS            =   RSOL * SIN(P) + 1. - (COS(P)/SOA)* SIN(P)-RSOL
     1 + COS(P)* SQRT( COS(P)*((2.* RSOL*SOA) -  COS(P))/ (SOA*SOA))
      GO TO 90
```

```
80 HOSP            =     1. - RSOL + SQRT(RSOL*RSOL - (1./(2.*SOA))
  1        *(1./(2.*SOA)))
   PC              =     ATAN(2.*SOA*( HOSP + RSOL - 1.))
   IF(P-PC)85,85,70
85 HOS             =     HOSP
90 RETURN
   END
```

```
      SUBROUTINE SURF1 (SOA, XOA, IX, H1, H2, B1, B2, S1, S2, X1, X2,
     1 X3, TO, T2O, ANX, ANY, P, Y2B, Y1B, RSOA)
      C(S)           =    (SOA - P*SOA) / (SQRT(1. + S*S) - 1.)
      A(S)           =    (P*SQRT(1. + S*S) - 1.) / (SQRT(1. + S*S) - 1.)
      Y3(X,H,B)      =    H + RSOA * SQRT(B*B - X*X)
      Y4(X,H,B)      =    H + RSOA * SQRT(B*B - (X - 1.)*(X - 1.))
    1 CALL RANDU (IX,IY,XOA)
      IX             =    IY
      IF (XOA - 0.005)  1,1,3
    3 IF (XOA - 0.995)  4,4,1
    4 ANY            =    XOA / SQRT(XOA*XOA + SOA*SOA)
      ANX            =    SQRT (1. - ANY*ANY)
      S1             =    SOA / XOA
      S2             =    SOA / (1. - XOA)
      H1             =    A(S1)
      H2             =    A(S2)
      B1             =    C(S1)
      B2             =    C(S2)
      D1             =    SQRT(1. + S1*S1)
      D2             =    SQRT(1. + S2*S2)
      X1             =    S1 * B1 / D1
      X2             =    XOA
      TO             =    ANX / ANY
      T2O            =    TO*TO
      X3             =    1. - S2 * B2 / D2
      Y1B            =    Y3(X1 ,H1,B1)
      Y2B            =    Y4(X3 ,H2,B2)
      RETURN
      END
```

```
      SUBROUTINE APROB (SOA,P , HOS, XSR1, XSR2, XP, YP, S1, PH, B1,
    1 H1, RSOA, Y1B, X1, Y2B, B2, H2, X3, S2, PROBN,ASF)
      AN1(X)          =    (XSR1 - SOA*(P - HOS)*SIN(X) / COS(X))
      AD1(X)          =    1. - XSR2 + XSR1 - AN1(X)
      Z1N(X)          =    F*AN1(X) / (F*AN1(X) + AD1(X))
      AN2(X)          =    (XP     - SOA*(P - YP)*SIN(X) / COS(X))
      Z1PN(X)         =    F*AN2(X) / (F*AN2(X) + AD1(X))
      AAA             =    ASF*SIN(PH) *SIN(PH) /(COS(PH) * COS(PH))
      F               =    EXP(AAA)
      XP              =    0.0
      YP              =    0.0
      PMO1            =    1.570796 - ATAN(S1)
      IF (PH - PMC1) 5,6,6
    6 XP              =    B1 * COS(PH)
      YP              =    H1 + RSOA * SQRT (B1*B1 - XP*XP)
    5 IF (HOS - Y1B) 1,2,3
    3 XSR1            =    SQRT (B1*B1 - (HOS - H1)*(HOS - H1)*SOA*SOA)
      GO TO 8
    2 XSR1            =    X1
      GO TO 8
    1 XSR1            =    (1. - HOS) * SOA / S1
    8 IF (HOS - Y2B) 10,20,30
   30 ROOT2           =    B2*B2 - (HOS - H2)*(HOS - H2) * SOA * SOA
      XSR2            =    1. - SQRT(ROOT2)
      GO TO 11
   20 XSR2            =    X3
      GO TO 11
   10 XSR2            =    1. -  SOA*(1. - HOS) / S2
   11 IF (PH - PMO1) 35,35,40
   35 PROBN           =    Z1N(PH)
      GO TO 100
   40 IF (XSR1 - XP)   45,45,50
   45 PROBN           =    Z1N(PH)
      GO TO 100
   50 PROBN           =    Z1PN(PH)
  100 RETURN
      END
```

```
      SUBROUTINE XYLFT (PS, S1, IX, XP, YP, XSR1, Y1B, P, SOA, X1B,H1,
     1 HO, B1, RSCA, X, Y)
      PSIC         =     1.5707963 - ATAN(S1)
      CALL RANDU (IX,IY,RA)
      IX           =     IY
      AB           =     COS(PS) / SIN(PS)
      IF (PS - PSIC) 5,6,6
    6 III          =     1
      IF (XSR1 - XP) 5,7,7
    7 XSR          =     XP
      HOS          =     YP
      GO TO 8
    5 HOS          =     HO
      XSR          =     XSR1
      IF (HOS - Y1B)  1,8,8
    1 Y2MY1        =     AB*XSR + (HOS - P)*SOA
      YQMY1        =     AB*X1B + (Y1B - P)*SOA
      RBAR         =     YQMY1 / Y2MY1
      III          =     2
      IF (RA - RBAR)  8,20,10
    8 COA          =     SOA*(P - H1) + RA*(AB*XSR + (HOS - P)*SOA)
      D            =     1. + AB*AB
      ROOT         =     B1*B1*D - COA*COA
      IF (ROOT) 20,20,21
   20 IF (III - 2) 23,22,22
   23 X            =     0.0
      Y            =     P
      GO TO 100
   22 X            =     X1B
      Y            =     Y1B
      GO TO 100
   21 X            =     (AB*COA - SQRT(ROOT)) / D
      ROOT2        =     B1*B1 - X*X
      IF (ROOT2)  20,20,50
   50 Y            =        H1 + RSOA*SQRT(ROOT2)
      GO TO 100
```

```
 10  X                    =    ((P - 1.)*SOA + RA*(AB*XSR + (HOS - P)*SOA))
     1   / (AB - S1)
         Y                =    -S1*X*RSOA + 1.
100  RETURN
     END
```

```
      SUBROUTINE XYRIT (PS, IX, HOS, Y2B, P, RSOA, X2B, XSR, SOA, XOA,
    1 H2, B2, X, Y)
      AB            =     COS(PS) / SIN(PS)
      CALL RANDU (IX,IY,RA)
      IX            =     IY
      IF (HOS - Y2B) 1,10,10
    1 Y2MY1         =     (P - HOS) + AB*(1. - XSR)*RSOA
      YQMY1         =     (Y2B - HOS) + AB*(X2B - XSR)*RSOA
      RBAR          =     YQMY1 / Y2MY1
      IF (RA - RBAR) 8,9,10
    8 X             =     (SOA*XOA + (1. - XOA)*(AB*XSR + HOS*SOA + RA*
    1 (AB*(1. - XSR) + SOA*(P - HOS))))/ (SOA + AB*(1. - XOA))
      Y             =     1. - (1. - X) / (1. - XOA)
      GO TO 100
    9 X             =     X2B
      Y             =     Y2B
      GO TO 100
   10 COA           =     SOA*(HOS - H2) + AB*XSR + RA*(AB*(1. - XSR) +
    1 SOA*(P - HOS))
      PART1         =     AB*COA + 1.
      PART2         =     COA*COA + 1. - B2*B2
      D             =     1. + AB*AB
      ROOT          =     PART1*PART1 - D*PART2
      IF (ROOT) 20,20,21
   20 X             =     1.
      Y             =     P
      GO TO 100
   21 X             =     (PART1 - SQRT (ROOT)) / D
      ROOT3         =     B2*B2 - (1. - X)*(1. - X)
      IF (ROOT3) 9,9,300
  300 Y             =     H2 + RSOA*SQRT(ROOT3)
  100 RETURN
      END
```

```fortran
      SUBROUTINE SURF2( X, Y, P, SOA, IX, X1, H1, B1, S1, ANY,ANX,BNY,
     1 BNX,XOA,X3,  S2, H2, B2, RSOA)
      PL            =     RSOA*(SQRT(1. + RSOA*RSOA) - RSOA)
      IF ( P-PL) 102,9,9
  102 IF (X3.LT.XOA.AND.XOA.LT.X1)  GO TO 101
      IF (XOA.LT.X1)  GO TO 201
      IF (X3.LT.XCA)  GO TO 301
      GO TO 9
  101 X1C           =     SQRT (B1*B1 - H1*H1*SOA*SOA)
      X2C           =     1. - SQRT(B2*B2 - H2*H2*SOA*SOA)
      IF (X.LT.X1C)  GO TO 10
      IF (X.LT.X2C)  GO TO 600
      GO TO 60
  201 X1C           =     SQRT (B1*B1 - H1*H1*SOA*SOA)
      IF (X.LT.X1C)  GO TO 10
      IF (X.LT.XOA)  GO TO 600
      IF (X.LT.X3) GO TO 50
      GO TO 60
  301 X2C           =     1. - SQRT(B2*B2 - H2*H2*SOA*SOA)
      IF (X.LT.X1)  GO TO 10
      IF (X.LT.XOA)  GO TO 30
      IF (X.LT.X2C)  GO TO 600
      GO TO 60
    9 IF (X-X1 )  10,10,20
   10 BNX           =     X / B1
      BNY           =     ((Y - H1) / B1)*SOA
      GO TO 100
   20 IF (X - XOA) 30,30,40
   30 BNX           =     ANX
      BNY           =     ANY
      GO TO 100
   40 IF (X - X3 ) 50,50,60
   50 T2            =     ATAN(S2)
      BNX           =     -SIN(T2)
      BNY           =     COS(T2)
      GO TO 100
```

```
 60 BNX           =    -(1. - X) / B2
    BNY           =    ((Y - H2)/B2)*SDA
    GO TO 100
600 BNX           =    0.0
    BNY           =    1.0
    Y             =    0.0
100 RETURN
    END
```

```
      SUBROUTINE REFLT (YN ,ZN ,P   ,RY,RZ,PSIR)
      YI            =    SIN(P)
      ZI            =    -COS(P)
      RY            =    (1.-2.*YN*YN)*YI - 2.*ZN*YN*ZI
      RZ            =    -2.*YN*ZN*YI+(1.-2.*ZN*ZN)*ZI
      IF (RY)   30,30,31
   30 IF(RZ)   32,33,33
   32 PSIR         =    -(180.0 -(ATAN(RY/RZ))*57.29578)
      GO TO 100
   33 PSIR         =    ATAN(RY/RZ)*57.29578
      GO TO 100
   31 IF   (RZ) 34,35,35
   34 PSIR         =    180.+(ATAN(RY/RZ))*57.29578
      GO TO 100
   35 PSIR         =    (ATAN(RY/RZ))*57.29578
  100 RETURN
      END
```

```
SUBROUTINE FRECO  (AN,AK,PSI,BNY,BNZ,R)
AB(P)    =  (AN*AN - AK*AK - SIN(P)*SIN(P))**2+(2.*AN*AK)**2
A2(P)    =  0.5*(SQRT(AB(P))+AN*AN -  AK*AK - SIN(P)*SIN(P))
B2(P)    =  0.5*(SQRT(AB(P))-AN*AN +  AK*AK + SIN(P)*SIN(P))
P        =  PSI  / 57.2958
RS       =  (A2(P)+B2(P)-2.*SQRT(A2(P))*COS(P)+COS(P)*COS(P))
       1 /  (A2(P)+B2(P)+2.*SQRT(A2(P))*COS(P)+COS(P)*COS(P))
        IF  (PSI - 90.) 40,45,40
40 Z     =  SIN(P)*SIN(P) / COS(P)
   GO TO 50
45 Z     =  0.0
50 RP1   =  (A2(P)+B2(P)-2.*SQRT(A2(P))*Z+Z*Z)
       1 /  (A2(P)+B2(P)+2.*SQRT(A2(P))*Z+Z*Z)
RP       =  RS * RP1
R        =  (RS + RP) / 2.
RETURN
END
```

```
      SUBROUTINE RTOL( SOA, P, XP, YP, XOA, S1, S2, H1, H2, B1, B2,
   1  X1, X3, PR, RSOA, Y1B, Y2B)
      X1B          =    X1
      X2B          =    X3
      PS           =    PR    / 57.29578
      R            =    (COS(PS) / SIN(PS))
      IF (YP - Y2B)5,5,10
   5  PSIL         =    -(1.570796 + ATAN(S2))
      GO TO 7
  10  PSIL         =    -(1.570796 + ATAN(((1. - XP)/(YP - H2)) * RSOA))
   7  IF (PS - PSIL) 90,6,6
   6  IF (Y1B - YP) 24,21,22
  21  PSIP         =    -1.570796
      GO TO 23
  22  PSIP         =    -ATAN (((XP - X1B)/(Y1B-YP))*RSOA )
      GO TO 23
  24  PSIP         =    -(1.570796 + ATAN(((YP - Y1B)/(XP - X1B))*SOA))
  23  AL           =    ATAN(((YP - H1)/ XP)*SOA)
      Q2           =    XP*XP + (YP -H1)*(YP - H1)*SOA*SOA
      BE           =    ATAN (B1 / SQRT(Q2 - B1*B1))
      PSIPP        =    -(1.570796 - (BE - AL))
      IF (PS - PSIP) 20,20,30
  20  XC           =    (SOA - YP*SOA + R*XP) / (R + S1)
      YC           =    R*(XC - XP)*RSOA + YP
      GO TO 60
  30  IF (PS - PSIPP) 40,40,50
  40  PART1        =    R*XP - (YP - H1)*SOA
      D            =    1. + R*R
      ROOT         =    B1*B1*D - PART1*PART1
      IF (ROOT) 50,42,43
  43  XC           =    (R*PART1 + SQRT(ROOT)) / D
      GO TO 44
  42  XC           =    R*PART1 / D
  44  YC           =    R*(XC - XP)*RSOA + YP
      GO TO 60
  50  XC           =    0.0
```

```
      YC              =    1. + P
      GO TO 60
   90 WRITE(3,111) PR     ,PSIL
  111 FORMAT (5X,' HECK - PS=',F10.5, 3X, 'AND PSIL=',F10.5)
   60 XP              =    XC
      YP              =    YC
      RETURN
      END


      SUBROUTINE LTOR ( SOA, P, XP, YP, XOA, S1, S2, H1, H2, B1, B2,
     1 X1, X3, PR, RSOA, Y1B, Y2B)
      X1B             =    X1
      X2B             =    X3
      PS              =    PR    / 57.29578
      R               =    (COS(PS) / SIN(PS))
      IF (YP - Y1B)5,5,10
    5 PSIL            =    1.570796 + ATAN (S1)
      GO TO 7
   10 PSIL            =    1.570795 + ATAN((XP/ (YP - H1))*RSOA)
    7 IF (PS - PSIL) 6,6,90
    6 IF (Y2B - YP) 24,21,22
   21 PSIP            =    1.570796
      GO TO 23
   22 PSIP            =    ATAN(((X2B - XP) / (Y2B - YP))*RSOA)
      GO TO 23
   24 PSIP            =    1.570796 + ATAN(((YP - Y2B) / (X2B - XP))*SOA)
   23 AL              =    ATAN (((H2 - YP) / (1. - XP)) * SOA)
      Q2              =    (H2-YP)*(H2-YP)*SOA*SOA + (1.-XP)*(1.-XP)
      BE              =    ATAN (B2 / SQRT(Q2 - B2*B2))
      PSIPP           =    1.570796 - (AL + BE)
      IF (PS - PSIP) 30,20,20
   20 XC              =    (SOA - YP*SOA - S2 + R*XP) / (R - S2)
      YC              =    R*(XC - XP)*RSOA + YP
      GO TO 60
   30 IF (PS - PSIPP) 50,40,40
```

```
40 PART1            =    1. + R*R*XP - (YP - H2)*R*SOA
   D                =    R*R + 1.
   PART2            =    R*R*XP*XP + 1. - B2*B2 - 2.*(YP-H2)*R*XP*SOA +
  1 (YP-H2)*(YP-H2)*SOA*SOA
   ROOT             =    PART1*PART1 - D*PART2
   IF (ROOT) 50,42,43
43 XC               =    (PART1 - SQRT(ROOT)) / D
   GO TO 44
42 XC               =    PART1 / D
44 YC               =    R*(XC - XP)*RSOA + YP
   GO TO 60
50 XC               =    1.0
   YC               =    1. + P
   GO TO 60
90 WRITE(3,111) PR     ,PSIL
111 FORMAT (5X,' HECK - PS=',F10.5, 3X, 'AND PSIL=',F10.5)
60 XP               =    XC
   YP               =    YC
   RETURN
   END
```

```fortran
      SUBROUTINE SELEC  (K,PSI,PSIM5,PSIP5,KK)
      DIMENSION  K(40) ,KK(10)
      I             =    ABS(PSI) / 5.
      IF   (PSI)   1,1,2
1 M             =    2*I + 2
  K(M)          =    K(M) + 1
  GO TO 3
2 M             =    2*I + 1
  K(M)          =    K(M) + 1
3 IF(PSI.GT.PSIM5.AND.PSI.LT.PSIP5)  GO TO 4
6 RETURN
4 MM            =    PSI - PSIM5 + 1.
  KK(MM)        =    KK(MM) + 10
  RETURN
  END
```

```
      SUBROUTINE COUNT (K , RAT)
      DIMENSION  K(40),D(40), RAT(40)
      J               =    1
      DO 10   I=1,36
      DIF             =    K(J) - K(I)
      IF (DIF) 9,9,10
    9 J               =    I
   10 CONTINUE
      D(J)            =    K(J)
      DO  20 K1=1,36
      D(K1)           =    K(K1)
      RAT(K1)         =    D(K1) / D(J)
   20 CONTINUE
      RETURN
      END
```

```
      SUBROUTINE RANDU( IX, IY, YFL)
      IY              =    IX * 65539
      IF (IY) 5,6,6
    5 IY              =    IY + 2147483647 + 1
    6 YFL             =    IY
      YFL             =    YFL * 0.4656613E-9
      RETURN
      END

      SUBROUTINE GAUSS (IX,S,AM,V)
      A               =    0.0
      DO 50 I=1,12
      CALL RANDU (IX,IY,Y)
      IX              =    IY
   50 A               =    A + Y
      V               =    (A-6.0)*S + AM
      RETURN
```

```
      SAMPLE DATA
1.0        0.1         0.6         10.0        0.1         4.0
   1111 10000   1000  1000   0.15
```

SAMPLE OUTPUT

SIGMA / LAMDA	=	0.10000
SIGMA / A	=	1.00000
INC-ANGLE	=	10.00000
P	=	0.60000
REF. INDEX	=	0.10000
ABS. INDEX	=	4.00000

AFTER. 200 BUNDLES, THE REFLECTED DISTRIBUTION IS AS FOLLOWS

REGIONS	1	3	5	7	9	11	13	15	17	19	21	23	25	27	29	31	33	35
	20	26	25	23	14	9	9	4	4	3	2	0	1	1	1	0	0	0
	0.769	1.000	0.962	0.885	0.538	0.346	0.346	0.154	0.154	0.115	0.077	0.0	0.038	0.038	0.038	0.0	0.0	0.0

REGIONS	2	4	6	8	10	12	14	16	18	20	22	24	26	28	30	32	34	36
	18	17	9	4	3	1	0	0	1	0	0	0	0	0	0	0	0	0
	0.692	0.654	0.346	0.154	0.115	0.038	0.0	0.0	0.038	0.0	0.0	0.0	0.0	0.0	0.0	0.0	0.0	0.0

5.00000   15.00000   50   40   20   100   50   40   50   50   60   50

LOSS NUMBER THROUGH THE SURFACE	5
ESCAPE NUMBER AFTER 1 REFLECTION	193
ESCAPE NUMBER AFTER 2 REFLECTIONS	2
ESCAPE NUMBER AFTER 3 REFLECTIONS	0
ESCAPE NUMBER AFTER 4 REFLECTIONS	0
NUMBER TRAPPED IN THE V-GROOVE	0

AFTER 400 BUNDLES, THE REFLECTED DISTRIBUTION IS AS FOLLOWS

REGIONS	1	3	5	7	9	11	13	15	17	19	21	23	25	27	29	31	33	35
	48	48	54	47	32	26	17	7	7	3	2	0	2	1	2	1	0	0
	0.889	0.889	1.000	0.870	0.593	0.481	0.315	0.130	0.130	0.056	0.037	0.0	0.037	0.019	0.037	0.019	0.0	0.0

REGIONS	2	4	6	8	10	12	14	16	18	20	22	24	26	28	30	32	34	36
	33	24	13	12	6	1	3	0	1	0	0	0	0	0	0	0	0	0
	0.611	0.444	0.241	0.222	0.111	0.019	0.056	0.0	0.019	0.0	0.0	0.0	0.0	0.0	0.0	0.0	0.0	0.0

5.00000   15.00000   100   70   60   180   70   80   130   130   120   80

LOSS NUMBER THROUGH THE SURFACE	10
ESCAPE NUMBER AFTER 1 REFLECTION	386
ESCAPE NUMBER AFTER 2 REFLECTIONS	3
ESCAPE NUMBER AFTER 3 REFLECTIONS	1
ESCAPE NUMBER AFTER 4 REFLECTIONS	0
NUMBER TRAPPED IN THE V-GROOVE	0

APPENDIX D

DETERMINATION OF THE IN-SURFACE PARAMETERS

The discussion that follows is representative of only a first approximation to determine by experimentation the parameter $\bar{a}$ and a flatness parameter introduced in Chapter V.

Consider a rough surface as presented in Figure D-1. The total macroscopic surface area is A_o with A representing the area of A_o that is effectively flat. Assume a uniform monodirectional radiant flux, F, incident on the surface at some angle ψ. The increment of incident energy that will make a contribution to the non-regular component is

$$dE = FdA \cos \psi \tag{D-1}$$

Thus the radiant intensity upon reflection is

$$dJ = \frac{R}{\pi} g(\psi;\theta,\varphi) \ dE$$

where R is a reflection coefficient and $g(\psi;\theta,\varphi)$ is a distribution parameter. So the total contribution to the radiant intensity due to the non-regular component from an isotropic surface is

$$J = \int dJ = \int \frac{R}{\pi} g(\psi,\theta,\varphi) \ F \cos \psi \ dA$$

$$= \frac{RFA_o}{\pi} g(\psi,\theta,\varphi) \left(1 - \frac{A}{A_o}\right) \cos \psi$$

The energy received in the solid angle $d\omega$ from the non-regular reflection is

128
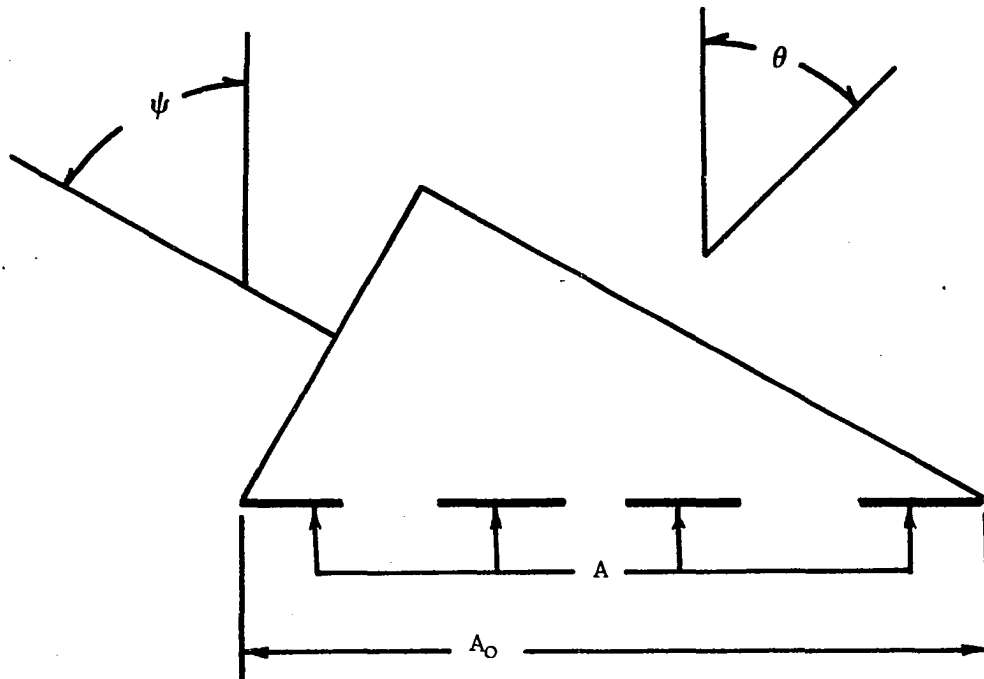
Figure D-1. Schematic of Rough Surface

$$E_1 = \int J d\omega = \frac{RFA_o}{\pi} g(\psi;\theta,\varphi) \cos \psi \left(1 - \frac{A}{A_o}\right) d\omega \qquad (D-2)$$

The increment of incident energy that will contribute to the regular component is of the form of equation (D-1). The reflected energy is then

$$E_2 = \int \rho dE = \rho F A \cos \psi$$

Therefore, the total energy received is

$$E = E_1 + E_2 \; \delta(\psi - \theta) \; \delta(\varphi)$$

$$= \frac{RFA_o}{\pi} g(\psi;\theta,\varphi) \left(1 - \frac{A}{A_o}\right) \cos \psi \; d\omega$$

$$+ \rho F A \cos \psi \; \delta(\psi - \theta) \; \delta(\varphi)$$

Thus $\quad \bar{R} = \dfrac{E}{A_o F \cos \psi} = \dfrac{Rg(\psi;\theta,\varphi)}{\pi} \left(1 - \dfrac{A}{A_o}\right) d\omega + \dfrac{\rho A}{A_o} \delta(\psi - \theta) \; \delta(\varphi)$

If $\psi = \theta$ and $\varphi = 0$

$$\frac{\bar{R}}{\rho} = \left[\frac{A}{A_o} \left(1 - \frac{Rg(\psi,\psi,0)d\omega}{\rho\pi}\right) + \frac{Rg(\psi,\psi,0)d\omega}{\rho\pi}\right]$$

$$\therefore \quad \frac{A}{A_o} = \frac{\bar{R}/\rho - \dfrac{Rg(\psi,\psi,0)d\omega}{\rho\pi}}{1 - \dfrac{Rg(\psi,\psi,0)d\omega}{\rho\pi}} \qquad (D-3)$$

By requiring a small acceptance angle

$$\frac{A}{A_o} \doteq \frac{\bar{R}}{\rho} \qquad (D-4)$$

This approximation should be quite good for metals since $R \simeq \rho$. For nonmetals, Equation (D-4) may not be very good since $R > \rho$. The quantities $\bar{R}$ and ρ are the general and ideal reflection coefficients for the material of interest.

The determination of the quantity $\bar{R}$ from an analysis such as MCR

must be handled carefully and at this point may be done only in approximate fashion. The actual non-regular reflected distribution is not known. A diffuse approximation of $N \cos (\theta^2 + \varphi^2)^{\frac{1}{2}}$ is quite mathematically unwieldy. For the analysis that follows, a parabolic approximation will be used. The total number of energy bundles reflected into the hemisphere above the specimen surface is

$$N_T \doteq 4N \int_0^{\frac{\pi}{2}} \int_0^m \left[1 - \frac{4}{\pi^2} (\varphi^2 + \theta^2) \right] d\theta d\varphi \qquad \text{(D-5)}$$

$$= 1.228 \, N \quad , \quad m = \sqrt{\frac{\pi^2}{4} - \varphi^2}$$

From the MCR analysis only 10,000 of the total N_T were received between a range of θ of $90°$ to $-90°$ and the range of φ of $2.5°$ to $-2.5°$. Changing the φ limits on equation (D-5) defines N to be approximately 10^5. Therefore N_T is approximately 1.2×10^5. Using the data from Figure 5-6, approximately 6,500 energy bundles were received about the regular reflection angle (i.e. 1,500 from the non-regular component and 5,000 from the regular). Thus

$$\bar{R} = \frac{6,500}{125,000} \doteq 0.052$$

The reflectance of nickel in the wavelength region where this data was taken is of the order of 0.8.

$$A = 0.065A_o$$

Thus for the particular example presented, approximately 6% of the total area of the surface is contributing directly to the regular component.

As stated previously, this analysis is a gross approximation and probably somewhat premature. That is, this research was conducted so as to aid in the development of a more general theory of reflection and this

coming theory must be used to carry out an analysis of the form presented here.